Progress in Polymer Science 115 (2021) 101374

Contents lists available at ScienceDirect

Progress in Polymer Science

journal homepage: www.elsevier.com/locate/progpolymsci

Recent progress in conjugated microporous polymers for clean energy: Synthesis, modification, computer simulations, and applications

Songhao Luo[a,1], Zhuotong Zeng[b,1], Han Wang[a,1], Weiping Xiong[a,1], Biao Song[a], Chengyun Zhou[a], Abing Duan[a], Xiaofei Tan[a], Qingyun He[a], Guangming Zeng[a,*], Zhifeng Liu[a,*], Rong Xiao[b,*]

[a] *College of Environmental Science and Engineering, Hunan University and Key Laboratory of Environmental Biology and Pollution Control (Hunan University), Ministry of Education, Changsha, 410082, PR China*

[b] *Department of Dermatology, Second Xiangya Hospital, Central South University, Changsha 410011, PR China*

ARTICLE INFO

Article history:
Received 5 October 2020
Accepted 10 February 2021
Available online 19 February 2021

Keywords:
Conjugated microporous polymers
Ultra-thin films
Density functional theory
Hydrogen storage
Lithium-ion batteries
Supercapacitor
Solar cells

ABSTRACT

Energy shortages and climate change call for the development of clean and sustainable energy. The development of green materials for clean energy storage and conversion is conducive to promoting the widespread use of clean energy. Conjugated microporous polymers (CMPs) have been synthesized with various structures and properties, which offer designability for the molecular structures and nanopores of conjugated skeletons. The research of CMPs in clean energy technologies is significant for the improvement of CMP-based materials and their application in energy and environmental engineering. CMPs have shown great potential for challenging energy and environmental issues such as gas adsorption, photocatalysis, solar energy conversion, and electrical energy storage and conversion. This review aims to summarize the advances of synthesis and design on CMPs, computer simulations on CMPs, and the applications of CMPs in the clean energy technologies including hydrogen evolution and storage, the adsorption and conversion of carbon dioxide, rechargeable batteries, supercapacitors, fuel cells, and photovoltaic cells. We also propose the challenges and potential chances of the synthesis and the clean energy applications of CMPs.

1. Introduction

1.1. Research background

Energy shortages and environmental pollution are global challenges. Traditional fossil energy reserves are limited. The use of large amounts of fossil energy can cause environmental pollution and global warming [1-3]. To meet this challenge, finding new energy systems that can replace fossil energy is needed urgently. Clean energy has a lower environmental impact than traditional energy [4-8], which is the most promising candidate for the energy future. However, the supply of these energy sources is volatile, so to develop strategies for storing and transforming clean energy is required. Today, many effective devices and techniques have been developed to store and transform clean energy including photocatalytic hydrogen production and hydrogen storage [9-11], rechargeable batteries [12-14], oxygen reduction devices [15-17], photovoltaic devices [18-20], and supercapacitors [21-23]. To improve the energy storage and conversion efficiency of these devices, many materials have been developed and used as catalysts or electrode materials [24-26].

The common choices are inorganic active materials such as transition metal oxides and graphite [27-29]. In 2014, the recent advances, mechanistic details, and new challenges and prospects in plasma-based nanogold catalysts in organic and clean energy conversion systems were reported [30]. Due to the surface plasmon resonance (SPR) effect in plasma-based catalysts, the near-field of local plasma and scattering effect were improved, and $e^-{-}h^+$ pairs were stimulated, thus greatly increasing the catalytic activity and

---

Abbreviations: SPR, surface plasmon resonance; SOFCs, solid oxide fuel cells; MOPs, microporous organic polymers; COFs, covalent organic frameworks; PAFs, porous aromatic frameworks; PIMs, polymers of intrinsic microporositys; AMPNs, anionic microporous polymer networks; CMPs, conjugated microporous polymers; HMOPs, hypercrosslinked microporous organic polymers; MO-CMPs, Metal-organic conjugated microporous polymers; BET, Brunauer–Emmett–Teller; TEB, 1,3,5-triethynylbenzene; CTFs, covalent triazine framework; NPs, nanoparticles; NTs, nanotubes; SCMPs, conjugated microporous polymers with thiophene segments; PCMPs, conjugated microporous polymers with pyridine units; HER, hydrogen evolution rate; AQY, apparent quantum yields; D-π-A, donor-π-receptor..

[*] Corresponding authors.

E-mail addresses: zgming@hnu.edu.cn (G. Zeng), zhifengliu@hnu.edu.cn (Z. Liu), xiaorong65@csu.edu.cn (R. Xiao).

[1] These authors contribute equally to this article.

https://doi.org/10.1016/j.progpolymsci.2021.101374
0079-6700/

Fig. 1. Historical development of microporous organic polymers (MOPs). Solubility film-forming PIMs. [53], Copyright 2004. Reproduced with permission from The Royal Society of Chemistry. Synthesis of crystalline COFs with exceptionally high surface areas. [54], Copyright2007, Reproduced with permission from the American Association for the Advancement of Science. CMPs which combine porosity with extended π-conjugation. [47], Copyright 2007. Reproduced with permission from the John Wiley & Sons Inc. More robust crystalline COF analogs. [55,56], Copyright 2008 and 2009. Reproduced with permission from the John Wiley & Sons Inc and American Chemical Society. Robust and highly porous aromatic frameworks. [42], Copyright 2009. Reproduced with permission from the John Wiley & Sons Inc. Metal-organic CMPs (MO-CMPs) comprising catalytic metal centers. [57], Copyright 2011. Reproduced with permission from the John Wiley & Sons Inc.

efficiency of solar-energy conversion. Hossain et al. highlighted the application of $BaCeO_3$ and $BaZrO_3$ electrolyte materials in proton-conducting solid oxide fuel cells (SOFCs) [31].

Furthermore, the novel microporous organic polymers (MOPs) are becoming to be new candidate materials for clean energy due to their large surface area, structural modularity, and excellent physicochemical properties [32-36], such as, covalent organic frameworks (COFs) [37-41], porous aromatic frameworks (PAFs) [42], polymers of intrinsic microporosity (PIMs) [43,44], anionic microporous polymer networks (AMPNs) [45,46], conjugated microporous polymers (CMPs) [47-51], and hypercrosslinked microporous organic polymers (HMOPs) [52]. The historical development of these MOPs is shown in Fig. 1 [42,47,53-57]. Javier's group critically reviewed the application and development of mesoporous materials in the field of clean energy [58], and gave many examples of the development of mesoporous structures, including the preparation of different scale pore systems with layered structures, which brings hope for better and cleaner energy production. Xia et al. discussed the application of COFs in the field of clean energy, and proposed the design principles laid the foundation for the rational design of COFs and the applications in clean energy [59]. CMPs are a class of amorphous structures that have recently received increasing attention due to their adjustability, expanded π-conjugation, and permanent building links [60].

CMPs have emerged as a powerful platform for solving deteriorating environmental and energy problems. For example, CMPs have been widely used as adsorbents [61,62], heterogeneous catalysts [57,63-66], light-harvesting materials [67,68], luminescent materials [49,69], photovoltaic materials [70,71], and photocatalysis [72], because they have many advantages, such as: (i) The π-conjugated structure extending along the polymer backbone provides excellent physicochemical stability, rich porous structure, and high surface area. (ii) The highly crosslinked polymeric structure and high surface area provide greater pore space to accommodate carriers and large contact surface areas to shorten ion diffusion distance, ensuring high electrochemical activity and fast kinetics [73-75]. (iii) The highly crosslinked polymer structure can effectively inhibit the dissolution of the active material in the organic electrolyte and improve cycle stability [73,76].

1.2. Representative advances

CMPs refers to the macromolecular compounds that hold microporous networks and π-conjugation resulting from alternating single and multiple bonds [48,77,78]. These bonds result from the overlap of two p-orbitals (or d-orbitals) crosswise with an intermediary σ-bond, which provides useful electronic properties (such as high conductivity) to CMP networks. The large variety of molecular building blocks that can be coupled in this way allows the control of functionality and structure in CMPs, and this structural diversity has led to the rapid growth of these materials since their discovery (Fig. 2) [47,57,67,76,79-94]. Almost all covalent bonds in CMPs are formed by irreversible kinetic routes, so all CMPs (excluding covalent triazine frameworks) are amorphous. In 2007, the unique porous materials, conjugated microporous poly(aryleneethynylene) networks with Brunauer–Emmett–Teller (BET) surface areas up to 834 $m^2\ g^{-1}$ were reported for the first [47]. In 2008, the CMPs with BET surface areas up to 1000 $m^2\ g^{-1}$ were produced [95]. Thomas et al. constructed CMPs based on spirobifluorene blocks and proposed for the first time to use these photoluminescent CMPs for photoelectric applications [80]. In the same year, CMPs prepared by homocoupling routes of 1,3,5-triethynylbenzene (TEB) were also reported [79] and confirmed to display visible-light catalytic activity for overall water splitting in 2017 [92]. In 2009, Thomas et al. also outlined a framework for a new generation of porous polymers for energy-related applications, presented potential applications, and proposed some outstanding issues and developments [96]. Metal-supported high surface area metal-organic CMPs (MO-CMPs) were synthesized in 2011 [57], etc. In recent years, these CMPs are becoming important functional materials [48,57,97] and are further explored for use in the field of clean energy.

In the development process of CMPs in the field of clean energy, Jiang's group comprehensively reviewed the design principles, structural research, and functional exploration, as well as potential application prospects of CMP materials [77]. Wang et al. briefly summarized the latest developments and trends in the field of photocatalytic water splitting using CMPs [98]. As well as, we reviewed the energy transfer phenomena of CMPs and the basic principles of photocatalysis, and proposed the strategy of improving the photocatalytic performance of CMPs [72]. To the best of our knowledge, there is no specific and detailed review for the CMPs in the field of clean energy. In recent years, CMPs have made rapid progress in the field of clean energy, and it is time to make a comprehensive and detailed summary and analysis of the topic of CMPs as a platform for clean energy. In this review, we aim to present the latest research advances in CMPs for clean energy including hydrogen storage materials, carbon dioxide capture and conversion, metal-ion rechargeable batteries, supercapacitors, fuel cells, and photovoltaic cells (Fig. 3). We first present an overview discussion and a summary of the synthesis strategies for CMP nanoparticles (NPs), nanotubes (NTs), and films. Then, a computer simulation that predicts and guides the synthesis and application of CMP materials is recommended. Furthermore, the use of CMPs with excellent properties in the field of clean energy is described. Finally, we discuss in detail the future trends and major challenges in the development of CMPs in the clean energy

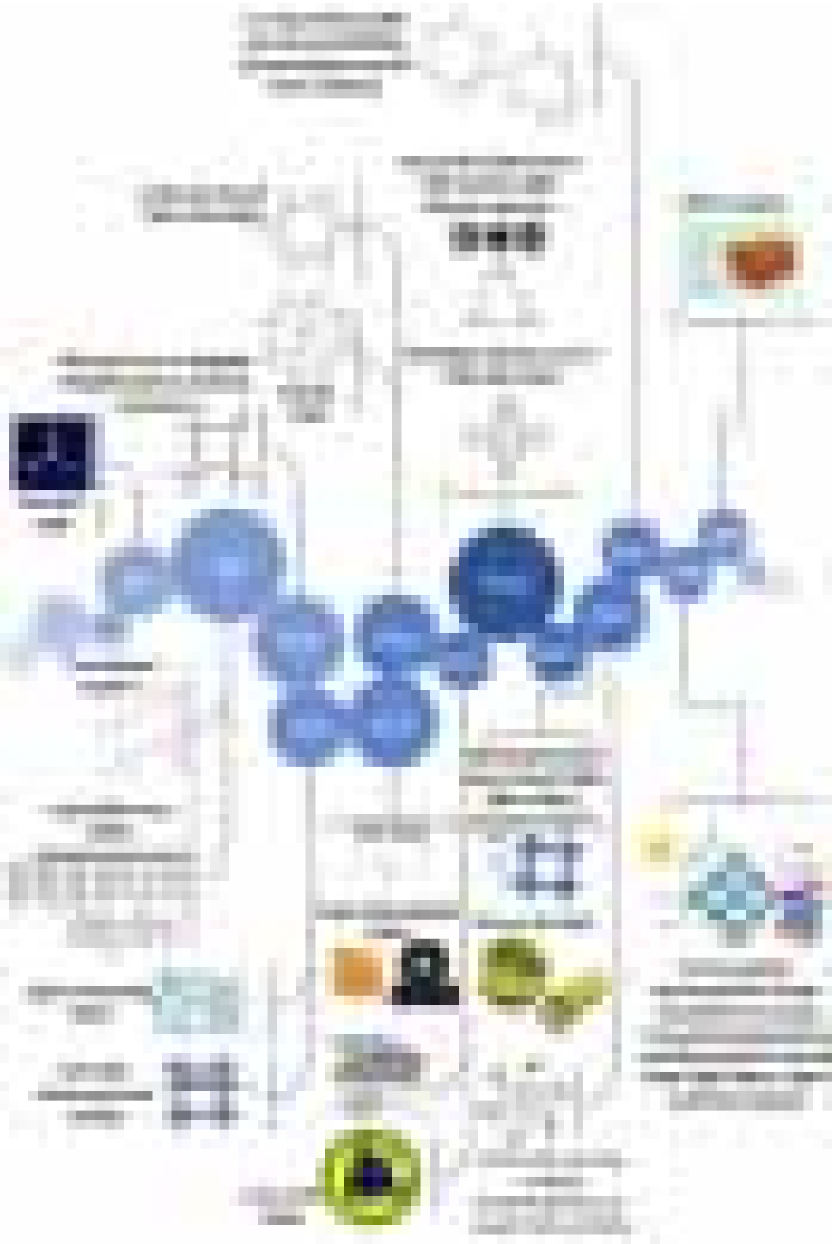

Fig. 2. Quintessential examples of CMP materials development. A milestone in the development of CMP materials. 2007. [47], Copyright 2007. Reproduced with permission from the John Wiley & Sons Inc. 2008. [79,80], Copyright 2008. Reproduced with permission from The Royal Society of Chemistry and the American Chemical Society. 2009. [81], Copyright 2009. Reproduced with permission from the John Wiley & Sons Inc. 2010. [67,82], Copyright 2010. Reproduced with permission from the American Chemical Society. 2011. [57,83], Copyright 2011. Reproduced with permission from the John Wiley & Sons Inc and The Royal Society of Chemistry. 2012. [84,85], Copyright 2012. Reproduced with permission from the John Wiley & Sons Inc and the American Chemical Society. 2013. [86,87], Copyright 2013. Reproduced with permission from the John Wiley & Sons Inc and The Royal Society of Chemistry. 2014. [76,88], Copyright 2014. Reproduced with permission from The Royal Society of Chemistry. 2015. [89,90], Copyright 2015. Reproduced with permission from the John Wiley & Sons Inc. 2016. [91], Copyright 2016. Reproduced with permission from the American Chemical Society. 2017. [92], Copyright 2017. Reproduced with permission from the John Wiley & Sons Inc. 2018. [93], Copyright 2018. Reproduced with permission from Elsevier Science Ltd. 2019. [94], Copyright 2019. Reproduced with permission from the John Wiley & Sons Inc.

field. We sincerely hope that this will stimulate readers' interest in the exploration of clean energy, who is advised to further read the cited articles.

2. Synthesis strategies of CMPs

The diversity of monomers and the variety of reactive groups make CMPs with diverse network structures and molecular functions. The reaction monomer of CMPs include π units such as arenes, fused aromatic rings, heterocyclic units phenylethynylene derivatives, macrocyclic systems, and so on, and the reactive groups such as iodoarenes, aromatic boronic acids, bromoarenes, cyano-substituted arenes, ethynyl-substituted arenes, and amino-substituted arenes, aromatic aldehydes [77]. CMP networks are usually formed by the reaction between two or more different monomers or, some by the homocoupling of a single monomer. The main challenge is to design a simple and productive synthesis route that can control the structural and photoelectric properties of CMPs to improve the performance of these networks in energy storage. This includes improved control at the molecular level, the establishment of topologies, the construction of porous structures, the regulation of band gaps, and changes in structural dimensions.

Fig. 3. CMPs as a powerful platform for the application in clean energy.

So far, a variety of synthetic methods have been developed for the preparation of CMPs, including the noble metal catalysis and non-noble metal catalysis methods. Quintessential examples of these synthetic methods are summarized in Table 1 [47,49,55,91,99-104].

2.1. Noble metal-catalyzed synthesis

Noble metal-catalyzed cross-coupling reactions are the first to be developed and are also the most versatile strategy for the synthesis of CMP materials. The structure of CMPs can be regulated by adjusting the comonomer molar ratio, and the reaction conditions. The advantages of these reactions are (i) mild reaction conditions, easy availability of substrates, good selectivity, easy post-synthesis functionalization, and good tolerance to functional groups, (ii) single synthesis precursor, simple reaction route, and high synthetic yield, (iii) high specific surface area. To date, various new CMP materials with adjustable structure and multifunction have been synthesized by noble metal-catalyzed cross-coupling reactions [83,105,106], which have great application prospects in clean energy systems. In this section, the up-to-date progress of this synthetic strategy is present in detail, including the Sonogashira-Hagihara reaction, the Suzuki cross-coupling reaction, the Yamamoto reaction, and the Buchwald-Hartwig coupling reaction.

2.1.1. Sonogashira-Hagihara reaction

The construction of the porous structure of CMPs requires the cross-coupling of building blocks of different geometric shapes. To construct conjugated porous structures, the monomers are first connected by the Pd-catalyzed Sonogashira-Hagihara cross-coupling reaction (Hereinafter referred to as Sonogashira-Hagihara reaction) with π-conjugated bonds [47,95,107]. In 2007, Jiang et al. combined the symmetrical core of C3 with the symmetrical linker of C2 through Sonogashira-Hagihara reaction to synthesize a series of polymer networks, namely CMP-1, CMP-2, CMP-3, and CMP-4 [47]. The pore size, surface area, and gas absorption of these materials can be attuned by changing the length of the link. CMP-1 contains two acetylene and one benzene on the arm, and its BET surface area is larger than the other three CMPs, indicating that the length of the polymer arm is inversely proportional to its surface area. In the following year, Jiang et al. then synthesized two other CMPs (CMP-0 and CMP-5) and the CMP-0 (S_{BET}: 1018 $m^2\ g^{-1}$) arm has only one ethylene and one benzene [95]. The BET surface area of CMP-0 exceeds that of CMP-1.

The polymer networks TCMP-0, TNCMP-2, TCMP-3, and TCMP-5 based on triazine were synthesized by Sonogashira-Hagihara reaction in 2012 [108]. In structural principle, these networks are isomorphic with the previously reported CMP-3 [47], CMP-0 and CMP-5 [95], and NCMP-2 [109]. As shown in Fig. 4, benzene nodes in these triazine-based network TCMP materials are replaced by 1,3,5-triazine units, which proves that nodes of CMPs can be adjusted and replaced reasonably. Meanwhile, the porosity of these polymers is comparable to that of previously reported 1,3,5-linked benzene CMP systems, but TCMPs showed better CO_2 absorption capacity. The TNCMP-2 displayed the highest surface area (995 $m^2\ g^{-1}$) and higher CO_2 absorption capacity (1.45 mmol g^{-1} at 1 bar at 298 K).

At the same porosity, selecting suitable monomers could effectively improve the physicochemical stability and adsorption capacity of the polymer network. Li's group used the Sonogashira-Hagihara reaction to synthesize CMPs with thiophene segments (SCMPs) [110]. Their electron-thiophene building units combine rich porosity and conjugated network structure, resulting in better adsorption capacity. In another example, Li's group used arylethynylenes and 2,6-dibromomethyl pyridine as raw materials, novel functional CMPs with pyridine units (PCMPs) were synthesized by Sonogashira-Hagihara reaction [111]. They find that the choice of vinyl monomer has a noteworthy effect on the BET specific surface area of the resulting CMPs. Furthermore, the molar ratio of the monomer has a significant effect on the surface area, which in turn affects the gas adsorption performance of CMPs [112,113]. Li's group synthesized a class of CMP networks using the Sonogashira-Hagihara reaction by using 1,3,5-triethylbenzene and 1,4-diethylbenzene as monomers (Fig. 5A) and used these CMPs as a porous model to reveal the influence of monomer ratio on the porosity of CMPs [112]. The results show that with the increase of the molar ratio of 1,3,5-triacetylene benzene to 1,4-diacetylene benzene, the surface area and total pore volume of these HCMP samples is decreased, but the mesopore and micropore volume is increased, which caused the improvement of the hydrogen adsorption capacity of HCMP samples (Fig. 5B). This can provide useful guidance for the design of new CMP hydrogen storage materials.

Recently, Xiang's group synthesized L-PDBT, L-PDBT-O, N-PDBT, and N-PDBT-O by Sonogashira-Hagihara reaction (Fig. 6A) [114]. In the field of clean energy, the design and synthesis of better hydrophilic CMP materials are beneficial to the exposure of photocatalytic active sites to the water environment, thus increasing photocatalytic activity. For these reasons, the morphology and surface polarity of these polymers can be adjusted by changing the structure block (Fig. 6A), so that CMPs have high hydrophilicity, which is more conducive to the production of hydrogen by photocatalytic water splitting. The measurement results of the water contact angle (Fig. 6B) show that N-PDBT-O has good water compatibility and adsorption performance. Compared with L-PDBT-O, polymer network N-PDBT-O exhibited better photocatalytic H_2 evolution activity [hydrogen evolution rate (HER): 366 μmol h^{-1}, AQY): 3.7%, $\lambda >$ 420 nm] because the synergistic effect of high hydrophilicity and BET surface area leads to more effective absorption of visible light by N-PDBT-O. The hydrophilic control strategy can also be applied to the design of other CMP-based photocatalysts to improve their photocatalytic activity, which provides an effective strategy for the design of higher hydrophilic CMP-based photocatalysts.

2.1.2. Suzuki cross-coupling reaction

Suzuki-Miyaura cross-coupling reaction (hereinafter referred to as Suzuki reaction), a reaction of aryl or alkenyl boric acid or boric acid ester with chlorine, bromine, aryl iodide or olefin catalyzed by noble metal Pd-based compounds, which was first reported by Akira Suzuki in 1979 [115,116]. This synthetic method has the advantages of commercial availability of boric acid, wide compatibility of functional groups, mild reaction conditions, etc. [117,118], so it has the potential of scale. However, the Suzuki reaction is sensitive to oxygen, which causes the homocoupling and the by-product of deboronated. Therefore, the gas should be eliminated strictly in

Table 1
Classic reaction routes for the preparation of CMPs

Category	Reaction type	Reaction formula	Representative CMPs	Ref.
Noble-metal catalyzed synthesis	Sonogashira-Hagihara coupling		CMP-1, CMP-2, CMP-3, CMP-4	[47]
	Suzuki coupling		DA-CMP1, DA-CMP2, Azo-CMP1, Azo-CMP2	[99]
	Heck coupling	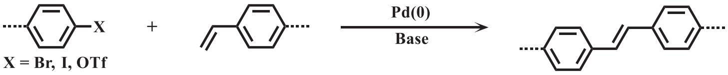	LMOP-1, LMOP-2, LMOP-3	[100]
	Yamamoto coupling	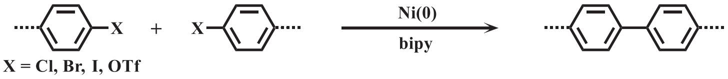	TBTPE, TPE-CMP, TPE-LP	[49]
	Buchwald-Hartwig coupling	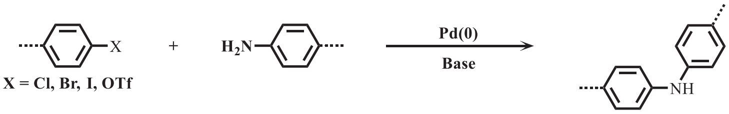	HCMP-1, HCMP-2, HCMP-3, HCMP-4	[91]
Non-noble metal catalyzed synthesis	Oxidative coupling		PCz–Cn–Cz (n = 3–6)	[101]
	Schiff-based reaction		KECMP-1	[102]
	Heterocycle linkages	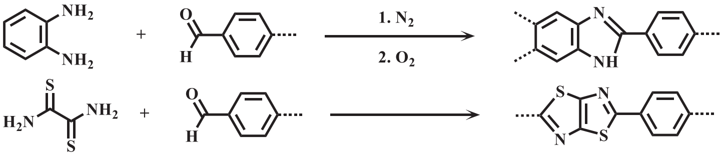	TzTz-POP-3, TzTz-POP-4, TzTz-POP-5	[103]
	Phenazine ring fusion reaction		TIPS-CMP	[104]
	Cyclotrimerization	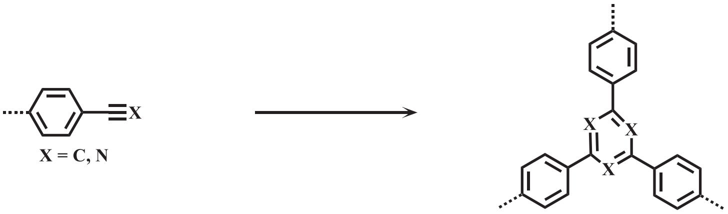	CTF-1	[55]

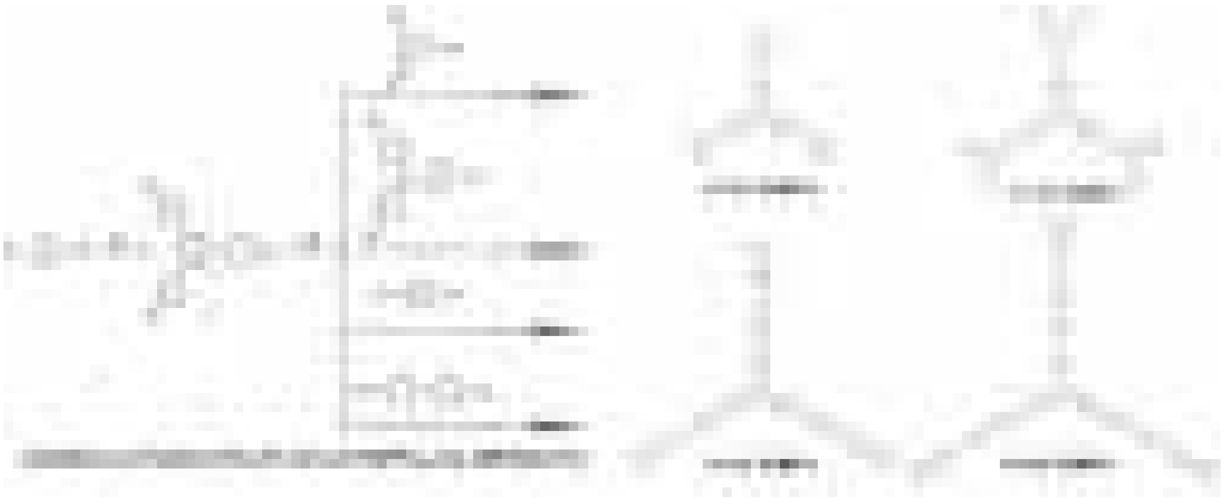

Fig. 4. Synthesis of the triazine monomer and molecular structures of TCMP networks. [108], Copyright 2012. Reproduced with permission from The Royal Society of Chemistry.

Fig. 5. (A) Synthesis route and structure for HCMP1–HCMP5. (B) Volumetric H2 adsorption isotherms for HCMP1–HCMP5 up to 1.0 bar at 77.3 K. [112], Copyright 2012. Adapted with permission from Elsevier Science Ltd.

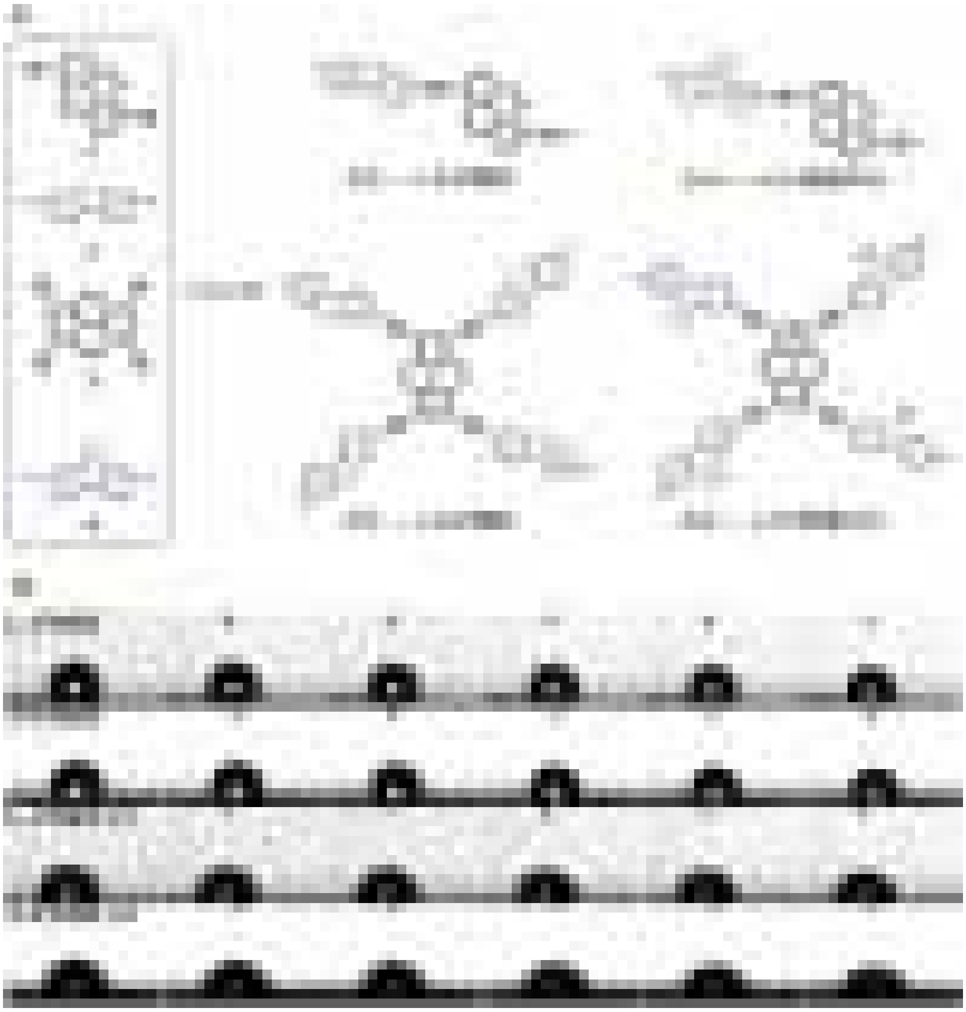

Fig. 6. (A) Synthetic route and representative structures of the L-PDBT, N-PDBT, L-PDBT-O, N-PDBTO. (B) Water contact angle measurements of L-PDBT, N-PDBT, L-PDBT-O, and N-PDBT-O. [114], Copyright 2018. Reproduced with permission from the John Wiley & Sons Inc.

the reaction process. Here, a series of donor-π-receptor (D-π-A) CMPs with different polymer structures and components are synthesized by Suzuki reaction using pyrene, benzothiadiazole, benzene (or biphenyl) as a donor, a receptor, and a crosslinking agent unit, respectively [65]. By adjusting the monomer species and the ratio of pyrene to benzothiazole in the reaction process, the molecular structure of CMPs can be adjusted (Fig. 7), and then improving their photocatalytic performance. This work highlights the molecular structure as one of the key factors in the design of efficient CMP photocatalysts, which provides a promising platform for efficient organic photocatalysts. Given the wide range of electron donor and acceptor units and the universality of the Suzuki reaction, there is an opportunity to produce a wide range of CMPs for use in clean energy.

Fig. 7. Suzuki reaction to the networks and the diversity of the molecular structure of CMPs. [65], Copyright 2018. Reproduced with permission from Elsevier Science Ltd.

2.1.3. Heck reaction

Heck reaction also is known as the Mizoroki-Heck reaction. Since Heck and Mizoroki independently discovered this reaction in the late 1960s, it has been applied more and more widely through continuous improvement of catalysts and reaction conditions, so that it has become one of the important reactions forming the C–C bond. In recent years, through the Heck reaction of 1,3,5-tri(4-ethenylphenyl) benzene and aromatic halides, a new class of luminescent microporous organic polymer LMOPs has been constructed (Fig. 8), which has a large surface area, narrow pore size distribution, and strong luminescent performance [100,119]. The one-pot synthesis strategy is expected to produce a variety of luminescent porous organic polymers, which could be widely used in the fields of organic photovoltaic and photocatalysis.

2.1.4. Yamamoto reaction

Yamamoto coupling reaction, also known as Yamamoto reaction, is a cross-coupling reaction in which halogenated aromatic hydrocarbons form C–C bonds under the catalysis of transition metal Ni [120-124]. The CMPs formed by Yamamoto coupling of tetrakis(4-iodophenyl)methane and tetrakis(4-bromophenyl)−1,3,5,7-adamantane monomers (Fig. 9) with BET surface areas of 3160 and 3180 m^2 g^{-1}, respectively, top all the CMPs in term of BET surface areas [107]. In 2009, Thomas et al. first prepared a series of spirobifluoren-based CMPs (YSN-CMPs) by Yamamoto coupling reaction, in which, when 2,2′,7,7′-tetrabromo-9,9′-spirobifluorene was self-polymerized, the specific surface area of the CMP was 1275 m^2 g^{-1} [125]. Results have shown that the bond length and configuration of different structural units can greatly affect the pore structure and BET surface area of CMPs. For example, when 2,2′,7,7′-tetrabromo-9,9′-spirobifluorene was copolymerized with p-dibromobenzene, the specific surface area of the polymer networks decreased to 887 m^2 g^{-1}, when it was copolymerized with m-dibromobenzene, the specific surface area decreased to 361 m^2 g^{-1}, when it was copolymerized with o-dibromobenzene, the specific surface area was only 5 m^2 g^{-1} [125].

Fig. 8. Syntheses of LMOPs by Heck reaction and representative molecular structures of LMOPs. [100], Copyright 2013. Reproduced with permission from The Royal Society of Chemistry.

Fig. 9. The Yamamoto reaction to the synthesis of polymer networks 1 and 3. [107], Copyright 2010. Reproduced with permission from the American Chemical Society.

Besides, p-aryl monomers are beneficial to the formation of porous structures [126]. Jiang's group used the Yamamoto coupling reaction to synthesize a novel conjugated microporous polymer (TPE-CMP) with a p-aryl monomer tetrakis(4-bromophenyl)ethene (TPTBE) [49]. In this reaction, the tetraphenylethene (TPE) units are directly connected to form a chain network, which limits the rotation of the phenyl group and enables the CMP to has a high luminescent activity, which has great potential in the production of hydrogen by the visible light solution of water. It should be noted that the disadvantage of the synthesis of CMP materials by the Yamamoto reaction is that the Ni catalyst is easy to oxidize and ab-

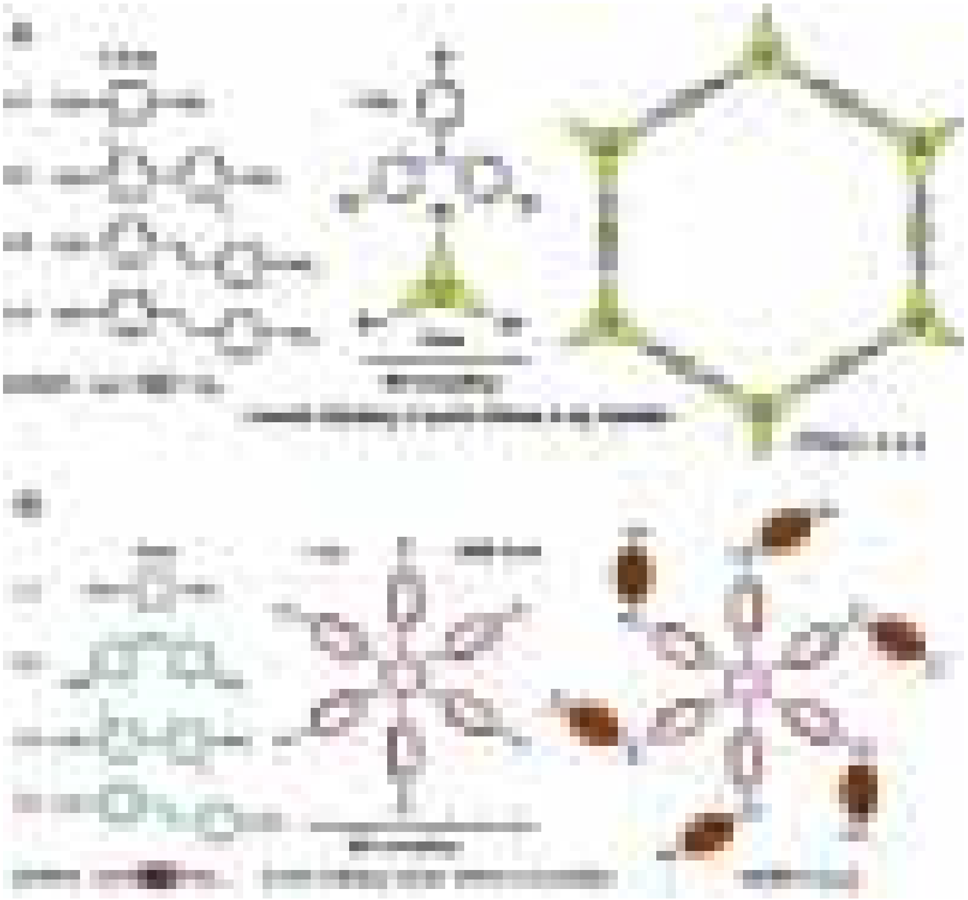

Fig. 10. (A) PTPAs synthesized by Buchwald-Hartwig coupling reaction. [128], Copyright 2010. Reproduced with permission from The Royal Society of Chemistry. (B) HCMPs synthesized by the Buchwald-Hartwig coupling reaction. [91], Copyright 2016. Reproduced with permission from the American Chemical Society.

sorb water, resulting in inactivation. Therefore, the condition of no water and no oxygen should be strictly controlled in the reaction process, which increases the preparation cost of CMPs to some extent.

2.1.5. Buchwald–Hartwig coupling reaction

Buchwald-Hartwig coupling reaction (B-H coupling) is a coupling reaction of halogenated aromatic hydrocarbons and aromatic amines to form C–N bonds under the action of a small amount of palladium catalyst. In 2008, Germain et al. first prepared the polyaniline network structure by B-H coupling and used it for hydrogen adsorption [127]. In 2014, Liao et al. extended this method to the efficient preparation of CMPs [91,128]. A series of conjugated microporous polytriphenylamine (PTPA) networks (Fig. 10A) and Hexaphenylbenzene (HPB)-based CMPs (HCMPs) (Fig. 10B) through the B-H coupling of tris(4-bromophenyl)amine core [128] and aromatic amine linkers or hexakis(4-bromophenyl)benzene (HBB) core and aryl diamine linkers [91]. The specific surface area and pore structure of PTPAs can be regulated by changing the conjugate length and rigidity of aromatic amine. Longer conjugate length and stronger rigidity of aromatic amine can synthesize CMPs with larger specific surface area up to 530 $m^2\ g^{-1}$.

2.2. Non-noble metal-catalyzed synthesis

Noble metal-catalyzed cross-coupling reactions are an important strategy for the synthesis of CMP materials. However, noble metal catalysts are expensive, sensitive to oxygen, difficult to recycle, and the catalyst solvents are toxic. Therefore, some non-noble metal-catalyzed synthesis reactions for the synthesis of CMP materials have developed. These reactions have advantages such as the use of cheap catalysts, ambient temperature reaction conditions, high yields, and only a single monomer is required, which are the keys to expanding the preparation of CMP materials. This section presents non-noble metal-catalyzed chemical synthesis methods for preparing conjugated microporous polymers in detail. It mainly includes oxidation coupling reaction, Schiff-base reaction, and Friedel-Crafts reaction, heterocycle linkages, phenazine ring fusion reaction, and cyclotrimerization reaction. These methods are providing an effective way for large-scale preparation of high-efficiency CMP materials for the clean energy field.

2.2.1. Oxidative coupling reaction

Oxidative polymerization is the process by which a compound containing active hydrogen atoms is dehydrogenated to form a polymer in the presence of an oxidation catalyst. According to the different oxidation forms, it can be divided into chemical oxidation polymerization and electrochemical oxidation polymerization. Chemical oxidation polymerization is the reaction of monomer dehydrogenation polymerization under the action of oxidants such as $FeCl_3$ [129].

Chen et al. used carbazole-based oxidative coupling polymerization to prepare various of microporous conjugated polycarbazoles (CPOP-2–7) with eternal porosity and special functions [130]. 2D and 3D conjugated structures with non-planar rigid conformation have been proved to be excellent candidate materials for the preparation of conjugated core structures. The synthesis routes of

Fig. 11. (A) Synthetic routes to monomers Cz-4, Cz-6, and Cz-7. (B) Preparation of microporous conjugated polymers CPOP-2~7. [130], Copyright 2013. Reproduced with permission from the John Wiley & Sons Inc.

monomers are shown in Fig. 11A, carbazolyl groups can be simply introduced into these conjugated core structures, which provide conditions for the preparation of multifunctional polymer networks. As shown in Fig. 11B, taking multipurpose carbazolyl-bearing 2D and 3D conjugated central with non-planar rigid conformation as linking units, a series of CPOPs are synthesized. Because no need boric acid, alkyl, halo groups, and other functional groups for the coupling polymerization reaction, so the properties get from monomer could be fully retained, and because each carbazole group in a monomer has two reaction sites, so makes the oxidation coupling polymerization of carbazolyl easy to form a porous polymer. As well as due to the high degree of crosslinking, the pore structure of the polymer is more stable and durable. The BET specific surface area of these porous polymer materials is between 510 and 1430 $m^2\ g^{-1}$, and the pore sizes are between 0.59 and 0.66 nm.

A carbazole-based CMP prepared by oxidative coupling polymerization has permanent micropores, high luminescent properties, and plentiful nitrogen activation sites, so it shows a high adsorption capacity of carbon dioxide with good selectivity and is an attractive functional material in clean energy applications [131]. In 2016, Yang's group reported four carbazole-based CMPs (PCz-Cn-Cz) by using $FeCl_3$ catalyzed oxidation coupling method [101]. These polymers have the same rigid backbone (carbazole) and different soft-bonded alkylene chains, but the pore width and pore size distribution of the four polymers not seem to differ significantly. These four polymers all have a high specific surface area (>750 $m^2\ g^{-1}$) and good adsorption capacity of gasses (H_2, CO_2, CH_4, CO), which have broad application prospects in the field of clean energy and environmental engineering. Meanwhile, because carbazoles are electron-rich group [132], so $FeCl_3$-catalyzed oxidative coupling reaction of carbazole and the electron-deficient unit can provide a greener and more environmentally friendly alternative to metal-free, visible light-driven solid CMP photocatalysts synthesis. In addition, two novel porphyrin-based CMPs (Porp-TPE-CMP and Porp-Py-CMP) formed by $FeCl_3$ catalyzed oxidative coupling reaction between pyrrole and aromatic aldehyde catalyzed also have the ability of gas adsorption [133]. Their BET specific surface areas are 547 and 31 $m^2\ g^{-1}$, respectively, and their CO_2/N_2 and CO_2/CH_4 selectivity are 55.28 and 4.11, respectively. These strategies provide a viable strategy for the storage of greenhouse gasses and chemical hydrides.

2.2.2. Schiff-Base reaction

In 2016, Chai et al. used Schiff-base reaction of 1,3,5-triformylphloroglucinol (TFP) and m-phenylenediamine (m-PDA) to synthesize an innovative β-ketoenamine-linked CMP (KECMP-1) [102]. The synthesis route is shown in Fig. 12, this preparation strategy uses only a single reactant and has the advantages of metal-free catalysis and template-free, as well as the BET specific surface area of the synthesized polymer network is up to 691 $m^2\ g^{-1}$. Meanwhile, the introduction of N–H groups into the polymer pore surface using a bottom-up strategy is conducive to the formation of the interaction between N–H•••O and CO_2, thus enhancing the CO_2 adsorption capacity of the polymer network. In 2018, CoCMP and ZnCMP were synthesized by a Schiff-base condensation reaction between metal-phthalocyanine tetra-amine and 4,4′-(2,5-bis(pentyloxy)1,4-phenylene)bis(ethyne-2,1-diyl)dibenzaldehyde (OPE-5) [134]. Among them, CoCMP, where Co^{2+} is steadied by the N_4-coordination of Phthalocyanines (PCs), and as a catalytic center. CoCMP showed stable and efficient electrocatalytic activity to oxygen evolution reaction (OER) (overpotential: 340 mV). This demonstrates the importance of Co^{2+} in OER catalysis. Meanwhile, the inactivity of ZnCMP to OER indicates that the introduction of metal ions should be wisely selected in addition to the selection of reaction conditions when designing CMP electrocatalysts.

Recently, the polymer network (FcTz-POP) formed by introducing iodine-affinity group ferrocene into the polymer network through Schiff-base reaction is quite stable, with a significantly increased iodine vapor adsorption capacity (396 wt.%, 348k, atmospheric pressure), higher than that of the ferrocene-free polymer (BpTz-POP) (216 wt.%, 348 K, atmospheric pressure) [135]. This guides the further introduction of other functional groups into the CMP networks through Schiff-base reaction to achieve specific effects for the application of clean energy.

2.2.3. Heterocycle linkages

A high porosity benzimidazole-chain polymer was synthesized by a simple template-free condensation reaction of 2,3,6,7,10,11-hexaaminotriphenylene with tetrakis(4-formylphenyl)methane, which has a wide application prospect in gas storage and separation [136]. As well as under solvent-heat conditions, catalyst-free condensation of aldehydes with dithiooxamide to form the thiazolothiazole-linked microporous polymer, which reveals high

Fig. 12. Schiff-base condensation polymerization to the synthesis of KECMP-1. [102], Copyright 2016. Reproduced with permission from Elsevier Science Ltd.

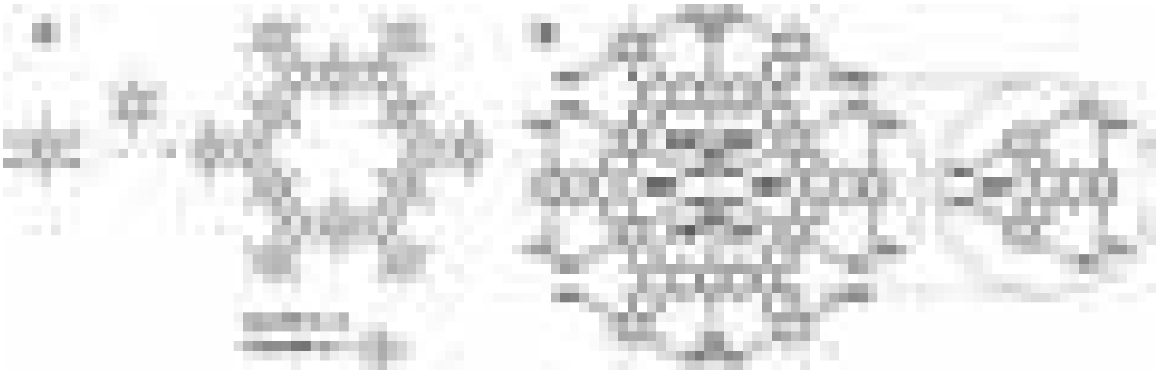

Fig. 13. (A) Solvothermal synthesis and structures of Aza-CMP and TIPS-CMP. (B) Chemical structure (with twist angles) of TIPS-CMP. [104], Copyright 2017. Reproduced with permission from the John Wiley & Sons Inc.

selective absorption of CO_2 at room temperature and pressure [137]. Recently, Feng's group systematically reported the formation of thiazolo[5,4-*d*]thiazole (TzTz) linkages, and three novel TzTz-linked POPs, namely TzTz-POP-3, TzTz-POP-4, and TzTz-POP-5 were synthesized by triphenylbenzene, tetraphenylpyrene, and tetra(hydroxyphenyl)methane cores, respectively [103], which exhibited excellent thermochemical stability and chemoselectivity.

2.2.4. Phenazine ring fusion reaction

Aza-CMP construction by built-in aza units and micropores, which has fused skeletons, compact aza units, and micropores to facilitate the formation of charge separation layers [138]. Therefore, it has great potential as a high-energy storage device. Compared to Aza-CMP, TIPS-CMP synthesis by the cyclocondensation of 1,2,3,4,5,6-hexaketocyclohexane and 3,6-di(triisopropylsilyl)ethynyl-1,2,4,5-benzenetetraamine after decontamination at reflux in a 1:4 mixture of dioxane and acetic acid (Fig. 13A) [104], has increased dispersion attributed to the highly distorted aromatic structure (Fig. 13B), which is conducive to the exfoliation of individual layers and the reduction of the interaction between dispersed layers in organic media. Uniform, coherent, optically transparent, and semiconducting films can be obtained with this enhanced dispersant. This shows that twist is a very powerful strategy for improving the dispersibility and processing properties of conjugated microporous polymers.

2.2.5. Cyclotrimerization reaction

Cyanocyclization is a method to prepare porous polymers under ionic heat after mixing $ZnCl_2$ with monomers, in which $ZnCl_2$ acts as a solvent, catalyst, and template pore-making agent. The CMPs obtained by this method is also called covalent triazine polymers (CTFs) [139]. For example, in 2008, Thomas' group for the first time obtained CTFs formed from nitrile molecules 1,4-dicyanobenzene in a $ZnCl_2$ melt at 400 °C (Fig. 14) [55]. CTFs with different pore structures and characteristics can be prepared by regulating temperature [140], monomer types [141], and reaction kinetics parameters [142]. Later, in 2010, Liu's group realized the precise regulation of the pore diameter and specific surface area of CMP by using the cyclotrimerization reaction of alkynyl monomers of different lengths [143].

2.3. Comparison of synthesis and processing

In general, CMPs with different characteristics can be obtained in different coupling reactions catalyzed by noble metals. For example, the CMP obtained through the Sonogashira-Hagihara coupling reaction contains an alkynyl group, which can be post-processed and functionalized. C–N bonds can be introduced into CMPs by using the Buchwald-Hartwig coupling reaction, which give them a certain degree of redox properties, making them better applicable to the field of clean energy. And Yamamoto Reaction is the first choice for the synthesis of high-surface-area CMPs.

These noble metal catalyzed synthesis reactions are the most commonly used and tend to mature, but the noble metal cata-

Fig. 14. Cyclotrimerization reaction of cyano monomer to the synthesis of CTFs. [55], Copyright 2008. Reproduced with permission from the John Wiley & Sons Inc.

lysts used in the synthesis process need to be removed through the cumbersome extraction process (such as Soxhlet extraction). Non-noble metal-catalytic processes are an option to avoid the use of metal catalysts that are difficult to eliminate. Meanwhile, these synthesis strategies have many other advantages, such as, the advantages of oxidative polymerization, such as the use of cheap catalysts, ambient temperature reaction conditions, high yield, and single monomer [144-148], to simplify production and reduce the cost, which required for large-scale preparation of porous materials. And Schiff-base reaction has the advantage of producing nitrogenous CMPs, which exhibit good electrocatalytic activity, and can be used for CO_2 adsorption [149-151].

Since the diversity of synthetic monomers and microporous structure of CMPs are two main characteristics of CMPs and generally affect the properties of materials. Therefore, it is important to investigate the differences in surface area and pore structure of different CMPs in different synthetic reactions. Surface area information of CMPs is usually calculated using physical adsorption isotherms [152-154]. The most common method is to use Brunauer-Emmett-Teller (BET) theory to get BET surface area and information about pore size distribution from the BET plot. However, before gas uptake measurements, it is necessary to investigate the chemical properties and structural changes of CMPs through thermogravimetric analysis (TGA) experiments [155-157].

In addition, when using CMP as a precursor material for porous carbon materials, the effect of the structure and composition of CMPs on these derived carbons should be considered, and the carbon yield of these CMPs should be reasonably assessed. CHN analysis techniques can provide information about the composition of CMP materials, including carbon, hydrogen, and nitrogen content [152], which are usually of concern when preparing derived porous carbon. Meanwhile, in order to further understand how the composition and structure of CMPs affect the performance and structure of these derived carbons, some auxiliary characterization experiments are usually needed, such as scanning electron microscopy image (SEM), transmission electron microscope (TEM), X-ray photoelectron spectroscopy (XPS) measurements, powder X-ray diffraction (XRD) analysis, ^{13}C solid-state nuclear magnetic resonance (NMR) spectroscopy, inductively coupled plasma emission spectrum (ICP-OES), etc.

3. Post-synthetic functionalization of CMPs

In addition to the selection of monomer molecular size, monomer ratio, and reaction conditions to regulate CMPs, post-synthetic modification of the CMPs backbone structure is another effective way to regulate their structure and properties. The functionalization of CMPs can be achieved by introducing different functional groups into the polymer networks. In the past few years, extensive research on the post-functionalization of organic materials have conducted, and often use so-called "click" chemistry [158-162], such as Huisgen reaction (copper-catalyzed 3 + 2 cycloadditions of azides), copper(I)-catalyzed alkyne-azide cycloaddition (CuAAC), thiol–yne click chemistry, and so on. In this section, post-synthetic modification to improve the properties of CMP materials is discussed.

Post-synthetic functionalization can modify the morphology and properties of CMPs by modifying their molecular structure [163,164]. As shown in Fig. 15A, radical thiol–yne chemistry of CMPs with aliphatic alcohols can adjust their functionalization degree and morphology, and then adjust their porosity and optical properties by changing the amount of thiol [165]. Similarly, an amine-functionalized CMP (CMP-1-NH_2) can modify amines into amides with different chiral alkyl chains to control surface functional groups and microporosity, and then reasonably adjust its BET specific surface area, pore-volume, CO_2 adsorption capacity, and isothermal heat capacity (Fig. 15B) [166].

“Clicking post-synthetic modification”, adjusts the fluoride content in the CMP framework by controlling the ratio of azide groups to improve gas capture ability. As shown in Fig. 16, first, a series of zinc-porphyrin CMPs (ZnP-XN_3-CMPs, $X = 5$, 25, and 50%) are synthesized from zinc porphyrin units, and then the azide groups are introduced into the pores of ZnP-XN_3-CMPs to form ZnP-XF-CMPs ($X = 5$, 25, and 50%) [167]. The measurement result represented the CO_2 capacity of ZnP-XF-CMPs, $X = 5$, 25, and 50% at 298 K and 1.0 bar was 34, 52, and 90 mg g^{-1}, respectively, which was 1.31, 1.68, and 1.84 times higher than that of the ZnP-XN_3-CMPs, $X = 5$, 25, and 50%.

Besides, the CMPs have a π-conjugated skeleton that also can be further adjusted by a postoxidation reaction to form a network with an extended π-structure [168]. Firstly, two CMPs with similar structure and high surface area, namely BO-CMP-1 and BO-CMP-2, are prepared using the Suzuki reaction. Afterward, the postoxidation process converts the biolefin benzoquinone blocks in the skeleton into the tetrabenzocoronene segments to form oBO-CMP-1 and oBO-CMP-2 with an extended π-structure. The method uses monomer with extended π-structures to prevent low polymerization problems caused by direct synthesis and can adjust the structure, porosity, and even the gas adsorption behavior of the main polymers, which provides a direct and simple post-modulation process for CMPs.

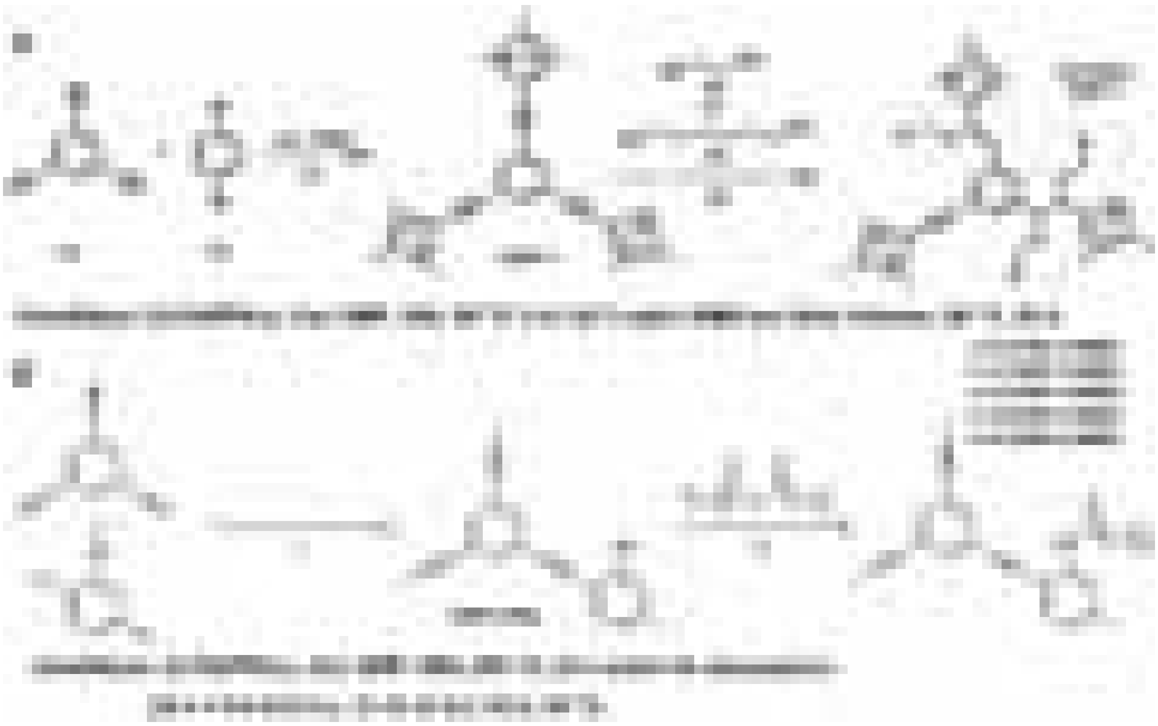

Fig. 15. (A) Post-modification of the structure of the CMPs by using –SH monomers. [165], Copyright 2011. Reproduced with permission from the American Chemical Society. (B) Post-modification of the CMPs with amidation reaction. [166] Copyright 2013. Reproduced with permission from Elsevier Science Ltd.

4. Morphological control of CMPs

Traditionally synthesized CMPs are amorphous powder materials, which are insoluble and infusible, and restrict further applications. With the in-depth study of CMP materials, other forms of CMP materials are synthesized one after another, such as nanospherical, nanotubular, thin-film, and bulk CMPs according to the actual application conditions under different synthesis methods. For example, CMP networks with nanospherical, nanotubular, and thin-film structures constructed by template synthesis can be used in high-performance energy-related applications. And high-quality CMP films are excellent materials in the field of clean energy, which are outstanding hole conductors with controllable thickness to be utilized directly in device fabrication.

4.1. CMP nanospheres and nanotubes

Nanospheres and nanotubes have promising applications in gas storage separation, energy storage, and solar energy conversion [169-171]. However, the control method of CMP nanospheres and nanotubes is still a great challenge owing to the poor dispersibility and solution processing of porous material. Both the structure of the monomer and reaction solvent may affect the morphology of CMPs, and the formation mechanism of the micromorphology of CMPs and the mechanism of the reaction conditions affecting their morphology still need to be further studied. As an example of the shape effect in materials science, hollow spheres exhibit better electrochemical and photocatalytic properties than non-hollow spheres, so many examples of hollow structures have been reported for the synthesis of porous materials [172,173]. After noble metal-catalyzed synthesis, template replication strategy [174-176] and layer-by-layer method [87,177] are effective methods for controllable synthesis of CMP networks with hollow structures. Among them, the hard template method based on silicon dioxide [178-180] has been used to construct a microporous polymer network with a quasi-zero-dimension structure.

Silicon dioxide can be easily removed by chemical etching in reaction with HF or NaOH. Therefore, hollow polymer networks are often obtained by chemical etching of silica templates. For instance, Kang et al. used the silicon spheres template method to prepare the shape-controlled hollow microporous organic networks (HMONs) [179]. Fig. 17 illustrated the synthetic route for the H-MONs using a silica template. Silica spheres were obtained by the Stöber method [181] and added to the polymerization process. The resulting mixture was then treated with HF solution to remove the silica template to obtain H-MONs. Meanwhile, the thickness of the shell of H-MONs can be well controlled by changing the synthesis conditions.

Besides, controlled synthesis of zinc porphyrin (TP-Zn)-based CMP (Zn-CMP) microspheres uniformly dispersed in solution is obtained by Sonogashira reaction of 5,10,15,20-tetrakis(4-ethynylphenyl)porphyrin-Zn(II) and brominated monomers directed by bidentate bipyridine (BP)-type ligands [182]. These spheres can be adjusted between 320 and 740 nm in diameter, and the coordination between BP and TP-Zn proved to be the key to forming the spheres. This strategy facilitates the handling and separation of polymer microspheres and is suitable for the most halogenated monomers. Given the universality of the chemical coordination method and the diversity of the monomer structure of CMPs, it is of great significance in the large-scale preparation of functional CMP spheres. However, it is important to note that these schemes significantly reduce the specific surface area while forming the desired morphology of the porous polymer [183,184], which may affect the application performance of CMPs.

The layer-by-layer template synthesis method maintains a layered CMPs with manageable chemical composition and regulating nanostructure. In 2016, Feng's group used the functionalized carbon nanotubes as templates to layer-by-layer prepare CMPs with controllable nanotube morphology and reasonable layered structure for the first time [177]. As shown in Fig. 18A, first, the preparation of *p*-bromobenzene functionalized carbon nanotubes (SWNT-Br) by SWNTs functionalized using the 4-

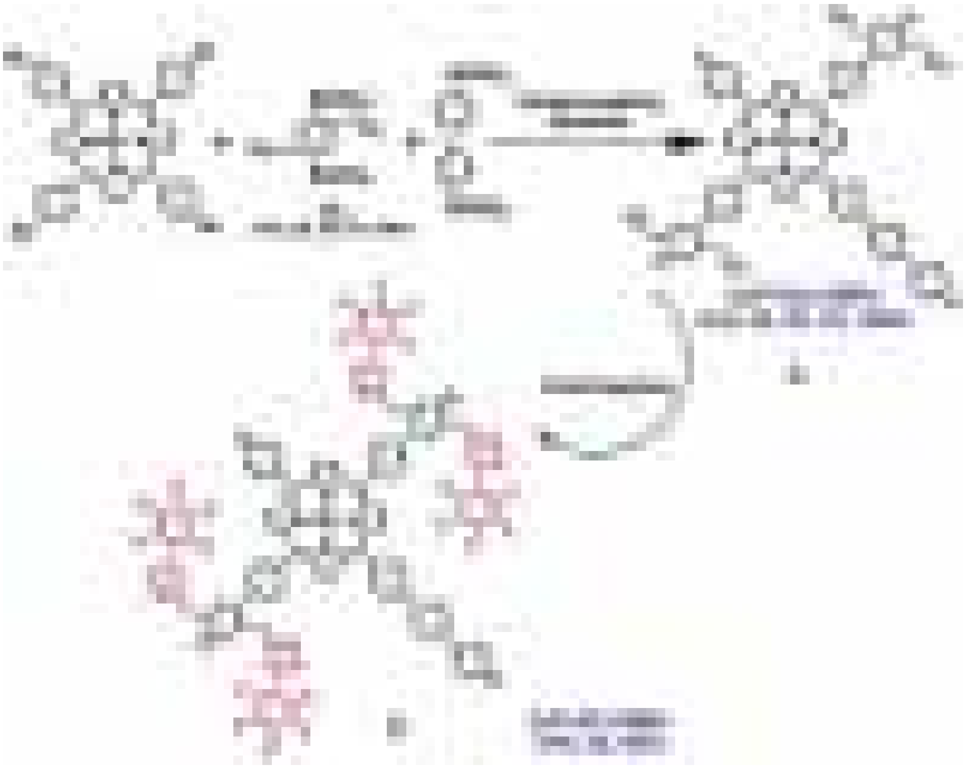

Fig. 16. Schematic representation of (A) ZnP-XN$_3$-CMPs ($X = 5$, 25, 50, 75 and 100%) and (B) ZnP-XF-CMPs ($X = 5$, 25 and 50%). [167], Copyright 2017. Reproduced with permission from The Royal Society of Chemistry.

Fig. 17. Synthetic route for H-MONs using a silica template. [179], Copyright 2013. Reproduced with permission from the American Chemical Society.

bromobenzodiazepine tetrafluoroborate. Later, CMP-PT was produced by Sonogashira reaction of SWNT-Br, M2, and M3. Finally, three-layered CMP PTbBbT was synthesized layer-by-layer using SWNT-Br or two-layered CMP-PTbB as template and M1 and M2 or M2 and M3 as monomers at the same conditions. The scanning electron microscopy (SEM) and transmission electron microscopy (TEM) confirm the nanotube morphology of the CMPs (Fig. 18B). The as-prepared CMP nanotubes own high specific surface areas (623 m^2 g^{-1}) and electronic interactions with electron acceptors (n-type) SWNTS, which has a high catalytic activity to ORR. Meanwhile, the prepared CMP nanotubes are also good precursors for the preparation of heteroatom-doped porous carbon nanotubes by pyrolysis (Fig. 18A). This novel synthesis route provides a new idea for the preparation of porous materials with excellent performance for energy storage, energy conversion, optoelectronic devices, and other clean energy fields. Meanwhile, it is worth noting that the drawbacks of these layer-by-layer templating methods are tedious operation processes and large energy consumption [113]. Therefore, there is still a great need to develop convenient, simple, easy to handle, and low energy consumption methods for producing CMP materials with controlled morphology.

4.2. CMP films

CMP films, an excellent hole conductor with controllable thickness, have many remarkable physical properties, covering high porosity, extended π-conjugated, facilitating exciton delocalization, and high electron transfer rate. The high-quality CMP films are excellent materials in the field of clean energy and can be directly used in the fabrication of devices [178,185]. Spreading the π-conjugated structure of CMPs to film structure can not only significantly enhance their charge transport, but also bring other good properties, such as excellent mechanical properties, flexibility, isotropy, and so on [186,187]. Common methods for the synthesis of CMP thin films are shown in Fig. 19:(A) solution spray-coating [84], (B) layer-by-layer self-assembly [188], (C) electrochemical deposition [189], (D) interfacial polymerization [190], and (E) surface-initiated polymerization [191].

Interfacial polymerization usually uses two incompatible solvents to dissolve monomers and/or initiators, catalysts, etc. [192] and has been developed for the synthesis of self-supporting and thick-controlled CMP nanometer-thin films, also known as a soft template synthesis method. In 2017, Chen et al. used interfacial polymerization based on the new polymerization strategy of Sonogashira-Hagihara reaction and oil-water interfacial Schiff-base reaction to prepare CMP nanofilms with independent and control-

Fig. 18. (A) Random and layer-by-layer controlled synthesis of 1D CMPs. (B) Morphology characterization of the as-prepared 1D CMPs. [177], Copyright 2016. Reproduced with permission from the John Wiley & Sons Inc.

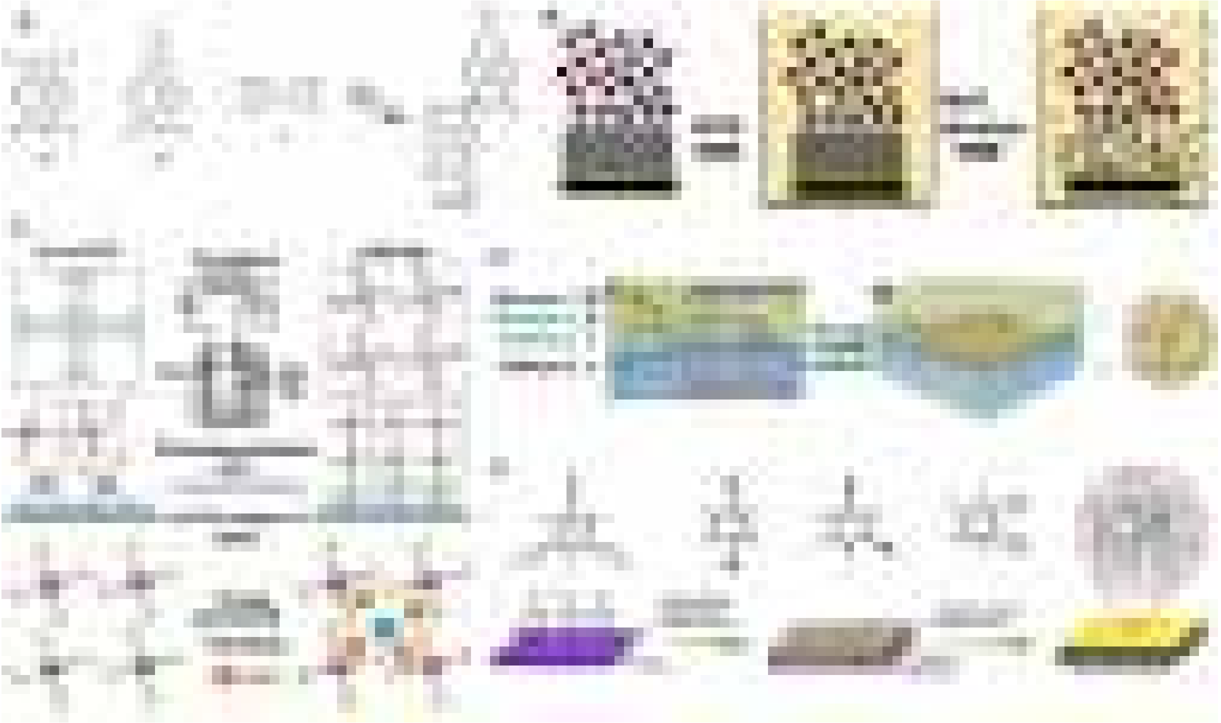

Fig. 19. (A) Solution spray-coating. [84], Copyright 2012. Reproduced with permission from the John Wiley & Sons Inc. (B) Layer-by-layer self-assemble. [188], Copyright 2014. Reproduced with permission from the American Chemical Society. (C) Electrochemical deposition. [189], Copyright 2015. Reproduced with permission from the John Wiley & Sons Inc. (D) Interfacial polymerization. [190], Copyright 2017. Reproduced with permission from The Royal Society of Chemistry. And (E) Surface-initiated polymerization. [191], Copyright 2018, Reproduced with permission from the Springer Nature. for the preparation of the CMP films.

lable thickness [190]. The thickness of CMP nanofilms can be controlled in 30–200 nm by changing the concentration of monomer, and independent macroscopic nanofilms can be easily transferred to various substrates, both are of great practical value in practical application.

Electrochemical deposition, an electrochemical route for the preparation of electroactive polymer films by solution polymerization and in situ deposition in one pot [71,193,194]. Compared with the usual spin coating, it only needs a slight amount of precursor solution to synthesize thin films that meet the thickness requirements [195-199], so it can effectively reduce the material consumption and thus reduce the cost. Electrochemical deposition films have the features of high crosslinking density, controllable structure, and good stability, which are applied in supercapacitors [189], organic light-emitting diodes (OLED) [195,197], induced emission devices [200], and so on [201].

In 2015, Jiang's group reported a strategy of preparing thiophene-based CMP films by electropolymerization at the solution electrode interface and revealed the conducting properties of CMP materials for the first time [71]. As shown in Fig. 20, the unique reaction site (Fig. 20A, blue arrows) of each thiophene subunit is electropolymerized via the C–C bond to form a thin film (Fig. 20B). Fig. 20C reveal the optimal single hole structure obtained by calculation, this multi-arm arrangement facilitates the formation of a porous π-skeleton. This strategy could be widely extended to the synthesis of other porous polythiophene films,

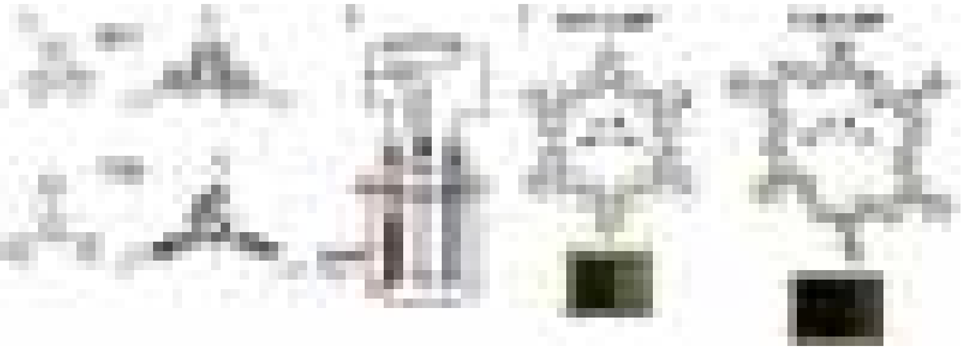

Fig. 20. (A) Structure of thiophene-based monomers BTT and TTB. The blue arrows indicate the carbon positions for the C–C bond formation in the polymerization reaction. (B) Setup of the three-electrode electrochemical cell. (C) The pore structures of the BTT-CMP and TTB-CMP films (inset: photos of the films). [71], Copyright 2015. Reproduced with permission from the John Wiley & Sons Inc.

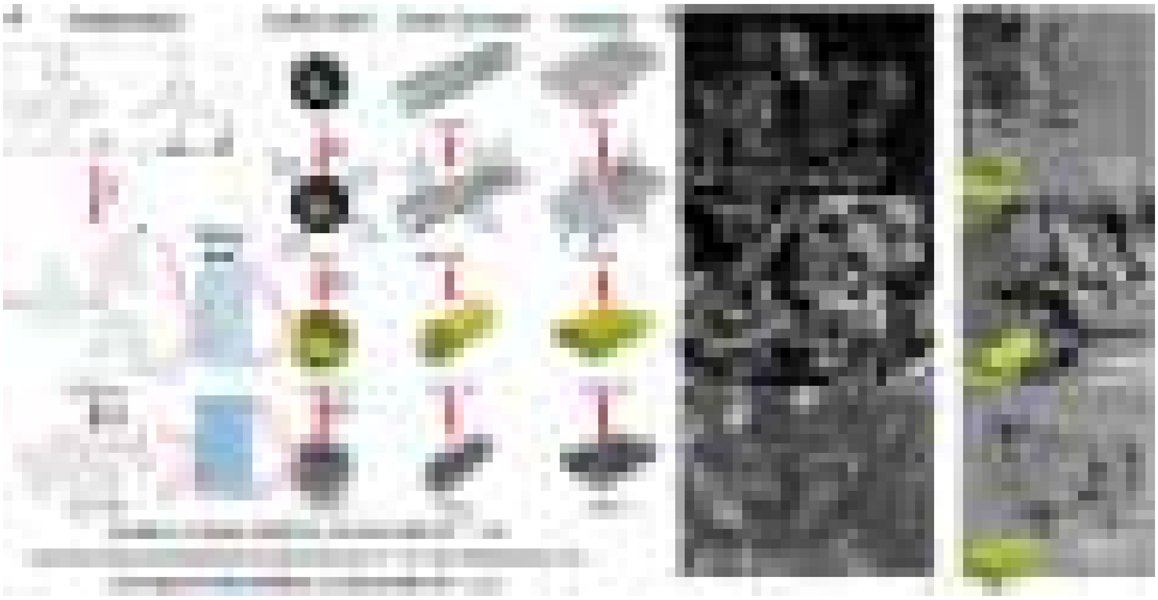

Fig. 21. (A) Dimensionally controlled synthesis of BODIPY-based CMPs. (B) SEM (left) and TEM (right) images of 0D, 1D, and 2D CMP. [90], Copyright 2015. Reproduced with permission from the John Wiley & Sons Inc.

which are expected to be used in high-performance photovoltaic devices and could stimulate further structural and performance exploration.

Besides, the template method can be used to prepare CMP films. Fig. 21A shows the route for the preparation of zero-dimension (0D), 1D, and 2D CMP materials that using carbon nanosphere (CSs), SWNTs, and reduced graphene oxide (rGO) as the templates, respectively [90]. The SEM and TEM of the as-prepared CMPs indicate that most monomers have polymerized on the surface of the template (Fig. 21B). Remarkably, dimensionality has an important impact on CMPs in terms of photoluminescence [90]. The inverse decay rate (τ_{eff}) reduction of nanocarbon directed CMPs up to 38–46% be superior to amorphous CMPs. Meanwhile, the porous carbons prepared by pyrolyzed of the corresponding dimension of CMPs showed more effective catalytic performance for the ORR compared to advanced noble-metal catalysts, and the relationship between electrochemical catalytic performance and dimension is 2D > 1D > 0D [90].

Lindemann et al. realized the surface modification of CMP thin films and nanofilms based on orthogonal click chemistry [202]. The reaction scheme of surface modification is shown in Fig. 22, first, the Cu(I)-catalyzed alkyne-azide cycloaddition (CuAAC) reaction is used for the preparation of the CMP nanofilms by a layer-by-layer method, then, the thiol yne reaction is used to modify the alkyne moieties of the surface of the last layer of the CMP films to realize the surface modification. This post-synthesis functionalization for the outer surface of CMP nanofilms plays a positive role in increasing the variability of them and facilitates the application of CMP materials in catalysis, sensing, or other optics/electronics devices.

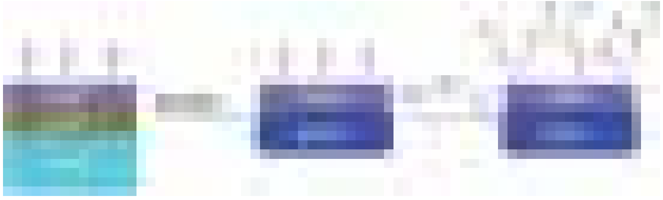

Fig. 22. Surface modification of CMP-nanomembranes using photoinduced thiol–yne click chemistry. [202], Copyright 2016. Reproduced with permission from The Royal Society of Chemistry.

Besides, the exfoliation is also a good strategy for CMP films [203]. However, due to the intense π-π overlapping interactions between the single-layers, the exfoliation usually requires additional aid to assist the exfoliating [204-207], and in most cases the exfoliated yield is low. Meanwhile, the auxiliary methods are not universal and may destroy the extended π-conjugated structure of

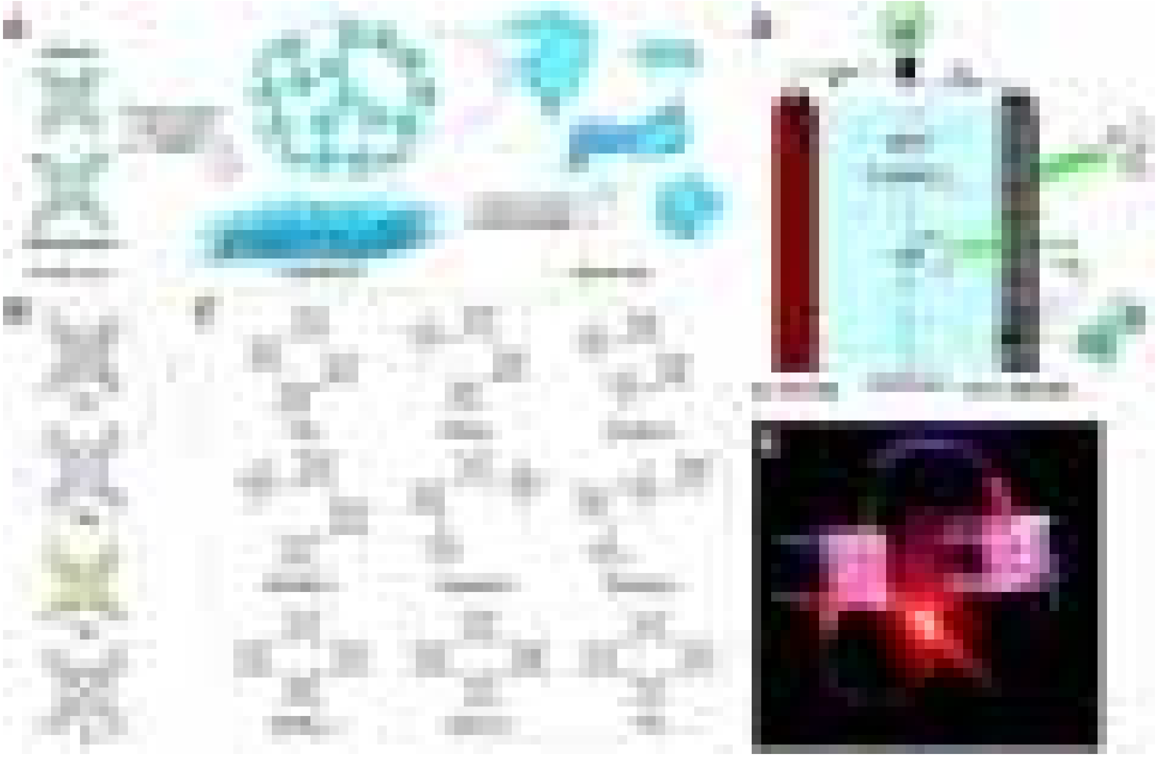

Fig. 23. (A) Synthesis of the amorphous ethynyl-linked phthalocyanine conjugated polymer (MPc-CP) films. (B) The four kinds of isomers (with D_{4h}, D_{2h}, C_{2v} and C_s symmetry) for tetra-β-substituted phthalocyanines. (C) Nine quadrilateral structure models fabricated from four phthalocyanine molecules with D_{4h} or D_{2h} symmetry. (D) Schematic of the Zn–air battery. (E) Photographs of a LED light (≈ 2 V) powered by two zinc–air batteries with a mixture of the films and RuO as the cathode in series. [208], Copyright 2019. Reproduced with permission from The Royal Society of Chemistry.

CMPs [138]. Therefore, the development of an efficient exfoliation method for the preparation of CMP films needs further exploration. Recently, Wang et al. reported a exfoliation for the synthesis of a series of ultra-thin CMP films, which has been proved to have good oxygen reduction reactivity and can be used in battery devices [208]. Fig. 23A describes the stripping method for preparing ultra-thin CMP films, and Fig. 23B is four isomers of phthalocyanine monomer. Taking D_{4h} and D_{2h} as examples, nine combined structures can be randomly formed (Fig. 23C). The introduction of intrinsic defects and disorder in a single layer reduces interlaminar overlap of the amorphous ethynyl-linked phthalocyanine conjugated polymer (MPc-CP) films, which in turn weakens the interlaminar interactions and ultimately yields an exfoliated yield of more than 50%. These well-dispersed thin film catalysts have more exposed catalytic active sites and more convenient material transport. The excellent ORR activity of these CMP films (open circuit voltage: 1.34 V; peak power density: ca. 180 mW cm^{-2}) is also confirmed for use in Zn-air battery devices (Fig. 23D) and two Zn-air batteries in series can deliver an enough open circuit voltage for the LED lamp (Fig. 23E).

5. Computer simulations of CMPs in clean energy applications

Computer simulations, including quantum calculations (ab initio, density functional theory, etc.), grand canonical Monte-Carlo (GCMC) simulations, and molecular dynamics (MD) simulations, are used to theoretically study the mechanism of CMPs transition, and to explore the structure-activity relationship between molecular structure and the final polymer. This is the basis for the further preparation of CMPs with precisely subdivided structures and is key for the synthesis and application of CMPs. With the further development of computer technology and the maturity of calculation methods, computer simulations and traditional experimental methods complement each other, which will bring a bright future to the development of porous polymer materials [209].

5.1. Quantum calculations guide functional design in CMPs

Density functional theory (DFT), one of the basic theory of quantum calculations, is a quantum mechanical method to study the electronic structure of multi-electron systems, which is often used to guide the functional design of CMP materials in recent years [210-214]. In 2014, Srinivasu and Ghosh reported the electronic structure and adsorption properties of the 2D CMPs, 1,3,5-triethynyl (CMP-1), and benzene, 1,3,5-tributadiyne (HCMP-1), based on the DFT [215]. Results found that lithium atoms exist on both sides of the C6 ring of the two CMPs. Each lithium-ion site carries almost a unit of positive charge, which can bind to H_2 molecules through ion-induced dipole interactions, thereby increasing the H_2 adsorption performance of CMPs. Furthermore, in 2017, Fan et al. reported the electron structure and adsorption properties of single-walled CMP nanotubes containing substituted benzene and ethylene units by the density-functional tight-binding method augmented with a van der Waals dispersion term [216]. The calculation results show that increasing the junction agent or adding substituents (AOH or ANH_2 substituents) in the node could reduce the bandgap of the nanotubes and bring about a larger expanded π-conjugation system, to improve the bonding strength of the adsorbent and adsorbents, which is conducive to improving the adsorption capacity in terms of energy.

Metal doping, the types of doped metals, and the doping amount could affect the catalytic performance of CMP catalysts. Therefore, Xu's group were used spin-polarized DFT method to design a novel 2D CMP of porphyrin units and thiophene chain and introduced a series of metal atoms (Fe, Mg, Mn, and Cu) into the center of the porphyrin ring to enhance their ability to reduce

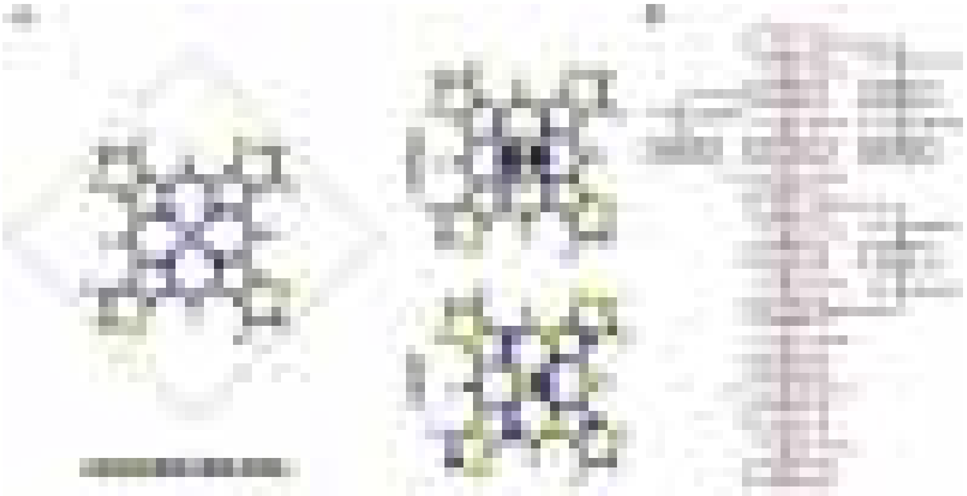

Fig. 24. (A) The optimized structure of the Fe-CMP unit cell; The HOMO and LUMO of the Fe-CMP with an isosurface of 0.03 $e\ \AA^{-3}$. (B) The overall pathway of CO_2 reduction and the activation barrier of each basic step. [217], Copyright 2018. Reproduced with permission from the Owner Societies.

CO_2 [217]. Calculations show that the CMPs are stable under environmental conditions, and the transition state (TS) search calculation shows that the Fe-modified CMP (Fe-CMP) has the highest catalytic activity for the reduction of CO_2. Fig. 24A shows the 2D geometric structure of Fe-CMP after optimization. The calculation of energy band structure and frontier orbital distribution further proved its semi-metallic properties and high electron occupancy, both of which are key factors affecting photocatalytic performance. Meanwhile, the possible mechanism of CO_2 photocatalytic reduction is calculated. As shown in Fig. 24B, CO_2 is eventually reduced to methane by the COOH* pathway and several thermodynamic steps.

Additionally, the Amsterdam density functional (ADF) program can guide conductive CMP materials. Xu has designed three different open-shell systems that contain thiophene building blocks, with a lower highest occupied molecular orbital (HOMO) and a lower unoccupied molecular orbital gap (LUMO) [218]. He calculated the electronic hopping rate k for the hole/electron transfer from one molecule to another molecule of the monomers and compared their conductivity at different geometry. The k is calculated based on the formula shown in Eqs. (1) [219,220]:

$$k = \frac{2\pi V^2}{h} \times \sqrt{\frac{\pi}{\lambda k_B}} \times exp\left\{-\frac{\lambda}{4k_BT}\right\} \tag{1}$$

In the equation, V is the electronic coupling for the hole/electron transfer, which is calculated by ADF, and h is Plank constant, and k_B is Boltzmann constant, T is the temperature in kelvin. If V is high, the electronic hopping rate k is high, and the conductivity of the materials is high. It is finding that for the same monomer, the electron coupling of the eclipsed configuration is higher, that is, the charge-transfer performance of the eclipsed configuration is better than that of the staggered configuration. On this basis, it is conducive to establish the design principles for constructing conductive CMP materials, such as build a similar open-shell system, adjust the properties of the connecting thiophene groups, switch groups with steric hindrance, and extend the π-conjugated structure.

5.2. Quantum calculations on solar energy conversion in CMPs

In 2013, Zwijnenburg et al. proposed the DFT method of pyrene-based CMP model ring fragment [221]. The calculations and the optical absorption and fluorescence spectroscopy complementary can explain the relationship between the significant redshift in the spectrum and the existence of the network structure of strained rings. The relationship denotes that the addition of strained rings can adjust the absorption and fluorescence spectra of polymers to optimize their potential applications, such as photocatalysis and photoelectricity, which can be used to explain the reason why bandgap engineering controls the photophysical properties of porous organic polymers. Although these model studies provide some significant preliminary insight, additional simulations of bulk systems can enable a more complete understanding of the mechanism of action of these types of CMPs.

Additionally, Wang et al. reported that cellular network-like aza-fused CMP nanosheets (aza-CMPNs) are an energy feasible photocatalytic OER under visible light irradiation [222]. All first-principles calculations are completed with the DFT method applied in the Vienna ab initio simulation package (VASP). The exchange-correlation functional of generalized gradient approximation (GGA) of Perdew, Burke, and Ernzerhof (PBE) and hybrid functional of Heyd, Scuseria, and Ernzerhof (HSE06) is used for geometric optimization and electronic structure calculations, respectively. As well as van der Waals correction of Grime's D3 scheme is incorporated to describe the weak interlayer interaction in aza-CMP multilayers. The optimized structures of the aza-CMPN and multilayer are illustrated in Fig. 25A and the optimized structure of bulk CMP is showed in Fig. 25B. The calculations reveal the possible active sites in the CMPs photocatalytic OER procedure. Fig. 25C summarizes each basic thermodynamic step involved in OER and Fig. 25D shows the optimized structures of *OH (S_1), *O (S_2), and *OOH (S_3) on active site 4. the carbon atom 4 gather holes under illumination to adsorb H_2O molecules and then release one proton to form *OH (S_1), and the S_1 site continue to release a proton to form *O (S_2). Then, H_2O and *O to form *OOH (S_3), and a proton released from *OOH, later, O_2 molecules are isolated from the surface of aza-CMPNs to begin a new cycle.

The first-principle predict the level of CMP nanosheets (CMPNs) theoretical conduction band minimum value (CBM) and valence band maximum value (VBM) (Fig. 26A), and to calculate the density of state (DOS) indicates that CMPNs VBM and CBM is mainly contributed by p orbitals of carbon atoms in benzene rings and 1,3-diyne links, and the delocalization of p-orbitals revealed by the charge of VBM and CBM at Γ k-point distribute over the entire polymer frameworks (Fig. 26B) [92], which demonstrated the energy feasibility of CMPNs photocatalytic OER from water splitting. Both single-site and dual-site procedures of OER in aqueous solution are considered here. The single-site procedure is denoted fol-

Fig. 25. (A) Top and side views of the optimized structures of aza-CMPN with the different number of layers. (B) Top and side view of the optimized structure of bulk aza-CMP. (C) Each basic thermodynamic step involved in OER. (D) Proposed photocatalytic pathway of the OER on the active site "4″". [222], Copyright 2017. Reproduced with permission from The Royal Society of Chemistry.

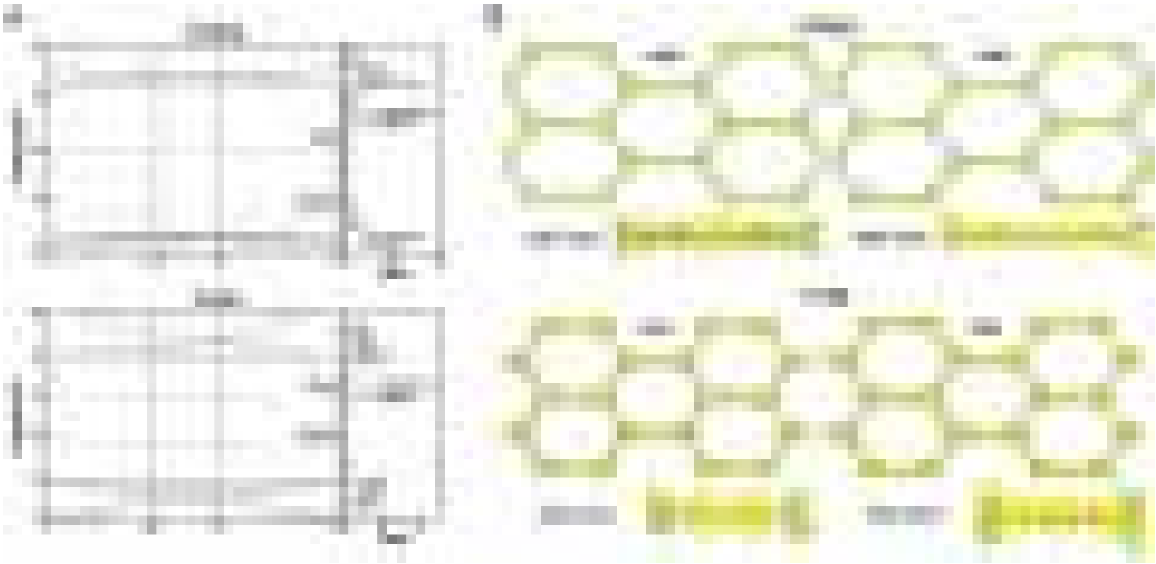

Fig. 26. (A) Calculated band structures for PTEPB and PTEB from Γ (0.0, 0.0, 0.0) to M (0.0, 0.5, 0.0) and K (0.333, 0.667, 0.0) k-point in the first Brillouin zone along with the calculated density of states (DOS). (B) The top and side views of charge distribution of VBM and CBM at Γ(0.0, 0.0, 0.0) k-point of PTEPB and PTEB. [92], Copyright 2017. Reproduced with permission from the John Wiley & Sons Inc.

low (stage 2 to 5):

$$S_0 + H_2O \rightarrow S_1^s + H^+ + e^- \tag{2}$$

$$S_1^s \rightarrow S_2^s + H^+ + e^- \tag{3}$$

$$S_2^s + \mathrm{H_2O} \rightarrow S_3^s + H^+ + e^- \tag{4}$$

$$S_1^s \rightarrow \mathrm{S_0} + \mathrm{O2} + H^+ + e^- \tag{5}$$

In these formulae, S_0 represents the bare surface, S_1^s, S_2^s, and S_3^s represent the intermediate products of *OH, *O, and *OOH at a single active site on the catalyst surface, respectively. In the dual-site procedure, stage (2) and (3) is identical as a single-site procedure ($S_1^s = S_1^d$, $S_2^s = S_2^d$), while the intermediate product of *OOH in the single-site procedure is substituted with an intermediate product of *O*OH at two adjacent active sites, and stage (5) is substituted with step (7) and (8).

$$S_2^d + \mathrm{H_2O} \rightarrow S_3^d + H^+ + e^- \tag{6}$$

$$S_3^d \rightarrow S_4^d + H^+ + e^- \tag{7}$$

$$S_4^d \rightarrow \ S_0 + \ O_2 \tag{8}$$

In these formulae, S_3^d and S_4^d represent the intermediate products of *O*OH and *O*O at adjacent active sites, respectively.

5.3. GCMC and MD simulations for prediction of properties of CMPs

GCMC and MD simulations, two common computer simulation methods, often used for the synthesis, design modification, and predict the application effects of CMP materials, and to gain additional insights into the relationship between structure and properties. They greatly reduce the data and analysis errors caused by

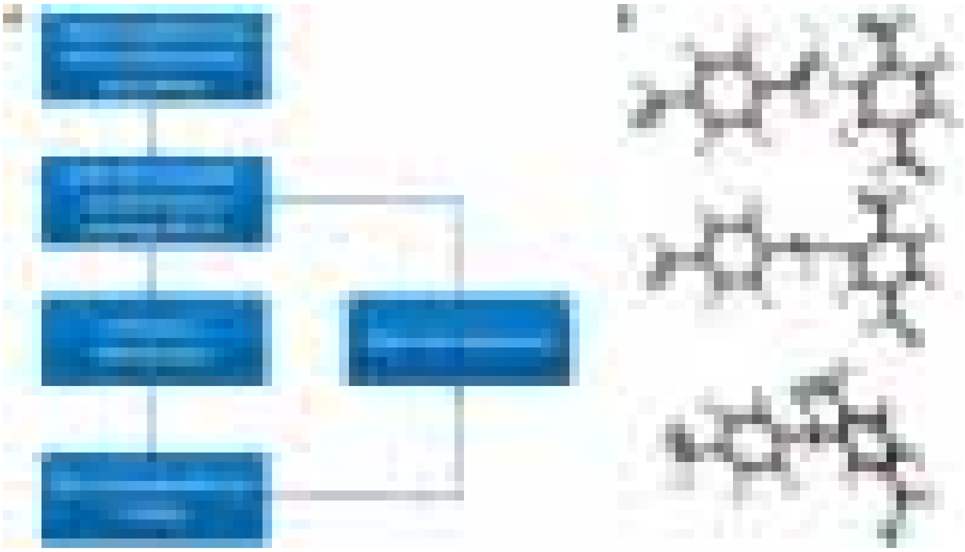

Fig. 27. (A) The theoretical technique for the formation of amorphous porous organic materials. [223], Copyright 2016. Reproduced with permission from the American Chemical Society. The route was adapted from Trewin et al. [224-226]. (B) Cross-linking exercise of dichloroxylene starting from (top) recognition of closest reactive pair of atoms (here a Cl atom and an H atom) followed by (middle) development of a bond linking the cross-linking sites corresponding to the closest pair of reactive atoms whereupon the reactive pair of atoms is removed and eventually ending with (below) equilibration. Carbon, chlorine, and hydrogen atoms are colored gray, green, and white, respectively. [227], Copyright 2011. Reproduced with permission from the American Chemical Society.

humans and help to save experimental costs, assist in improving the accuracy of experimental results, and accelerate research progress. The rational simulation and analysis of newly designed polymer materials include the analysis of reported monomers and links to ensure that the structural characteristics of the model can be maintained with minimal energy. The rationalization of porous polymer materials is conducive to the realization of optimal structural properties of these materials and the stimulation of potential functions. However, to accurately model their structures is a challenge owing to the randomness of amorphous porous polymers. To meet this challenge, many research groups have used MD simulations to study these porous polymer materials. The motion of atoms in a material system determines the overall structure and properties of the material. Therefore, a series of steps repeated many times to implement the analysis of larger systems or small clusters are needed. Fig. 27A [223-226] explains a general simulation pathway, and the formation of bonds and the number of atoms is the key to achievement. Fig. 27B [227] shows the cross-linking procedures achieved during synthesis. Meanwhile, the GCMC simulations with the assistance of prediction of gas adsorption.

Jiang et al. used model clustering to study structural geometry, flexibility, and porosity, and pointed out that these fragments are unlikely to capture entanglement and connectivity of the extended networks, resulting in excessive pore volume [47,95]. Therefore, the relaxed state of the polymerized main chain in the calculation to maintain consistency with the experimental gas absorption at higher pressure is needed to consider. In 2014, Suresh et al. used MD and GCMC simulations to assist in the design of a new type of CMPs with large surface area and gas storage capability, and introduced the structure model of tetraphenylethene-based amorphous CMP (TPE-CMP) and its gas storage performance [228]. This structural model takes all future characteristics into calculations, and MD simulations are carried out on the model oligomer of TPE-CMP in a force field. The binding energy (~30 kJ mol^{-1}) of CO_2 and the polymer is obtained in the calculation based on the force field, and the density of the polymer is calculated to be 0.8 g cm^{-3}. Fig. 28A shows the reasonable structural model for TPE-CMP, the yellow areas shown in Fig. 28B represents the gaps in the polymer and Fig. 28C displays the optimized configuration of CO_2 in TPE-CMP attained through MD simulations. The GCMC simulations shown in Fig. 28D considers the relaxation of the polymer during gas absorption, the blue circle is an estimation from the GCMC simulations that recreates the CO_2 adsorption isotherm of the polymer materials. In contrast, as can be seen from the red box in Fig. 28D, the gas absorption predicted by GCMC simulations is slightly lower than the experimental value under high pressure because the relaxation effect of the polymerized main chain is not considered in the calculation.

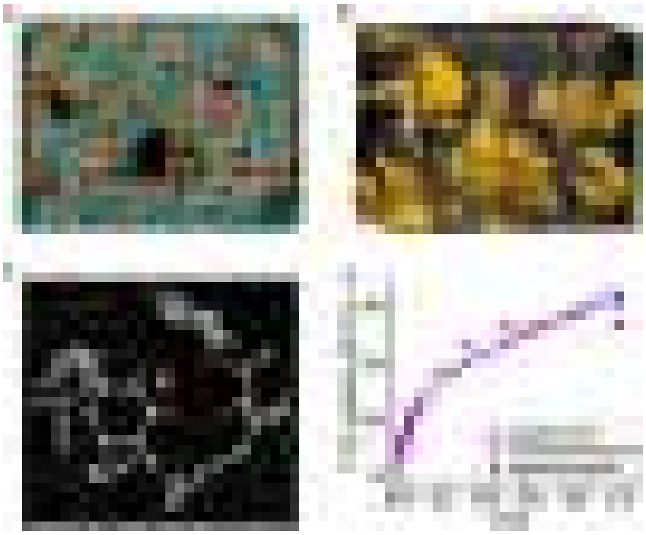

Fig. 28. (A) Computed model structure for TPE-CMP at a density of 0.798 g cm^{-3}. (B) Pore architecture in the structural model. (C) Optimized geometry of CO_2 in TPE-CMP. (D) Comparison of the adsorption isotherms at 195 K between the experiment (violet line) and that calculated from GCMC simulations (red squares). [228], Copyright 2014. Reproduced with permission from the American Chemical Society.

The addition of the A4 monomer is conducive to increasing the porosity of the polymers [69], while the B2 monomer is used to ameliorate the solubility of the polymer networks [84]. Here, Abbott and Colina used MD simulations to study a series of pyrene-based CMPs with different monomer ratios to provide insight into porosity and ring construction in bulk models [229]. The LAMMPS simulation package [230] was used to simulate all energy minimization and molecular dynamics in the polymerization and equilibrium processes. During the polymerization process, the Lennard-Jones cutoff time was adjusted according to the previous work [231] to simulate the solvation state of the system more accurately. The simulations are finding that the surface area of the system increased with the ratio of four functional monomers to two functional monomers because the cross-linking degree of the polymers is effectively improved. These results support the rationalization of the spectral displacement based on the network ring induced strain, which can limit the rotation of the benzene ring to prepare larger conjugated structures to improve the optical properties of CMPs.

6. CMPs as platforms for clean energy

Clean energy refers to the technology system of clean, efficient, and systematic application of environmentally friendly energy. (i) Clean energy is not just a simple classification of energy; (ii) Clean energy focuses on cost and efficiency while ensuring environmentally friendly; (iii) The environmentally friendly of clean energy means that the environmental impact is under control. In recent years, CMPs and their composites/derivatives have been widely used in the fields of energy generation, conversion, and storage owing to their unique expanded π-system, controllable electronic energy levels, and unique morphological properties. Their applications in clean energy include: (i) Storing energy molecules (such as hydrogen molecules) in pore structures; (ii) Store the energy in a polymer pore structure, such as batteries, in the form of chemical bonds; (iii) The energy is stored in the structural recombination and secondary valences of the pore structure, such as the compressed double-layer structure of the supercapacitor; (iv) The semiconductor structure of CMPs generates photoelectron hole pairs under photoexcitation, which are then converted into electrical energy (photovoltaic cells) or chemical energy (artificial photosynthesis).

6.1. CMPs as platforms for hydrogen energy

Hydrogen as an efficient, clean, and sustainable renewable energy source, comes mainly from water splitting, has high calorific value, and carbon-free emissions during combustion [232-234], and has attracted the attention of research institutions and industry over the past decade. On January 17, 2017, a total of 13 leading clean energy-related companies launched a global initiative called the Hydrogen Council at the World Economic Forum in Davos, Switzerland [235]. This initiative expresses the important role of hydrogen energy in promoting energy transformation. Promoting the globalization of hydrogen energy can help achieve the goal of mitigating global warming. Therefore, advanced materials need to be developed for hydrogen production and storage.

CMPs with the adjustable high porosity and controlled structural properties are an excellent candidate in the hydrogen energy field. Here, our discussion includes (i) CMPs for hydrogen storage, (ii) CMP materials applied to photocatalytic hydrogen evolution from water splitting, and (iii) they as catalysts supports or precursors for hydrogen evolution.

6.1.1. CMPs for hydrogen storage

The use of hydrogen requires a safe, compact method of storage, but hydrogen is often stored in cylinders in an energy-intensive manner, posing additional risks. Therefore, it is best to convert the hydrogen into a condensed state, or the most direct method is to use a hydrogen adsorption material. Hydrogen, as an energy storage medium, has attracted the attention of research institutions and industry over the past decade. The weak bonding strength of hydrogen and adsorbent is the key obstacle to fabricate hydrogen storage materials with good hydrogen storage properties under ideal hydrogen storage kinetics. CMP materials are the adsorption materials which has made much progress in recent years [126,236,237], the progress of hydrogen storage capacity of CMPs in recent years is summarized in detail in Table 2 [79,84,143,147,150,238-244]. Most of the reported adsorption values were measured at a temperature of 77 K, which is well below the usual temperature range required for practical applications. Also, some reports give maximum adsorption values, while others report adsorption values at specific pressures (usually 1 bar). Therefore, it is difficult to synthesize all the reported values to make a judgment. Here, we discuss quintessential examples of strategies to improve hydrogen adsorption in recent years.

At a specific pressure and temperature (1.13 bar, 77.3 K), micropores rather than mesopores are the main reason for H_2 adsorption. High surface area HCMP-1 and HCMP-2 were synthesized using homocoupling of 1,3,5-triethynylbenzene or 1,4-diethynylbenzene [79]. Although the apparent BET surface area (827 $m^2\ g^{-1}$) of HCMP-2 is slightly smaller than that of HCMP-1 (842 $m^2\ g^{-1}$), the adsorption capacity of HCMP-2 (131 $cm^3\ g^{-1}$) on H_2 is higher than that of HCMP-1 (107 $cm^3\ g^{-1}$), which can be attributed to the higher micropore surface area and ultramicropore volume observed in HCMP-2. Microwave-assisted rapid synthesis is a new synthesis technology, which has great industrial application potential in organic synthesis and material preparation and is conducive to enhancing the hydrogen adsorption capacity of organic microporous polymers. In 2010, microwave-enhanced ionothermal polymerization is used in the synthesis of porous polymer materials, can be in a few minutes to obtain high surface area (2390 $m^2\ g^{-1}$) triazine-based CMPs (CTFs), they have higher adsorption capacity of hydrogen (1.78 wt.%, 1 bar, and 77 K) [245]. It is worth noting that this method is a simple and efficient method for the preparation of this kind of triazine-based porous material, which provides an opportunity for the large-scale preparation of highly efficient and economical polymer-based hydrogen adsorption materials.

Besides, lithium gives CMPs an extremely high ability to store H_2, which is a big step forward in their application [238,242,246]. In 2016, with the guidance of computer simulations, methyl lithium (MeLi) was designated as a new lithium dopant for the preparation of lithium-doped CMPs [246]. MeLi, as a cluster of positive charges, creates a more intimate bonding condition for H_2 molecules, and naphthalene-containing CMP (N-CMP) was designated as the matrix material to inhibit the gathering effect of lithium. It is more noteworthy that through strong interaction, MeLi can be selectively fixed to the pre-designed active site, which is conducive to obtaining the optimal doping amount. This significantly improves the hydrogen storage capacity of CMPs. MeLi doped N-CMP (MeLi@N-CMP) has enhanced the absorption capacity of H_2 not only at low temperatures but also at close to ambient temperature. Compared with undoped N-CMP, the hydrogen adsorption capacity of MeLi@N-CMP at 77 K and 80 bar (6.5 wt.%) and at 273 K and 80 bar (1.0 wt.%) maintained an increase of 150% and 100%, respectively.

Recently, Yang et al. designed and synthesized triazatruxene (TAT) with three coplanar indole moieties (Fig. 29A and B), and using $FeCl_3$ catalytic oxidative coupling polymerization (Fig. 29C) to further prepare high crosslinking poly(triazatruxene) (PTAT) [242]. The point-to-face metal-coordination interaction (cation–π) between the surface of PTAT aromatic structures and the cation is beneficial to capture more lithium ions, and the captured lithium ions are well dispersed on the PTAT surface to ensure adequate Li^+ content in the PTAT (Fig. 29D and E). The lithium-doped CMP (Li^+–

Table 2
Summary of hydrogen storage in CMPs

CMPs	Molecular structure	S_{BET} (m^2 g^{-1})	V_{total} (cm^3 g^{-1})	P (bar)	T (K)	H_2 (wt.%)	Ref.
Li–CMP	–	795	1.61	1	77	6.1	[238]
POP-1	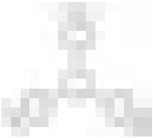	1031	0.641	60	77/87	2.78/2.31	[143]
POP-2	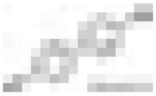	1013	0.712	60	77/87	2.71/2.14	[143]
POP-3	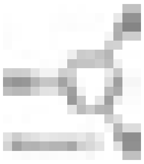	1246	0.729	60	77/87	3.07/2.51	[143]
POP-4	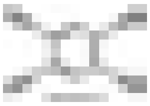	1033	0.730	60	77/87	2.35/1.75	[143]
BLP-1(Cl)		1364	0.746	1	77	1.10	[239]
BLP-1(Br)	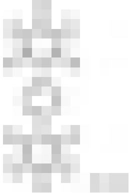	503	0.303	1	77	0.68	[239]
BLP-2(Cl)		1174	0.649	1	77	1.30	[239]
BLP-2(Br)		849	0.571	1	77	0.98	[239]
BLP-10(Cl)		924	0.67	1	77/87	1.3/0.9	[240]
PCTF-1	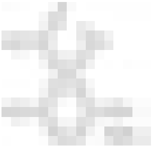	2235	1.56	1	77	1.86	[241]

(continued on next page)

Table 2 (*continued*)

CMPs	Molecular structure	S_{BET} ($m^2\ g^{-1}$)	V_{total} ($cm^3\ g^{-1}$)	P (bar)	T (K)	H_2 (wt.%)	Ref.
PCTF-2	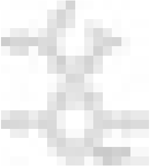	784	0.38	1	77	0.9	[241]
ThPOP-1	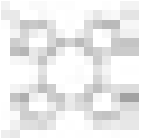	1050	0.69	1	77	2.23	[147]
ThPOP-2	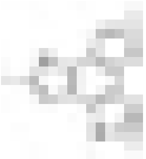	160	0.27	1	77	1.03	[147]
PTAT	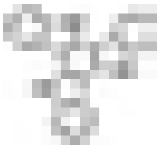	304	–	1	77	1.9	[242]
Li^+–PTAT	–	281	–	1	77	7.3	[242]
CMP-G1	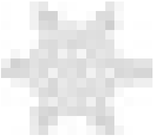	997	1.32	1/20	77	1.27/2.69	[243]
CMP-G2	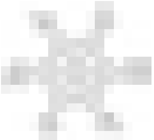	786	0.87	1/20	77	1.01/2.14	[243]
HCMP-1	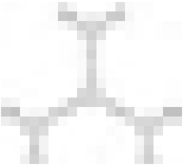	842	1.16	1.13	77.3	107[a]	[79]
HCMP-2	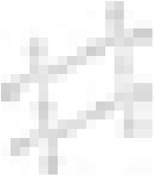	827	1.35	1.13	77.3	131[a]	[79]
p-PPF		269	0.20	45	77	67[b]	[244]
m-PPF	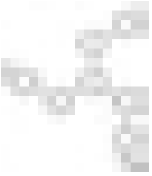	229	0.15	45	77	56[b]	[244]

(*continued on next page*)

Table 2 (*continued*)

CMPs	Molecular structure	S_{BET} (m^2 g^{-1})	V_{total} (cm^3 g^{-1})	P (bar)	T (K)	H_2 (wt.%)	Ref.
SCMP-1	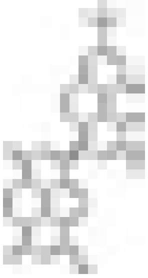	505	1	1	77	3.8[c]	[84]
BILP-10	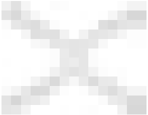	787	–	40	77	27.3[d]	[150]

[a] H_2 uptake (cm^3 g^{-1}).
[b] H_2 uptake (mL g^{-1}).
[c] H_2 uptake (mmol g^{-1}).
[d] H_2 uptake (g L^{-1}).

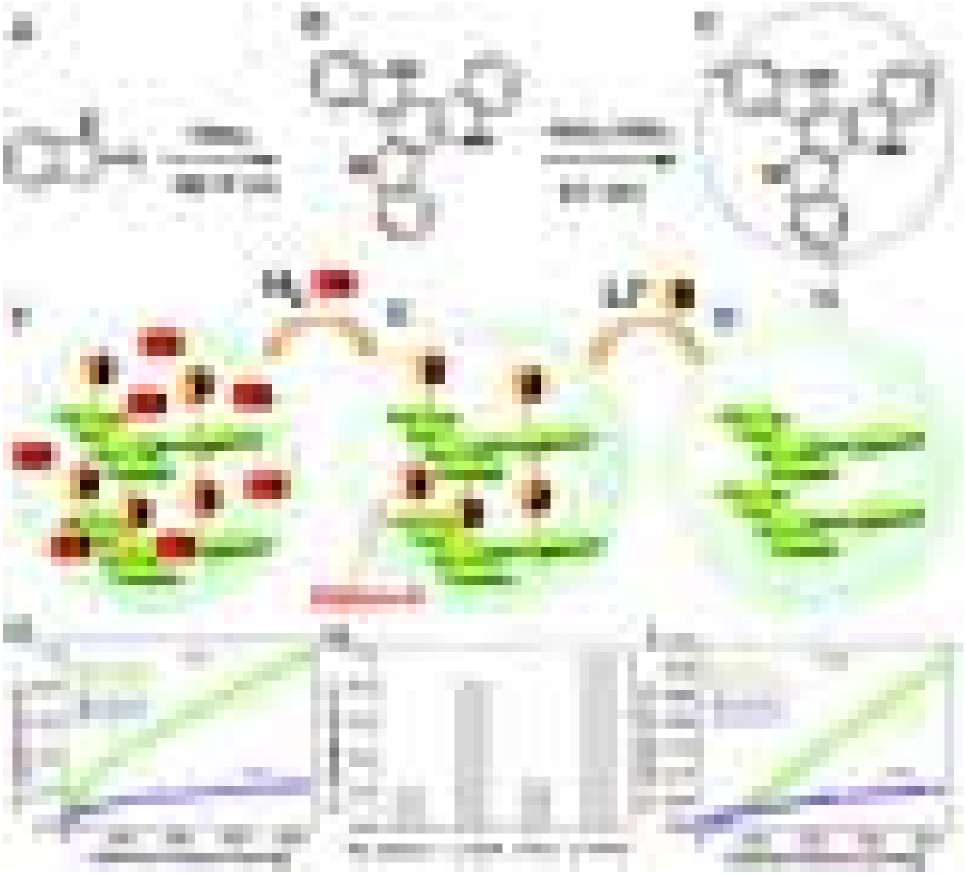

Fig. 29. (A-F) Synthetic route of the conjugated microporous polymer PTAT. (G) Hydrogen adsorption and desorption isotherms of the Li^+–PTAT and PTAT at 77 K; (H) The hydrogen uptake capacities of reported lithium-doped MOF [251], and CMP [242], PTAT and Li^+–PTAT; (I) Hydrogen adsorption and desorption isotherms of the Li^+–PTAT and PTAT at 273 K. [242], Copyright 2019. Reproduced with permission from The Royal Society of Chemistry.

PTAT) can spontaneously adsorb hydrogen molecules by electrostatic charge-quadrupole and charge-induced dipole interactions to obtain excellent hydrogen absorption properties (Fig. 29F). Fig. 29G shows that Li^+–PTAT has a higher hydrogen absorption value of 7.3 wt.% (1 bar, 77 K) than PTAT at 1.9 wt.% (1 bar, 77 K) under the same conditions. The adsorption value is also higher than the previously reported lithium-doped MOF [247] and lithium-doped CMP [242] (Fig. 29H). Also, the high hydrogen absorption value of 0.32 wt.% is maintained for Li^+–PTAT at 273 K at 1 bar (Fig. 29I), which proves its potential application value.

Furthermore, the development of selective hydrogen adsorption has attracted much attention. Membrane separation is a promising way to selectively adsorb hydrogen from mixed gasses. Currently, the gas permeability of commercial films is low, and it is often necessary to prepare large-size films in order to maintain sufficient gas production [44], which obviously increases the cost of commercial applications. To improve the permeability and selectivity of the films, zeolite and MOFs with rigid skeletons and uniform pores were investigated extensively [248-251]. However, presently, commercial films are mainly prepared from polymers with low permeability and high selectivity [252]. Therefore, a more ideal choice is to prepare MOPs with high permeability and good selectivity and machinability. For example, the porous organic cages (POCs) prepared by Cooper's group is a class of MOP with good processability and shows the potential for selective gas separation [252-254]. And polymers of intrinsic microporosity (PIMs) is a kind of MOPs with gas permeability, selectivity and good solubility and machinability [44,255-257]. CMPs have good chemical stability and can maintain functional stability under high pressure and temperature [34,48,77]. However, the extremely rigid framework of CMPs makes it difficult to reprocess. Therefore, the development of machinable, structurally stable CMPs with high gas selectivity and permeability is a major obstacle to be solved.

Recently, Loh et al. succeeded in synthesizing a solution-processable conjugated microporous thermoset (CMT) [258], which has outstanding H_2 permeability and solubility and processability, and maintains stable microporous structure and internal pore connectivity even under high temperature and pressure. Due to the internal pore connectivity of CMT can promote the redistribution of gas molecules, CMT can obtain H_2 permeability higher than the most advanced ultra-pore PIM while possessing similar selective hydrogen adsorption capacity [44,257]. Meanwhile, noteworthily, the solubility and machinability of CMT plus its centrally distributed pore diameter distribution is conducive to the production of large-area film products.

6.1.2. CMPs for photocatalytic hydrogen evolution

Photocatalytic technology has many important features [259-261], such as: (i) It can be operated under mild temperature and pressure; (ii) The mother and intermediate products can be completely mineralized without secondary pollution; (iii) Low operating cost. Hydrogen produced by photocatalytic water splitting has been regarded as a popular technology to solve the energy crisis and environmental pollution [262-266]. At present, most used inorganic photocatalytic materials have complex preparation strategies, limited reserves, and low photocatalytic activity in visible light, which is not conducive to further development [267,268]. In terms of sustainable development, it is necessary to develop a metal-free, flexible design, synthesis of diverse organic polymer photocatalysts with adjustable structure and properties for photocatalytic hydrogen evolution [269-273]. Wang et al. presented the basic theory of photocatalysis and the key factors affecting photocatalysis, and then discussed the development of new photocatalysts for inorganic materials, carbon-based materials and semiconductor composite materials developed in the past ten years [274]. They also investigate and explore highly efficient optical drive materials for converting solar energy into sustainable fuels. Finally, the future development of photocatalysis technology is discussed. CMP materials as photocatalyst have followed advantages [275-279]: (i) Expand π-conjugated structure and open pores are advantageous to the photocarrier migration and separation; (ii) High chemical stability and thermal stability provide excellent photocatalytic stability for CMPs; (iii) Wide range of raw materials including many economical, earth-rich raw materials can be used as synthetic monomers; (iv) Wide spectral absorption range is beneficial to improve the efficiency of light absorption; And (v) they have high flexibility in adjusting bandgaps and surface-active sites.

In 2016, Cooper's group reported the relative importance of junction geometry, comonomer length, and planarization degree to the photocatalytic hydrogen evolution rate of CMPs, demonstrating the potential of CMPs as a photocatalyst for hydrogen evolution [280], but the relevant design rules are not well understood. For example, it is still necessary to investigate the catalytic efficiency of CMP materials with different surface areas, geometric shapes, and bandgaps, as well as to investigate the effects of substituent patterns and conjugate lengths on the photocatalytic performance of CMP materials to establish a more detailed structural-performance relationship. Therefore, Jiang's group synthesized three perylene-containing CMPs (Pr-CMPs) through the Suzuki reaction of hydroquinone as raw material for photocatalytic hydrogen evolution [281]. The results show that the pore properties and band gaps of Pr-CMPs are adjusted by changing the kind and the connection positions of the substituents. By adjusting the benzenes connection site, is a good way to adjust the structure and optical properties of polymers, among them, the hydrogen evolution rate of 1,2,4,5-linked polymer (Pr-CMP-3) under ultraviolet irradiation is the highest (12.1 mol h^{-1}) in the three kinds of polymers, this is because Pr-CMP-3 has high surface area, wide light absorption spectrum, and the extension of the π-conjugate structure. These results indicate that bond geometry is one of the key factors affecting the photocatalytic activity of CMPs.

Subsequently, the effect of the length of the crosslinking agent on the photocatalytic properties of hydrogen production is reported. Jiang et al. reported a series of dibenzothiophene dioxide containing CMP (DBTD-CMP) photocatalysts [66]. Among them, there is a short benzene cross-linked photocatalyst DBTD-CMP1 exhibit the most active hydrogen evolution rate of 2460 μmol h^{-1} g^{-1} without Pt cocatalyst in visible light. This may be because the increase of the length of the crosslinking agent leads to the increase of the polymer skeleton distortion, which reduces the conjugation degree and planeness of the main molecular chain, hinders the photoinduced carrier transport and separation, and thus reduces the photocatalytic activity. Furthermore, it is worth noting that after the loading of 3 wt.% Pt catalyst, the Pt-loaded DBTD-CMP1 displays a remarkable high hydrogen evolution rate (9200 μmol h^{-1} g^{-1}).

Rigid pyrene unit is a common building unit of CMP materials [65,282,283]. Jiang's group designed a series of donor-π-acceptor (D-π-A) CMP photocatalysts using pyrene, benzothiadiazole, and benzene (biphenyl) as the donor, acceptor, and π-crosslinker units, respectively, and compared the effects of the molecular structure and the ratio of donor to the receptor on the photocatalytic properties of CMPs [65]. The donor unit, π-crosslinker unit, and acceptor unit are indispensable in enhancing the photocatalytic performance. Meanwhile, the ratio of donor to acceptor has a big impact on the photocatalytic performance of the CMPs, when the ratio of pyrene to benzothiadiazole is 9:2, the photocatalytic hydrogen evolution rate of the CMP (PyBT-2) is as high as 106 μmol h^{-1} under ultraviolet irradiation. Furthermore, they designed two CMP photocatalysts (PyDOBT-1 and PyDOBT-2) copolymerization of pyrene and dibenzothiophene-S,S-dioxide as building blocks, and investigated the effect of a connection mode of dibenzothiophene-S,S-dioxide on photocatalytic hydrogen evolution [283]. The results showed that the photocatalytic activity of PyDOBT-1 (Fig. 30A) with 3,7-connection mode was higher than that of PyDOBT-2 with 2,8-connection mode. The photocatalytic hydrogen production rate of "naked" PyDOBT-1 was 5697 μmol h^{-1} g^{-1} under visible light irradiation, and the photocatalytic hydrogen production rate of Pt-load PyDOBT-1 reached a maximum of 12,986 μmol h^{-1} g^{-1} (Fig. 30B). The higher photocatalytic activity of PyDOBT-1 may be due to the 3,7-connection mode, which enhances the conjugated chain length and improves the coplanar property of the polymerized main chain to facilitate the transfer of charge along the polymer chain. Their work suggests that rational molecular design is the key to the development of effective CMP photocatalysts.

Fig. 30. (A) molecular structure of PyDOBT-1; (B) Hydrogen generation of the polymers under visible light. [283], Copyright 2018. Reproduced with permission from the American Chemical Society.

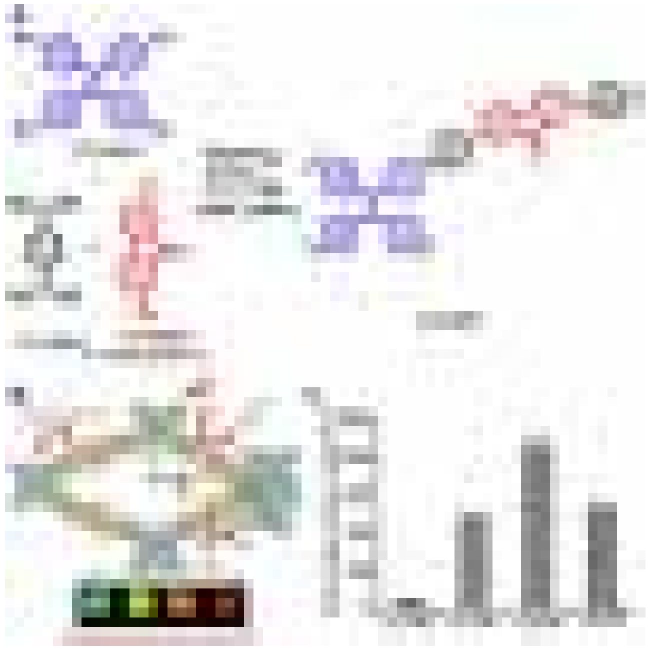

Fig. 31. (A) The preparation route of F_xCMPs. (B) F_xCMPs with adjustable bandgap photocatalytic water splitting for hydrogen production. (C) Hydrogen evolution rate of F_xCMPs. [284], Copyright 2019. Reproduced with permission from the John Wiley & Sons Inc.

Recently, Maji et al. synthesized a series of CMPs ($F_{0.1}CMP$, $F_{0.5}CMP$, and $F_{2.0}CMP$) using tetraphenylethylene (TPE) as the donor and 9-fluorenone (F) as the acceptor (Fig. 31A), and adjusted the optical properties of these CMPs by bandgap engineering to enhanced photocatalytic water splitting for hydrogen production [284]. As shown in Fig. 31B, by increasing the content of F, the emission color of CMP materials changes from green to red, and the bandgap of F_xCMP can be adjusted from 2.8 eV to 2.1 eV, thus enhancing its visible light absorption. Among all the CMPs, $F_{0.5}CMP$ (2.3 eV) displayed the highest hydrogen evolution rate under broad-spectrum irradiation (Fig. 31C). Compared with CMP materials without F, the photocatalytic activity of the D-A CMP containing F is observably enhanced. Interestingly, the CMPs display emissions in the 540–580 nm with the assistance of energy transfer in the TPE segment.

As amorphous polymers, the effect of crystallization on photocatalytic behavior of CMPs needs to be further discussed. In 2018, Cooper et al. targeted investigated the difference of photocatalytic hydrogen production between benzobis(benzothiophene sulfone) moiety-based COF crystals and amorphous similar organic polymers [285]. Although the photocatalytic hydrogen evolution performance of COFs with ordered crystal structure is superior to that of their amorphous organic analogues in this case, this does not indicate that the photocatalytic activity of crystallized COFs is necessarily higher than that of amorphous CMPs. This is because crystallinity is not the only factor affecting photocatalytic activity [286-288], such as, amorphous CMPs also have much lower specific surface area and charge transfer capacity, and some CMPs also have poor hydrophilic performance, which may result in reduced photocatalytic performance of them.

Besides, the stability of photocatalysts should also be considered. CMP materials have been shown to have a more stable structure than the crystallized ordered COFs originally reported [37,47,54,80]. But things are still changing, and researchers studying COFs materials are exploring the use of more stable chemical bonds to build super-stable COFs materials [206,289,290]. But in meanwhile, noteworthily, the amorphous properties of CMPs provide more design possibilities, and more possible multi-component CMP catalysts are constructed by using multi-step tandem reactions, which are difficult to be completed by COF materials.

6.1.3. CMPs as supports or precursors of catalysts for hydrogen evolution

In addition to being used as catalysts directly, CMPs can also be used as (electro-) catalysts carriers to assist in the synthesis of composite catalysts with excellent catalytic properties. This type of composite catalysts usually combines the properties of two or more materials with different properties and can have a synergistic effect in an application. As well as, CMPs can also be used as precursors of catalysts for hydrogen production through pyrolysis.

Alkordi's group used pyridine-based porous polymer materials and graphene composites (PyPOP@G) as carriers and then electrodepositing Pt metal uniformly in the pores for forming the composite material (PyPOP-Pt@G) (Fig. 32A) [291]. The main chain of PyPOP in this system is rich in Lewis-base binding sites and microporous matrix, which can provide support for Pt species and binding sites for G. The properties of the material were evaluated by cyclic voltammetry (CV), linear sweep voltammetry (LSV), and controlled potential electrolysis (scan rate of 100 mV/s for the CVs and 10 mV/s for the LSVs). Fig. 32B indicates that the initial performance of the electrode is improved after the reduction of Pt(IV) in the cycling process. As shown in Fig. 32C, the overlaying CV scan no observe the deterioration of the electro-catalytic properties of the composite, indicating its high durability and stability. And as shown in Fig. 32D, the Tafel inset (~37 mV/decade) of the catalyst indicates that there is a rate-limiting step of Heyrovsky type in PyPOP-Pt@G catalyzed hydrogen evolution reaction, which provides an in-depth understanding of the mechanism of proton electric reduction. The core of Heyrovsky-type step is the hypothesis of the active site of a single metal atom (Eqs. 9 – 11) [291]:

$$H_3O^+ + e^- + M \leftrightarrow M - H + H_2O \quad \text{Volmerstep} \tag{9}$$

$$M - H + H_3O^+ + e^- \leftrightarrow H_2 + H_2O + M \quad \text{Heyrovskystep} \tag{10}$$

$$2M - H \leftrightarrow H_2 + 2M \quad \text{Tafelstep} \tag{11}$$

The Heyrovsky step mentioned above may be caused by the delay of the diffusion of hydrated protons into the electroactive catalytic site in the microporous matrix.

Meanwhile, CMPs are an effective precursor of functional heteroatomic doping of porous carbon [292-295]. Cui et al. reported that a nitrogen-rich porous carbon material derived from a novel

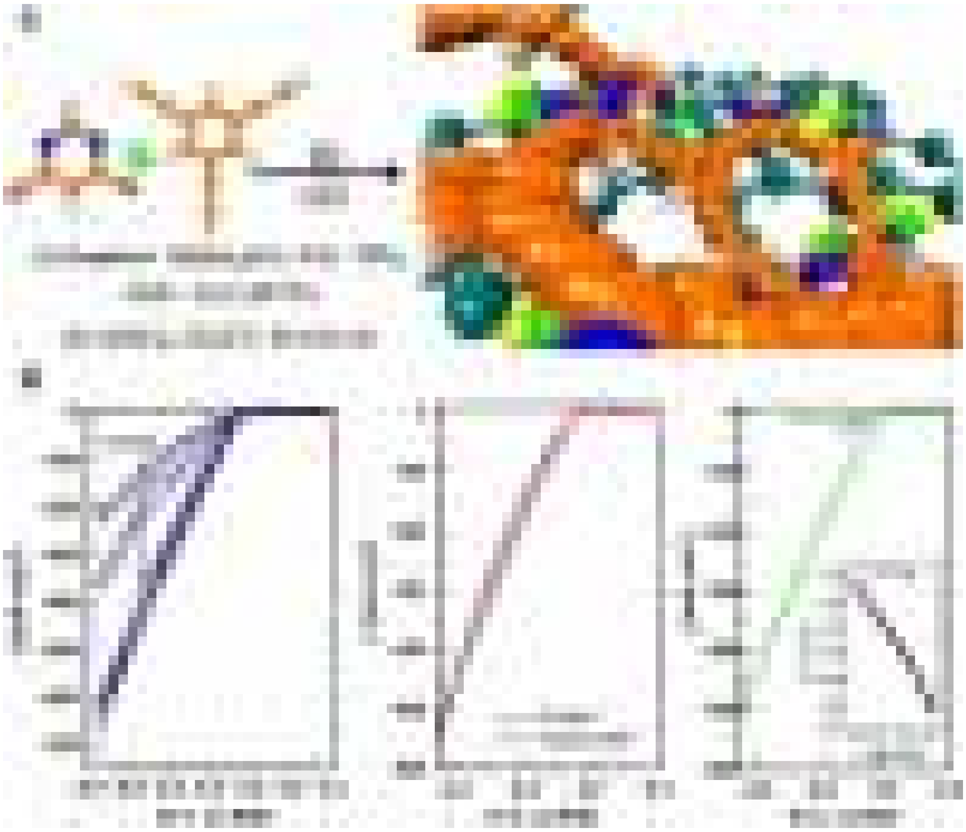

Fig. 32. (A) Synthesis route of the PyPOP-Pt@G, C (Orange, Teal in Graphene Sheet), N (blue), Br (Break Red), Cl (Yellow), Pt (Green), H (White). (B) The first few cyclic voltammetry (CV) scans for a fresh electrode of the PyPOP-Pt@G on a glassy carbon electrode (GCE) (left); The CVs for GCE casted with the PyPOP-Pt@G with scan rate 100 mV/s (middle); Linear sweep voltammetry (LSV) for GCE casted with PyPOP-Pt@G with scan rate 10 mV/s with inset (right). [291], Copyright 2017. Reproduced with permission from the American Chemical Society.

copper-porphyrin-based CMP (Cu-CMP) has a high surface area and a inimitable tubular nanostructure that can be used as a functional catalyst for encapsulating copper/copper oxide nanoparticles for hydrogen evolution [296]. Among them, the use of Cu-CMP850 as the catalyst, show the good performance of electrical catalytic hydrogen evolution, with relatively low potential (0.19 V, 1.0 mA cm $^{-2}$) and high current density of 50 mA cm $^{-2}$ at an overpotential of 0.47 V, and Tafel slope of ~135 mV decade $^{-1}$, the Faraday efficiency of 90% under the application potential of 0.34 V, as well as high durability.

Doping some single or double hetero atoms such as N, S, Ru, and Co can significantly improve the performance of carbon materials [292,297-299]. Wang et al. used carbon fiber cloth to chemically deposit a kind of heteroatom-rich CMP (PAQTA), then adding Co salt pyrolysis to prepare Co nanocrystalline composite porous carbon materials doped with heteroatoms for efficient and stable electrocatalytic hydrogen evolution reaction [300]. PAQTA was impregnated with Co(acac)$_2$ solution and then pyrolyzed in nitrogen at high temperature, followed using acid etching to prepare the CoNOC catalysts (Fig. 33A). Among them, the CONOC-900 showing a Tafel slope of 21 mV decade $^{-1}$, an approximate rectangular CV curve, and negligible polarization curve attenuation and loss of current density (the green line in Fig. 33B). DFT calculations show that the excellent electrochemical performance of the catalysts is due to (i) rapid transfer of electrons from cobalt nanocrystals to graphene layers, and (ii) the reduction of Fermi level of the neighboring C atom owing to N,O-dual doping. This results in a decrease in the free energy of hydrogen adsorption, which enhances the performance of electrocatalytic hydrogen evolution.

6.2. CMPs for adsorption and conversion of carbon dioxide

The constant emission of carbon dioxide (CO$_2$) caused by the heavy use of fossil fuels is a major factor causing global climate change [301,302]. The progress of efficient methods of CO$_2$ capture, storage, and conversion of CO$_2$ into useful fuels is a significant aspect in the effective reduction of CO$_2$ emissions, and has important implications for alleviating the current energy crisis and global warming [303]. Currently, some solid porous materials (such as zeolite, carbon, aluminum oxide, and metal organic frameworks (MOFs) with gas selection capabilities [304,305] are used to adsorb and separate CO$_2$. To meet the requirements of sustainable development, researchers should give priority to the development of advanced materials that can not only absorb CO$_2$ but also catalyze its conversion into liquid fuels [306,307]. The materials used in this strategy first need to be able to capture and convert CO$_2$ without the need for additional energy at environmental conditions to avoid the generation of new CO$_2$. CMPs as a platform for CO$_2$ storage and catalytic conversion to provide a feasible clean energy technology.

6.2.1. CMPs for carbon dioxide adsorption

Due to the high porosity and regulable pore surface function of CMPs [102,308-311], they are promising in enhancing CO$_2$ capture and storage. Table 3 summarizes the CO$_2$ uptake by CMPs reported in recent years [63,131,144,147,241,244,293,312-321].

Some polar groups, such as –NO$_2$ [322], arylamines [323], –OH [324], –COOH [313], –SO$_3$H [324], and heterocyclic nitrogen atoms [325] can modify the surface of porous materials, which can significantly increase the binding energy of CO$_2$, thus increasing the

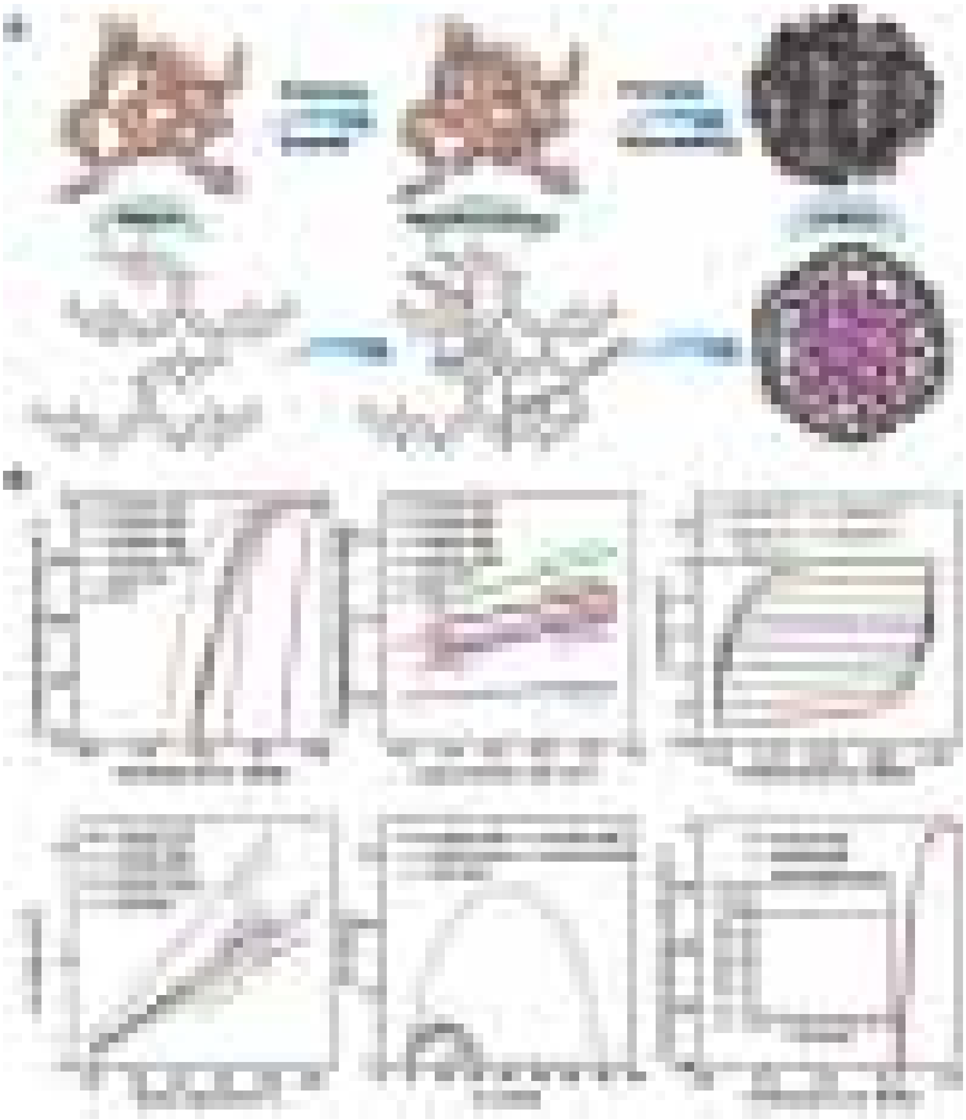

Fig. 33. (A) Synthesis route of CoNOCs. (B) Polarization curves and corresponding Tafel plots obtained in 0.5 M H_2SO_4, CV curves of CoNOC-900, capacitive current density as a function of scan rate, Nyquist plots, and durability. [300], Copyright 2018. Reproduced with permission from the John Wiley & Sons Inc.

absorption rate and/or selectivity of CO_2. Therefore, Zhu's group investigated the influence of –COOH, $–NH_2$ and –OH on the CO_2 adsorption capacity of polymer networks [312]. The groups –COOH, $–NH_2$, and –OH are merged into the networks of the PAFs synthesized Sonogashira–Hagihara reactions of tri(4-ethynylphenyl)amine with various aryl halides. Noteworthily, compared to "naked" PAFs, the $–NH_2$ functionalized PAF-33–NH_2 displays the highest CO_2 isosteric heat (32.9 kJ mol $^{-1}$) and the –COOH functionalized PAF-33–COOH shows the maximum CO_2 uptake per unit areas (4.37 and 2.71 μmol m^{-2}) at 273 and 298 K. This indicates that the integration of functional groups is conducive to enhancing the interaction between PAF networks and CO_2 molecules, thus enhancing their adsorption properties. Furthermore, PAFs can be modified by post-metallization (such as Li, Na, K, Mg) [314]. Interestingly, the CO_2 isosteric heats of adsorption are depending on the type of light metal ion and follow the order of PAF-26-COOMg < PAF-26-COOLi < PAF-26-COOK < PAF-26-COONa.

Considering the highly modular nature of CMPs, the introduction of chemical functions after functionalization can make them more absorbent and selective to CO_2 absorption. Thomas et al. prepared PCZNs by Yamamomo reaction and introduced a series of secondary building units by post functionalization (Fig. 34A) [126]. The porosity and N-content of the polymers are both key factors affecting the absorption of CO_2. Both factors can change with the change of chemical structure and concentration of the secondary monomer. In this case, these factors are enhanced by introducing functional groups using post-functionalization, such as PCZN-8 can obtain a higher CO_2 absorption value and high-efficiency CO_2/N_2 selective separation (the green line in Fig. 34B; Table 3).

The pore properties of polymer networks can be well adjusted by adjusting the length and geometry of the links to enhance CO_2 adsorption property. Xu et al. prepared a series of A6 + Mx ($x = 2$, 3, 4, 6) type polyphenylene CMPs (A_6CMPs) through modulating the monomer length and geometry by the polymerization reaction of 1,3,5-tris(3,5dibromophenyl)benzene (A6) and a series of benzene polymerization boronic or ethynyl (MX, X represents the number of functional groups) [326]. A6CMP-4 (M3), A6CMP-3 (M2), and A6CMP-6 (M4) showed BET specific surface area of 960, 1042, and 1115 m^2 g^{-1}, respectively, correspond to the CO_2 adsorption capacity of 1045, 963, and 925 mg g^{-1} at 60 bar and 318 K, respectively, and A6CMP-7 (M6) showed BET specific surface area of 571 m^2 g^{-1} corresponds to the CO_2 adsorption capacity of

Table 3
Summary of Carbon dioxide capture and storage in CMPs

CMP sample	Molecular structure	S_{BET} ($m^2\ g^{-1}$)	V_{total} ($cm^3\ g^{-1}$)	T (K)	CO_2 ($mmol\ g^{-1}$)	Ref.
PAF-33	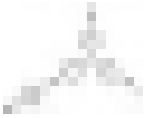	821	–	273	2.16	[312]
PAF-33–NH_2	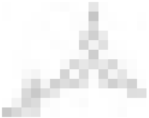	370	–	273	1.19	[312]
PAF-33–COOH	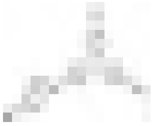	445	–	273	1.94	[312]
PAF-34		953	–	273	2.50	[312]
PAF-34–OH	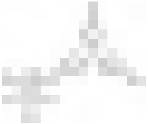	771	–	273	2.21	[312]
PAF-35	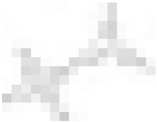	567	–	273	1.77	[312]
CMP-1	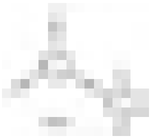	837	0.45	298/273	1.18/2.05	[313]
CMP-1-$(CH_3)_2$	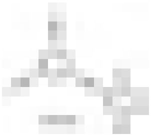	899	0.75	298/273	0.94/1.64	[313]
CMP-1-$(OH)_2$	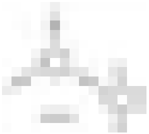	1043	0.71	298/273	1.07/1.80	[313]
CMP-1-NH_2	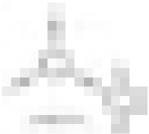	710	0.39	298/273	0.95/1.64	[313]
CMP-1-COOH	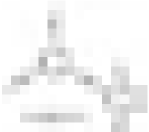	522	0.30	298/273	0.95/1.60	[313]
CMP		772	1.21	298	71.0	[63]
Co-CMP		965	2.81	298	79.3	[63]

(*continued on next page*)

Table 3 (*continued*)

CMP sample	Molecular structure	S_{BET} (m^2 g^{-1})	V_{total} (cm^3 g^{-1})	T (K)	CO_2 (mmol g^{-1})	Ref.
Al-CMP		798	1.41	298	76.5	[63]
MFCMP-1	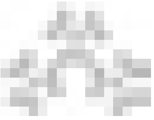	840	0.52	273	3.69	[131]
PAF-26-COOH	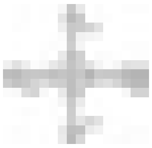	717	0.36	273	286[a]	[314]
PAF-26-COOK	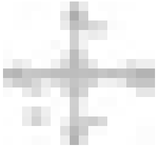	430	0.20	273	572[a]	[314]
p-PPF	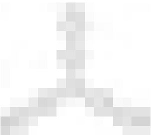	269	0.20	195/273	73.0/44.9[b]	[244]
m-PPF	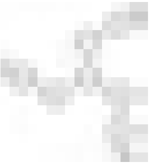	229	0.15	195/273	41.5/24.2[b]	[244]
Cz-POF-1	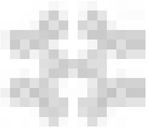	2065	1.57	273	202[b]	[315]
Cz-POF-2		671	0.42	273	77[b]	[315]
Cz-POF-3	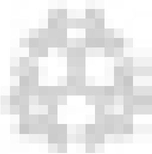	1927	1.35	273	210[b]	[315]
Cz-POF-4	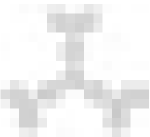	914	0.60	273	121[b]	[315]
PON-1		1447	1.0	195/298	976/109[c]	[316]
PON-2	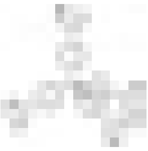	189	0.83	195/298	482/34[c]	[316]

(*continued on next page*)

Table 3 (*continued*)

CMP sample	Molecular structure	S_{BET} ($m^2\ g^{-1}$)	V_{total} ($cm^3\ g^{-1}$)	T (K)	CO_2 ($mmol\ g^{-1}$)	Ref.
PON-3		44	0.09	195/298	525/37[c]	[316]
P-1		611	0.95	273	8.9[d]	[144]
P-2		1222	1.55	273	14.5[d]	[144]
P-TCzPhSi		1856	1.7	273	23.5[d]	[317]
P-TCzTAT	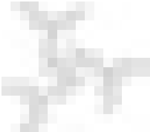	1028	0.76	273/298	18.15/10.69[d]	[318]
P-BCz	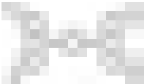	640	0.85	298	9.27[d]	[319]
P-TCz	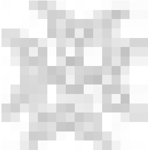	1109	1.31	298	16.02[d]	[319]
P-HCz	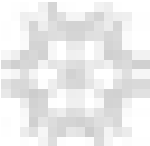	790	1.20	298	9.41[d]	[319]
TEPO-1		485	0.82	273/298	6.52/3.65[e]	[320]
TEPO-2	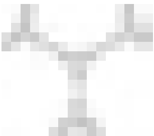	534	0.30	273/298	7.62/3.93[e]	[320]
TEPO-3	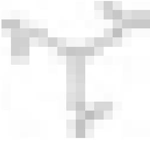	592	0.30	273/298	8.40/5.33[e]	[320]
ThPOP-1	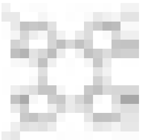	1050	0.69	273	15.0[e]	[147]

(*continued on next page*)

Table 3 (*continued*)

CMP sample	Molecular structure	S_{BET} (m^2 g^{-1})	V_{total} (cm^3 g^{-1})	T (K)	CO_2 (mmol g^{-1})	Ref.
ThPOP-2		160	0.27	273	4.0[e]	[147]
NCMP1	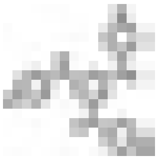	58	0.15	273/298	6.1/3.5[e]	[293]
NCMP2	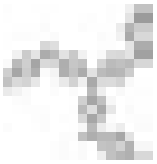	280	0.30	273/298	8.2/4.4[e]	[293]
NCMP3	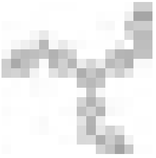	485	0.57	273/298	11.0/6.5[e]	[293]
PCTF-1	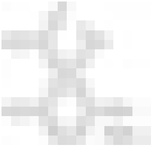	2235	1.56	273	44.9[f]	[241]
PCTF-2	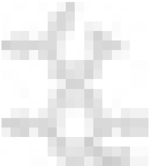	784	0.38	273	24.2[f]	[241]
CMP-LS1		493	0.32	273/298	31/17[f]	[321]
CMP-LS2		1576	1.06	273/298	87/47[f]	[321]
CMP-LS3		643	0.37	273/298	42/24[f]	[321]

[a] CO_2 uptake (mg cm^{-3}) at 101 kPa.
[b] CO_2 uptake (cm^3 g^{-1}) at 30 bar.
[c] CO_2 uptake (mg g^{-1}).
[d] CO_2 uptake (wt.%) at 1.1 bar.
[e] CO_2 uptake (wt.%).
[f] CO_2 uptake (cm^3 g^{-1}).

~875 mg g^{-1}. Interestingly, A6CMP-1 has a low BET specific surface area of 571 m^2 g^{-1}, exhibited the largest CO_2 capture capacity of 740 mg g^{-1} yet it showed the maximum CO_2 adsorption capacity of 1218 mg g^{-1}. In 2017, Thomas et al. further investigated the relationship between carbon dioxide adsorption performance of CMPs and the number of functional groups [327]. They synthesized a series of cyanovinyl-based nitrogen-rich microporous polymers by metals-catalyzed polymerization (Fig. 35A) for the capture of carbon dioxide. A point diagram reveals that the structure-adsorbability relationship is linear, with the adsorption capacity of CO_2 proportional to the number of functional groups. As shown in Fig. 35B, as the number of functional groups from P4 to P1 increases, their CO_2 adsorption capacity gradually increases, which are 32, 99, 103, and 111 mg g^{-1} at 1 bar and 273 K, respectively.

6.2.2. CMPs for carbon dioxide conversion

Capturing CO_2 and converting it into useful chemicals or high-calorific energy is a promising clean energy technology to effectively combat global warming. Adding metal-organic molecules to CMP networks can produce materials that capture and simultaneously convert CO_2. The salen-Co/Al has previously been reported as a homogeneous catalyst for cyclic carbonates generation from

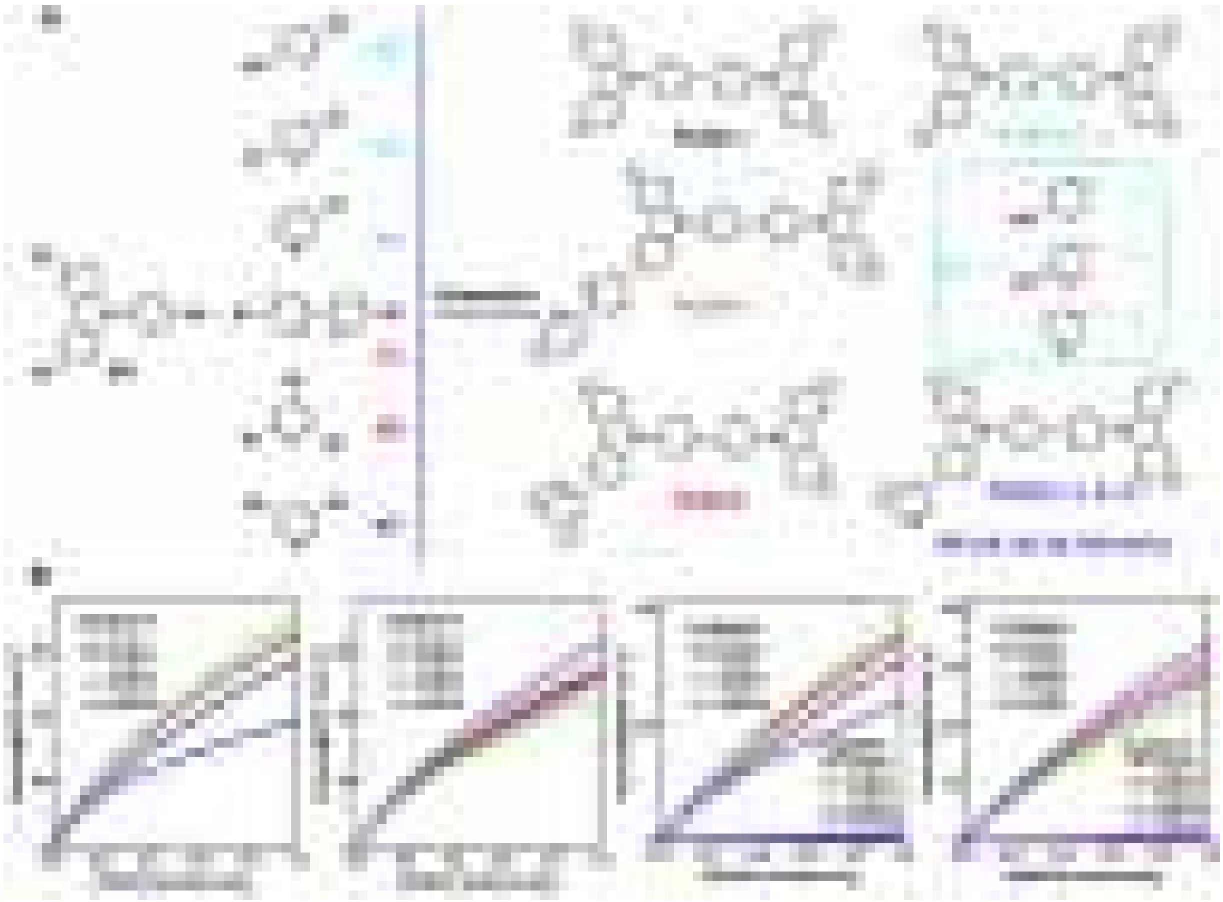

Fig. 34. (A) The functionalized route to polycarbazole networks (PCZNs); (B) CO_2 adsorption isotherms of PCZNs at 273 K, and CO_2 and N_2 adsorption isotherms measured at 298 K. [126], Copyright 2017. Reproduced with permission from The Royal Society of Chemistry.

Fig. 35. (A) Metal-catalyzed reactions for P2, P3, and P4, and molecular structure of P1, P2, P3, and P4. (B) The CO_2 adsorption capacity of P1, P2, P3, and P4 at 273 K. [327], Copyright 2017. Reproduced with permission from the John Wiley & Sons Inc.

carbon dioxide and epoxides at low temperatures and pressures [328]. The introduction of this component into CMP networks has resulted in a serious of Co/Al-coordinated CMPs [63], which have outstanding CO_2 capture and conversion properties at ambient conditions, and their adsorption capacity is comparable to that of some previously reported inorganic catalysts [329,330]. Meanwhile, these CMPs also can be used as heterogeneous catalysts catalytic CO_2 with propylene oxide (PO) reaction to propylene carbonate (PC) under environmental conditions. In the existence of quaternary ammonium salt nBu_4NBr (TBAB), Co-CMP and Al-CMP showed remarkably high catalytic activities in the conversion of CO_2 at ambient conditions. Single catalyst Co-CMP has good durability, which can be reused for 22 times without significant reduction in catalytic activity. This strategy combines the functions of gas storage and catalysis, and provides a new idea for one-step, low-cost CO_2 emission reduction, which is worthy of further study.

Based on the module features of 2D CMPs and the excellent catalytic activity of metalloporphyrin derivatives to CO_2 conversion, Chen et al. designed a new 2D CMPs constituted by metalloporphyrin serves as the main structural and functional unit and thiophene as the link for the emission reduction of CO_2 [217]. Furthermore, to improve the ability of CMP to catalyze the conversion of carbon dioxide, a series of metal atoms (Fe, Mg, Mn, and Cu) were introduced into CMP networks to modify the electronic properties

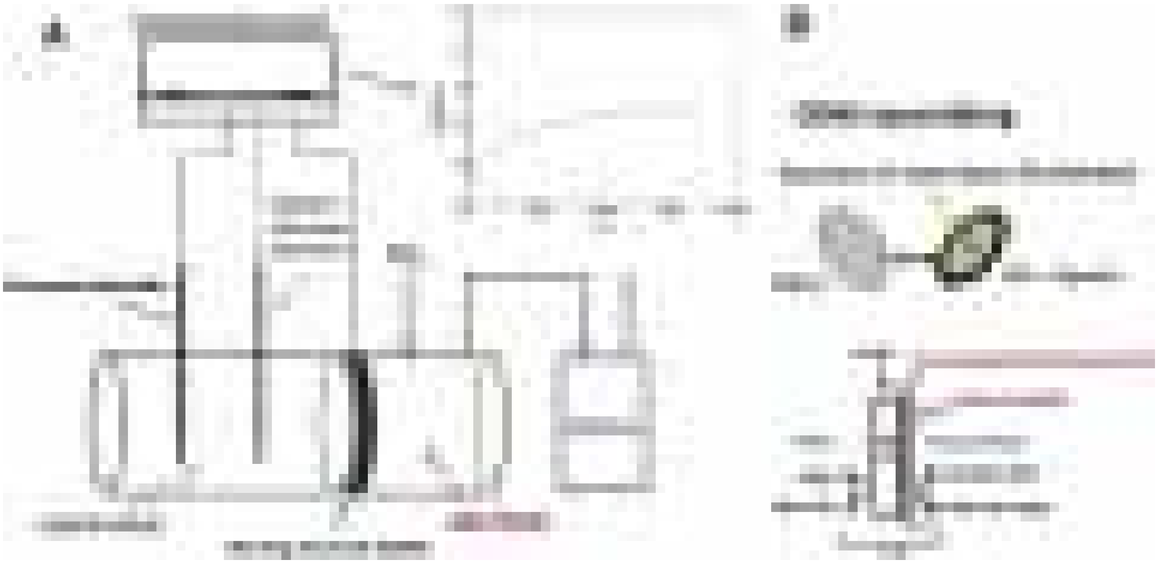

Fig. 36. (A) The schematic of the electrochemical device for the gas-phase CO_2 reduction, and (B) Gas diffusion membrane (GDM) assembly. [120], Copyright 2015. Reproduced with permission from Springer Nature.

of metalloporphyrin units. The calculation results show that these CMPs have the properties of catalysis, high stability, and adjustable electronic structure, and Fe-modified thiophene-linked metalloporphyrin (Fe-TMP) has the highest catalytic activity for the reduction of CO_2.

To our best knowledge, the single homogeneous catalytic process has the disadvantages of difficult separation of catalysts, difficult purification of products, and difficult recovery of expensive catalysts, as well as the residual metals in products that may cause serious problems for environmental applications. To solve the above problems, it has been reported that loading a homogeneous catalyst on a solid porous carrier is an effective strategy. CMPs are promising materials that can selectively adsorb CO_2 and reduce CO_2 back to liquid fuel under mild conditions when loaded with homogeneous metal nanoparticles as an electrocatalyst.

Ampelli et al. synthesized tetrakis-phenylethene CMPs (TPE-CMPs) by Yamamoto reaction, and then Pt (or Fe) nanoparticles were deposited on their surface by sol immobilization method to modify TPE-CMP to create and the active catalytic CO_2 reduction site on the CO_2 adsorption site of the polymers [120]. The gas diffusion membrane (GDM) based on the metal-doped CMPs is used as part of an electrochemical device for CO_2 reduction to liquid fuel. The schematic of the experimental apparatus and the GDM assembly are shown in Fig. 36. The anode working in the liquid phase is in contact with one side of the Nafion membrane, and the cathode working in the gas phase is in contact with the free side of gas diffusion layer (GDL). CO_2 penetrates through GDL and is absorbed on the surface of metal-doped TPE-CMP, then, it reacts with metal nanoparticles (Pt or Fe) at the catalytic active site to form liquid fuel. The characterization and testing of electrocatalytic materials by a small device between the working electrode and the counter electrode indicate that this electrocatalytic device has advantages over common liquid phase electrochemical systems in that it does not take into account the solubility of CO_2, does not require the recovery of liquid-phase products, and has better selectivity for high-chain hydrocarbons and oxygen-containing compounds. Polymer electrocatalysts loaded with appropriate metal catalysis sites are one of the keys to the preparation of high-efficiency electrode materials. The other one, the assembly of multilayer composite electrode materials to ensure good proton mobility and conductivity is also the key to improve the overall efficiency of the electrocatalytic device.

Although electrochemical systems vary greatly in operating conditions and product distribution, to improve the efficiency of the system, the key points should be considered. Besides the key issues mentioned above, the rate-determining steps of the CO_2 reduction process are not yet clear [331,332]. An increase in the number of CO_2 adsorption sites could be an advantageous measure to accelerate reduction, especially since these sites selectively adsorb and catalyze carbon dioxide, which requires further investigation.

6.3. CMPs for batteries

CMPs can be used as electrode materials and as precursors to electrical energy storage materials for lithium-ion batteries (LIBs). (i) The high surface area of CMPs can improve the contact area with the electrolyte, which provides more surface locations for reversible reactions to occur. (ii) CMPs have a short ion migration distance, fast kinetic speed, and high energy storage capacity, which is conducive to the development of high-performance LIBs. (iii) CMPs can crosslink redox-active modules into highly stable porous electrodes, which has been sought after in the exploration of the next generation of green batteries. Furthermore, CMPs can also be used as electrode materials for potassium-ion batteries (KIBs) and sodium-ion batteries (SIBs). Here summarize CMP materials as a platform for metal-ion batteries (Table 4) [74-76,333-346].

6.3.1. CMPs for lithium-ion batteries

LIBs are a clean energy storage device, which has the advantages of recyclability, low-cost application, and high-energy-density, and plays a significant role in the application of mobile electronic products and electric vehicles [24,347-349]. To widely apply LIBs, to develop high-performance electrode material is needed, which is the core component of LIB systems [24]. To date, the electrode materials of LIBs mainly include inorganic active materials [350-354], organosulfur compounds [24], organic radical compounds [355,356], organic carbonyl compounds [357-359], and conducting polymers [360-362]. Due to the rapid growth of energy demand and serious environmental problems, there is still a great need to develop electrode materials for green batteries. Organic polymer materials have been widely studied as electrode materials due to their ease of synthesis, reproducibility of raw materi-

Table 4
Summarizes CMP materials as a platform for metal-ion batteries

CMPs	molecular structure	S_{BET} (m^2 g^{-1})	V_{total} (cm^3 g^{-1})	CR/CN	RC/rate	CE%	Ref.
Lithium-ion batteries							
PDCzBT	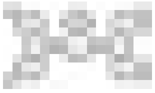	1166	0.7	312/400 (200 mA g^{-1})	215/500	>98 (10th)	[333]
HATN-CMP	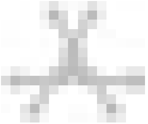	616	0.63	61.9%/50	147/100	100 (50th)	[76]
NG-HCP	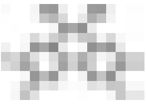	72.56	0.2548	76.9%/230	1320/20	100	[334]
PTDATA	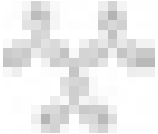	560.58	–	98.2/100 (20 mA g^{-1})	125.4/50	95 (45th)	[74]
PTPAn	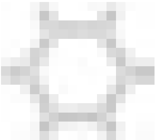	11	–	93%/50	81/50	92	[335]
PTTPAB	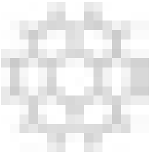	595	0.13	96%/150	84/50	98	[335]
HATNPF1		384	0.27	92%/1200	312.5/100	100	[336]
PBIM	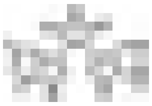	711	0.317	807/ (0.05 C)	1172/50	99.2 (60th)	[337]
PTTE	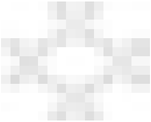	312	–	80.8%/100	834/200	46 (initial)	[338]
PT	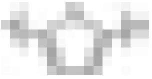	13	0.07	90/1000 (500 mA g^{-1})	141/3000	–	[75]
P33DT	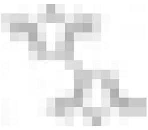	696	0.53	79.9%/1000	387/5000	43.1 (initial)	[75]
PTPADTz	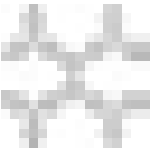	~657	–	95/20 (20 mA g^{-1})	80/50	–	[339]

(*continued on next page*)

Table 4 (*continued*)

CMPs	molecular structure	S_{BET} ($m^2\ g^{-1}$)	V_{total} ($cm^3\ g^{-1}$)	CR/CN	RC/rate	CE%	Ref.
NGA-CMP400	–	521.3	0.31	701.2/500 (1 A g^{-1})	874.3/100	46.6 (initial)	[340]
IEP-11-E12		2000	–	90%/5000	47/30C	100	[341]
TzThBT	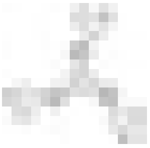	406	–	326/1500 (5 A g^{-1})	1599/50	100 (500th)	[342]
Sodium-ion batteries							
PDCzBT	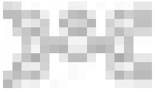	1166	0.7	119/200 (50 mA g^{-1})	145/20	>96 (15th)	[333]
PYT-TABQ/rGO	–	–	–	98%/1400	245/200	>92 (initial)	[343]
ALP-8	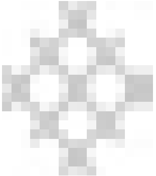	550	–	90%/150	180/0.3C	96 (150th)	[344]
PTTE		312	–	88.1%/50	326/50	100 (100th)	[338]
Potassium-ion batteries							
PyBT	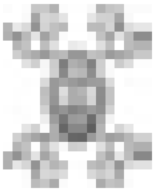	493	–	272/500 (50 mA g^{-1})	428/30	99.5 (500th)	[345]
PI-CMP	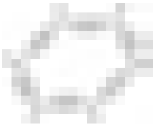	110	–	60.2%/200	–	–	[346]

CR: capacity retention (mA h g^{-1}); CN: cycle number; RC: reversible capacity (mAh g^{-1})/rate: current density (mA g^{-1}); CE: coulombic efficiency.

als, structural diversity, and design flexibility, as well as the redox properties of their synthetic monomers [363-365]. In the past years, important progresses have been achieved for CMPs as electrode materials in LIBs (Table 4).

6.3.1.1. CMPs as electrode materials for LIBs. Due to the high surface area and multisurface reaction sites, the robust porous network and insoluble organic solvent properties, as well as monomer diversity and the variety of synthesis methods, a series of CMP electrode materials have been used for LIBs [74,333,336,366,367]. For example, Jiang et al. reported that the hexaazatrinaphthalene CMP (HATN-CMP) cathode material of LIBs has a first cycle capacity of 147 mAh g^{-1} and the capacity retention rate of 61.9% after 50 charge-discharge cycles [76]. Yang et al. used carbazole and benzothiadiazole based CMPs as free anodes, with capacities of 1047 and 215, 161 and 117, 117 mAh g^{-1} at 20, 500, 1000 and 2000 mA g^{-1}, respectively [333].

The construction of CMP networks is helpful to prevent the leakage of electroactive units. A newly designed hexaazatrinaphthalene CMP (HATN-CMP) prepared by haxaazatrinaphthalene (HATN) unit to construct the skeleton with redox activity and the crosslinked porous skeleton with high surface area for LIB energy storage (Fig. 37A and B) [76]. The HATN edge may leak during the recharging and discharging cycle process, while the HATN unit can be interwoven into the network of HATN-CMP to greatly reduce the leakage of the HATN unit into the electrolyte. In the crosslinked skeleton, the redox-active units and graded nanopores work together to facilitate the electrochemical processes involved in energy storage and release. Therefore, the CMP network structures not only make efficient use of the active cell of the batteries but also enhances their cycling performance. The redox-active unit in the HATN-CMP skeleton serves as the active unit of the energy storage and power supply module, and the high surface area of its inherently open nanopores contact with lithium

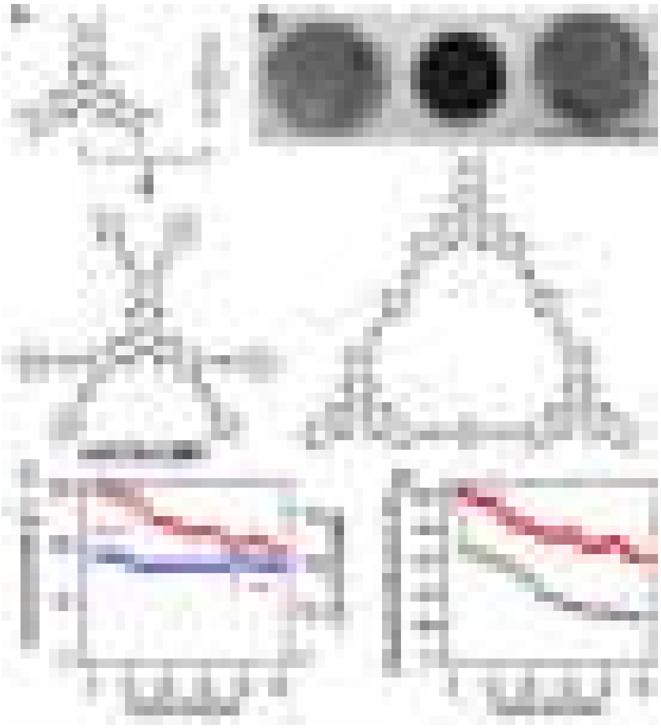

Fig. 37. (A) Schematic representation of the synthesis of hexaazatrinaphthalene CMP (HATN-CMP) and the elementary pore structure. (B) The photos of HATN-CMP electrodes and lithium batteries thus fabricated. (C) Cycle stability and (D) capacity retention ratio of HATN-CMP (filled circle) and monomer (open circle) cathode electrodes within 50 cycles under 100 mA g^{-1}. [76], Copyright 2014. Reproduced with permission from The Royal Society of Chemistry.

ions to promote charge dynamics. Compared with the HATN, the HATN-CMP with built-in redox-active skeleton and permanent nanopores has a nearly uniform coulomb efficiency, high capacity, and excellent cycling stability. HATN-CMP shows the capacity of 91 mA h g^{-1} (Fig. 37C) after 50 cycles, which is much higher than that of monomer HATN (13 mAh g^{-1}), and compared with HATN monomer, which only lost 30% of its original capacity (Fig. 37D, black curve) in 2 cycles and only retained 25% after 50 cycles, HATN-CMP still retained 62% of its original capacity after 50 cycles (Fig. 37D, red curve). This significant reduction in capacity is related to the ease with which the HATN monomer on the cathode surface dissolves into the electrolyte. Meanwhile, the discharge-charge capacity reflects that HATN-CMP maintains a coulomb efficiency of up to 100% over 50 cycles, which proves the high efficiency of charge and ion in the electrochemical reaction.

The high surface area of CMPs improves the contact area with the electrolyte, which provides more surface locations for electrode reversible reactions, and is beneficial to the reversible redox reaction of Li^+ and shortens the Li^+ diffusion path resulting in reduced charge transfer resistance, thus improving the performance of the battery [75,337,368]. PTTPAB was designed and synthesized by chemical oxidation polymerization of triphenylamine derivative 1,3,5-tris(4-diphenylamino-phenyl)benzene (TTPAB) (Fig. 38A) [335]. The corresponding PTTPAB powder has the unique microporous structure (the average micropore diameter of 0.68 nm, the mesopore diameter of ~2–5 nm) and flowering spherical shape (BET specific surface area, 595 m^2 g^{-1}) (Fig. 38B), which are beneficial to enhance the rate performance of the battery. Compared with a typical p-doped radical polymers polytriphenylamine (PTPAn), The PTTPAB shows a more stable cycle-specific capacity (Fig. 38C, 86.7 mAh g^{-1}) over 50th charging/discharging cycle, and higher coulomb efficiency (Fig. 38D, 98%), as well as better rate

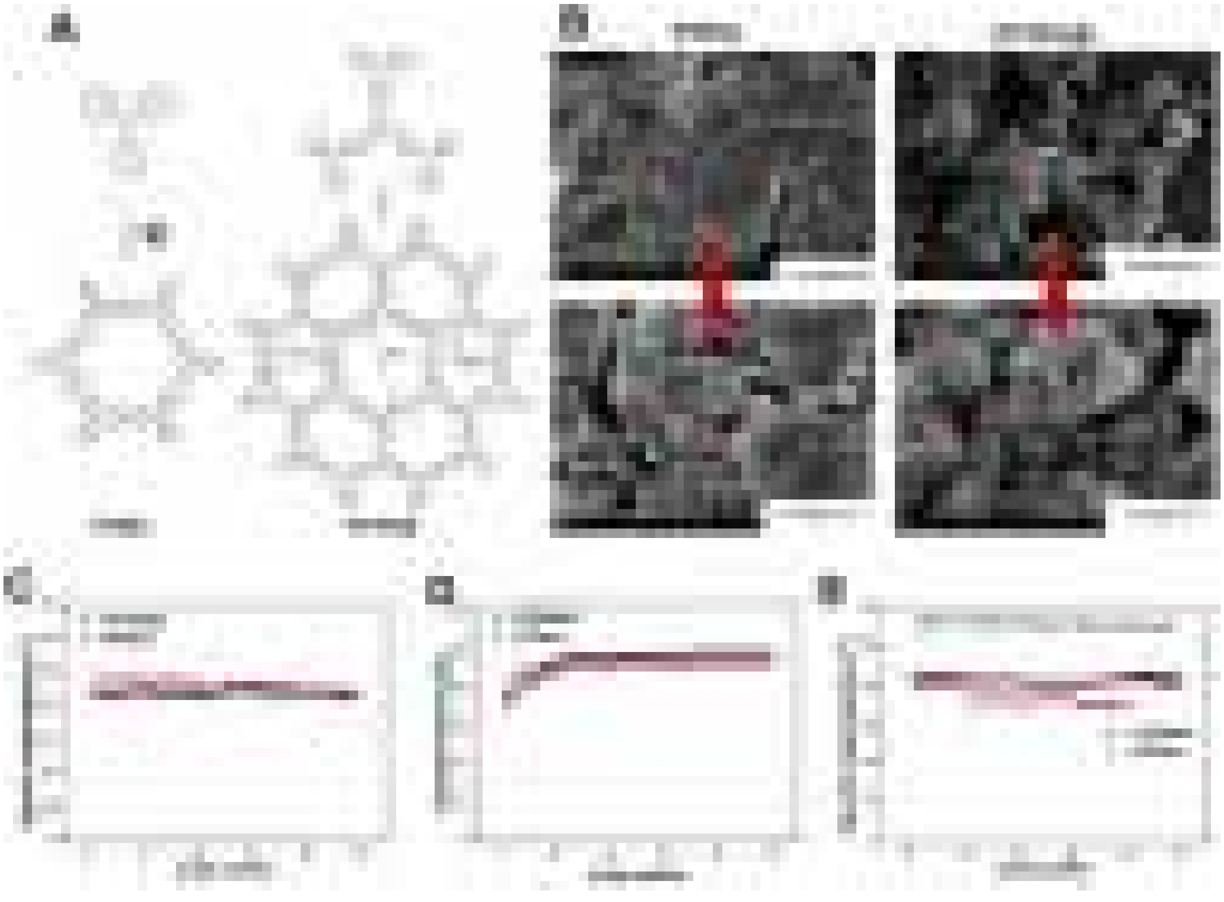

Fig. 38. (A) The synthetic route of PTPAn and PTTPAB samples. (B) SEM images of powder samples of PTPA and PTTPAB. (C) Cycling stability of PTTPAB and PTPAn at a current of 20 mAg h^{-1} between 2.5 and 4.2 V. (D) Coulomb Efficiency of PTTPAB and PTPAn. (E) Rate performance of PTTPAB and PTPA polymers. [335], Copyright 2018. Reproduced with permission from Elsevier Science Ltd.

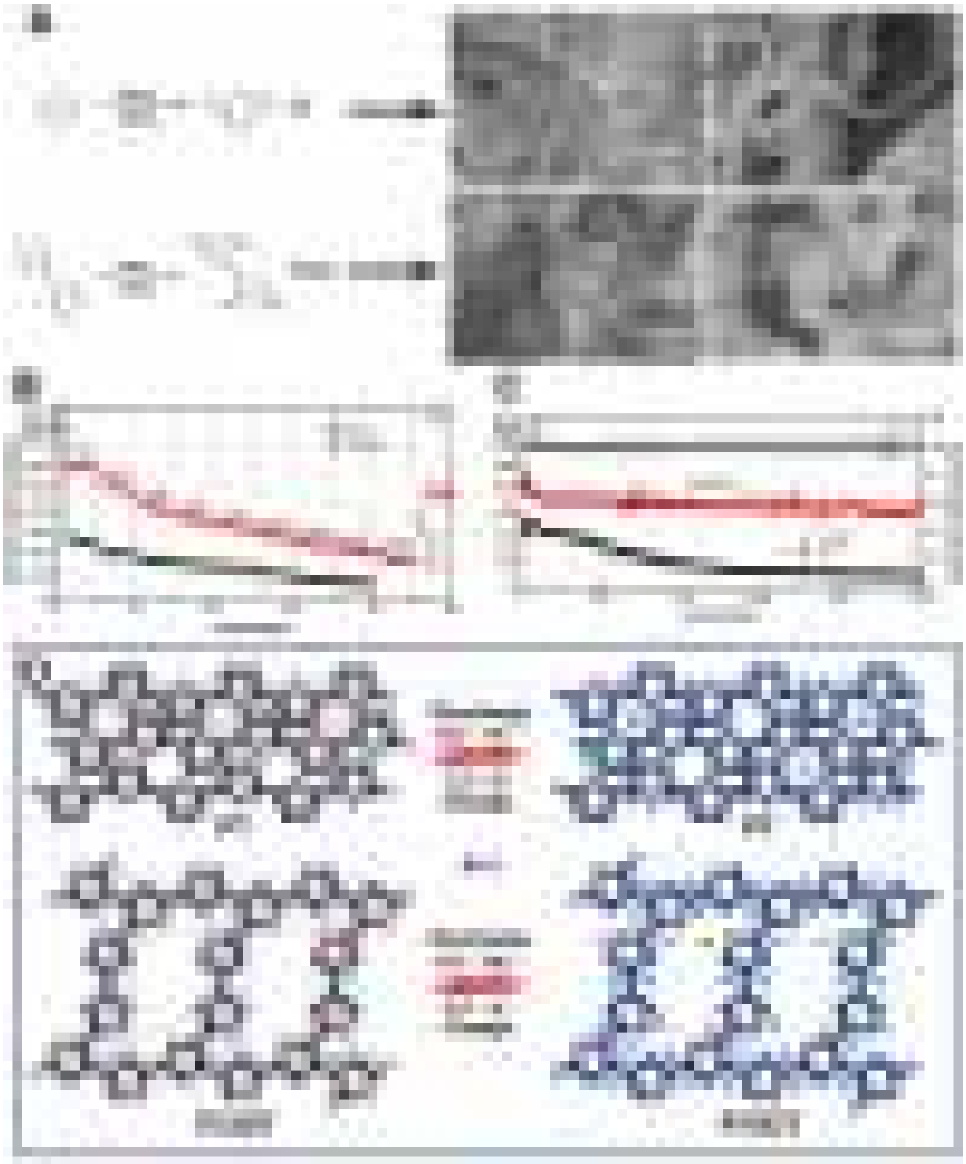

Fig. 39. (A) Synthetic routes to the polymers of PT and P33DT and their notional polymer structures (left) and SEM images (right) for PT and P33DT. (B) The rate performance at different current densities from 45 to 5000 mA g^{-1}. (C) the cyclability at 500 mA g^{-1} of PT and P33DT. (D) The schematic redox reaction mechanisms of PT (top) and P33DT (bottom). [75], Copyright 2017. Reproduced with permission from the John Wiley & Sons Inc.

performance (Fig. 38E, 84, 82, 81, 80, 84 mAh g^{-1}) at a current rate of 50–500 mA g^{-1}.

In addition to the high surface area of the fine pore structure that can enhance the electrochemical performance of CMPs, the molecular structure also greatly affects the electrochemical performance. Polythiophene, an N-doped conjugated polymer with reversible redox behavior, the content, cross-linked porous structure and surface area of thiophene play an important role in improving its electrochemical performance. Through the structural design and synthesis of a series of thiophene-containing CMPs with different thiophene contents and specific surface areas, namely poly(thiophene) (PT) and poly(3,3′-bithiophene) (P33DT) (Fig. 39A), the influence of the molecular structure of CMPs on the electrochemical performance of LIB was compared [75]. The results show that the content of thiophene, crosslinked pore structure, and specific surface area play an important role in improving the electrochemical properties of thiophene. Compared with PT (Fig. 39B, 141 mAh g^{-1} at 3000 mA g^{-1}), P33DT has better rate performance (Fig. 39B, 387 mAh g^{-1} at 5000 mA g^{-1}). P33DT anode has a high capacity (Fig. 39B, 1215 mAh g^{-1} at 45 mA g^{-1}) and longer cycle life (Fig. 39C, 663 mAh g^{-1} at 500 mA g^{-1} after 1000 cycles) due to its unique structure of highly crosslinked porous characteristics, high thiophene content and large specific surface area. Fig. 39D shows the charging and discharging mechanism of thiophene conjugated polymer.

Cation$-\pi$ interaction [369-371], effectively aggregates Li^+ around the polymer chain and further reduces the diffusion distance of lithium ions, allowing Li^+ to react more quickly with the active groups on the polymer surface. As a representative aromatic compound, indole has abundant electronic structure [372,373], makes it easier to form a cation-interaction with Li^+. Meanwhile, introducing heteroatoms such as O and N into conjugated systems can promote redox reactions at active sites with lone pair electrons [374-376]. The unique aromatic structure of indoles containing N-heteroatoms also provides high redox activity and many active sites to receive Li^+ through a reversible electrochemical Li addition reaction to form a cation$-\pi$ interaction. As shown in Fig. 40A, indole-based CMP poly(bisindolylmaleimide) (PBIM) obtained by

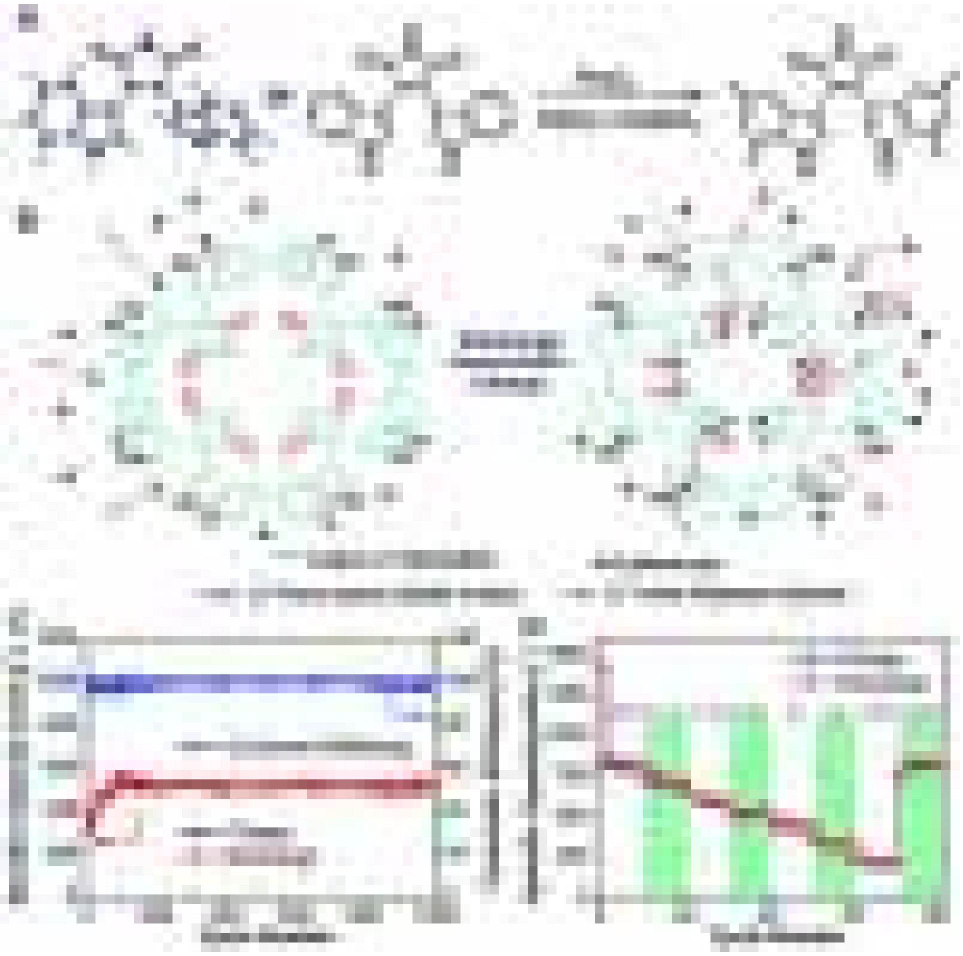

Fig. 40. (A) The synthetic route of PBIM and (B) reaction mechanisms. (C) Cycle performance at a current density of 1000 mA g^{-1}. (D) The rate performance at different current densities from 0.05 C to 2.5 C. [337], Copyright 2018. Reproduced with permission from The Royal Society of Chemistry.

$FeCl_3$ catalytic oxidative coupling reaction [337]. The cationic-π interaction formed and unconfined at the discharge-charging process are shown in Fig. 40B. The PBIM prepared as the anode material of LIB showed high capacity (Fig. 40C, 1172 mAh g^{-1} at 50 mA g^{-1}), high coulomb efficiency (Fig. 40C, 99.2%), excellent cycle life (Fig. 40C, 1000 cycles), and ascendant rate performance (Fig. 40D, 0.05, 0.1, 0.3, 0.5, 1, 2, and 2.5 C at 807, 701, 589, 525, 427, 323, and 214 mAh g^{-1}, respectively; 1 C = 1967 mA g^{-1}), which are attributed to the reversible cationic interaction and the unique aromatic structure containing N heteroatoms. To develop new electrode materials for large-scale energy storage applications, further exploration of CMP materials is still needed, especially the development of diverse CMP materials in terms of application.

6.3.1.2. CMPs as precursors for electrode materials of LIBs. Porous activated carbon, a special hard carbon, has high surface area and abundant internal porous structure, and is a promising candidate for high-performance LIB anode materials. There are various preparation methods and precursor substances for the preparation of activated carbon. For example, the use of plant tissues with supporting structures [377-379] as precursors of activated carbon materials can significantly reduce not only the economic costs and environmental pollution from agricultural waste disposal, but also the raw material costs for the preparation of activated carbon. However, these plant tissues can become contaminated with many minerals during extraction and transportation [378]. The ash produced by the high temperature calcination of these minerals may reduce the catalytic performance and mechanical strength of the derived activated carbons [378,380]. Therefore, a series of pretreatment processes are required for the preparation of activated carbon materials derived from plant tissues [377,378].

Besides, for MOFs materials [381-385], it has adjustable pore structure and ultra-high surface area, and there are plenty of combinations to try. A good strategy is to use MOF materials as precursors to prepare more stable conductive carbon materials. In this way, it can solve the problems of instability and poor conductivity of MOF precursors, and endowing MOF-derived carbon materials with high porosity, large surface area, multiple layers and adjustable structure of the precursors. However, it should be noted that although thousands of MOFs materials have been reported so far, the selection of suitable precursor materials is limited [383]. Therefore, more efforts are needed to explore more alternative and cheap MOFs materials.

The surface properties and pore structure of CMPs can be adjusted by changing the geometric shape and chain length of CMP monomers, or by doping different heteroatoms or metals. CMPs can also be modified by the post-synthesis method. Therefore, CMP is also an ideal precursor material for preparing porous carbon. Meanwhile, CMP materials are simple in composition and mainly composed of C and H, as well as can provide more suitable options for preparation of derived porous carbon. Based on the easily adjustable porosity of CMPs, the performance of CMP-derived porous carbon can be changed by adjusting the length of the monomer pillar in the CMP precursors [386]. This also means that CMP-derived porous carbon electrode materials with ideal structure can

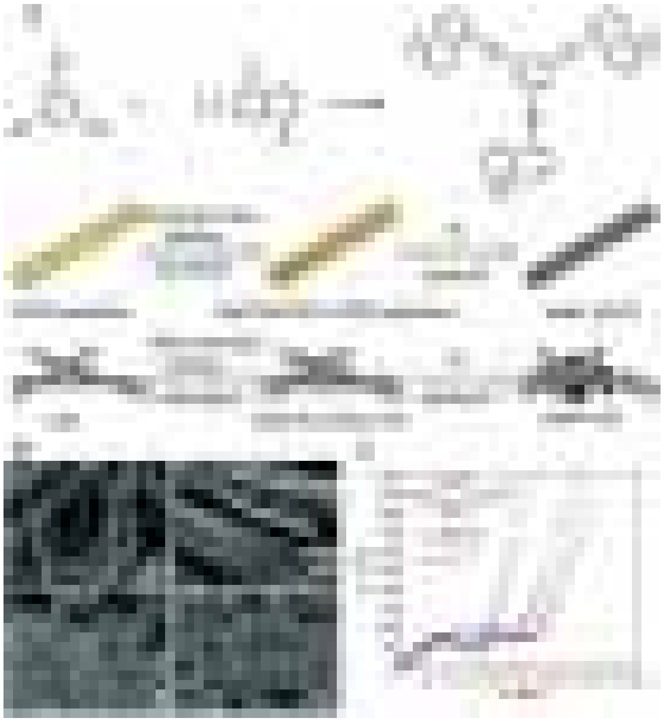

Fig. 41. (A) Schematic illustration of the reaction for the CMP nanotubes synthesis (top). Schematic illustration of the fabrication of MnO–PCNTs and MnO–CNTs (below). (B) SEM image of MnO–PCNTs (top), and SEM images of MnO–CNTs (control, below). (C) EIS of the fresh cells loaded with PCNTs, MnO–PCNTs, and MnO–CNTs. [392], Copyright 2016. Reproduced with permission from The Royal Society of Chemistry.

be more rational designed and prepared by adjusting the structure of CMP materials, which may provide an idea for the rational design and preparation of CMP-derived porous carbon anode materials as high-performance LIBs. Nitrogen-doped porous carbon nanoparticles (NPCN-KOH) with the improved porous structure were obtained by pyrolysis of nitrogen-containing conjugated porous polymer (NCMP) and high-temperature activation of KOH [387]. NPCN-KOH has a more disordered structure and a high specific surface area of 1845 m^2 g^{-1}. These unique functions ensure that NPCN-KOH has a high reversible capacity of 818 mAh g^{-1}, a high rate performance of 818 mAh g^{-1} at 0.1 C, and long cycle life (527 mAh g^{-1}, the capacity retention rate of 97.6% after 600 cycles). As well as the reversible capacity of NPCN-KOH is 857 mA h g^{-1} at 0.1 C, which is exceeding other porous carbon [388-390].

More stable composites can be obtained by embedding metals or metal oxides into the CMP-derived materials [391-394]. After the synthesis of porous carbon nanotubes (PCNTs) by the simple pyrolysis of CMP nanotubes, the incorporation of MnO nanoparticles into PCNTs (Fig. 41A, MnO-PCNTs) can further improve the performance of PCNTs [392]. As shown in Fig. 41B, the microstructure of MnO-PCNTs is like that of PCNTs, and the MnO nanoparticles are located inside the PCNT. Compared to PCNTs (276.4, 228.0, 199.7, 170.1, 155.7, 138.1, 114.6, 93.3, and 79.7 mAh g^{-1}) and MnO-CNTs (545.9, 466.1, 419.5, 351.1, 301.2, 235.4, 170.1, 127.6, and 101.9 mAh g^{-1}), MnO-PCNTs have better rate performance MnO-PCNTs (539.3, 447.7, 392.2, 345.1, 313.0, 282.2, 227.4, 179.2 and 160.8 mAh g^{-1}) at 0.2 to 0.5, 1, 2, 3, 5, 10, 20 and 30 C, respectively. This suggests that the addition of MnO nanoparticles can greatly improve the performance of PCNTs and that MnO-PCNTs have a unique structure to prevent MnO from being crushed in the process of repeated charging-discharging cycles. The impedance data of the equivalent circuit (Fig. 41C, inset) represent, compared with PCNTs (235 U) and MnO-CNTs (258 U), the charge transfer resistance of MnO-PCNTs is 173 U (Fig. 41C), which is because MnO nanoparticles are dispersed in PCNTs, which made the composite materials have high electron conductivity and ion diffusion ability.

Recently, Fe_3O_4-SPC is successfully prepared by simply pyrolysis SCMP and mixing it with $Fe(NO_3)_3$•$9H_2O$ and $Fe(CH_3COO)_2$•$4H_2O$ [394]. The protection of SPC avoids the huge volume change caused by the crushing of Fe_3O_4 during the repeated discharge/charge cycle. Fe_3O_4-SPC is a graded polymer composed of nanoparticles and containing Fe_3O_4 crystals with a face-centered cubic structure. Compared to naked Fe_3O_4, these special structures enable Fe_3O_4-SPC to exhibit good cyclic capacitance of 897.2 mAh g^{-1} at 0.6 A g^{-1} over 300 cycles, which can be attributed to the reversible growth of the gelatinous polymer layer under the action of transition metal oxides [395,396]. Furthermore, the reversible capacity of Fe_3O_4-SPC (926 mAh g^{-1} at 100 mA g^{-1}) is higher than the Fe_3O_4, which are attributed to sulfur-enriched host and an open porous structure to provide more lithium storage site.

6.3.2. CMPs for sodium-ion batteries

Energy storage is critical to the sustainable development of energy, leading to a growing demand for energy storage devices, especially for integrated energy storage systems, and the development of advanced energy storage technologies beyond LIBs is expected. SIBs are expected to complement this field because they are lighter, more flexible, more environmentally friendly, and have a high global stockpile. CMPs provide an effective platform for the development of the next generation of advanced SIBs with multi-functional organic/polymer electrodes [343].

Recently, highly porous azo-linked polymers (ALPs) have been used for the first time as redox-active electrode materials for a new rechargeable SIBs [344]. ALPs are highly cross-linked polymers with high surface area and a π-conjugated microporous property, which eliminates the solubility problem of organic electrodes in common electrolytes, facilitates the absorption of electrolytes, and assist ion transport and charge transfer. Among them, the theoretical capacity of ALP-8 polymer with azo-linked was calculated based on a four-electron redox reaction (Fig. 42A). The tilt of the charge-discharge curve (Fig. 42B) is due to the complex electronic properties and redox reactions in the amorphous structure as well as the embedding of Na^+ [397,398]. As can be seen from Fig. 42B, the contribution of Na^+ embedding to capacitance is small. The ALP-8 electrode showed high cycling performance, and the reversible capacity (2nd) is 194 mAh g^{-1} (70% of the theoretical capacity) at 0.3 C (Fig. 42C), and maintain a specific discharge capacity of 170 mAh g^{-1} after 150 cycles. In the case of high current density, the limited mobility of Na^+, and the decrease of electronic conductivity of the cathode material tend to reduce the capacity. Therefore, the discharge capacity of the battery at different current densities was measured to verify its rate capacity, as shown in Fig. 42D, ALP-8 shows excellent rate performance of 108, 88, 70, 57, 42 mAh g^{-1} at 1, 4, 10, 20, and 40 C (1 $C = 278$ mA g^{-1}), respectively.

6.3.3. CMPs for potassium-ion batteries

Additionally, KIBs also are competitive energy storage devices due to the K^+/K redox potential (2.93 V relative to the standard hydrogen electrode) similar to Li^+/Li (3.04 V) [399]. However, the cycle stability of the KIBs is generally poor due to the large volume changes caused by the insertion/extraction of K^+ [400-404]. The extended π-conjugated structure of CMPs is conducive to improving the cyclic stability and rate performance of KIBs [346]. However, the relationship between the structural and performance of CMPs needs further exploration.

Recently, two series of CMPs (Fig. 43A, bromated benzene (Bz)-containing CMPs and benzothiadiazole (BT)-containing CMPs) with different structural units were used as the anode for KIBs [345]. A

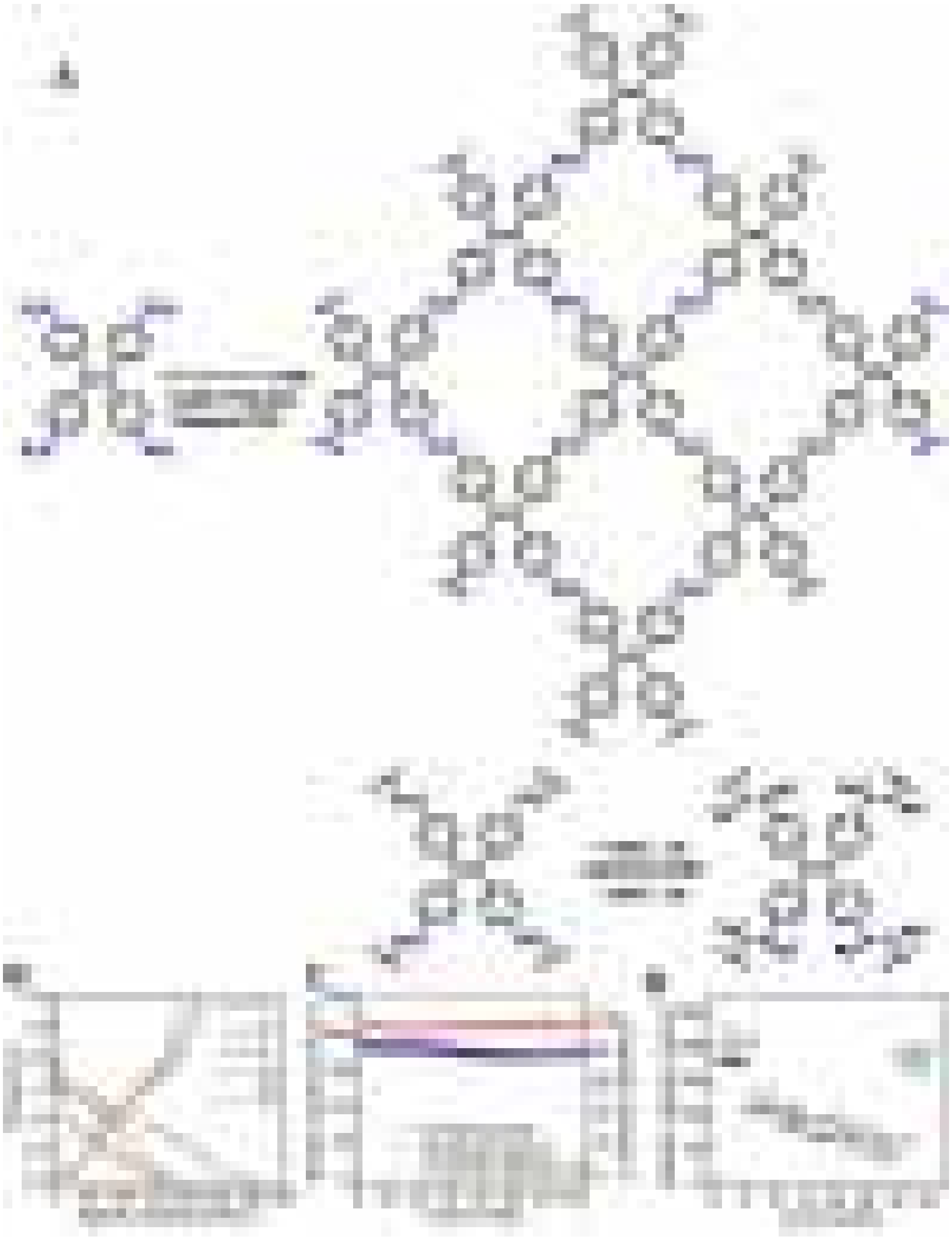

Fig. 42. (A) Synthetic route of ALP-8 and its redox mechanism with sodium ions. (B) Galvanostatic charge/discharge profiles of ALP-8 battery at 0.3 C, (C) cycle stability and Coulombic efficiency up to 150 cycles at 0.3 C, and (D) rate capability at different current densities. [344], Copyright 2019. Reproduced with permission from the American Chemical Society.

comparative study of the structure-performance relationship shows that the LUMO distribution, LUMO energy level, and bandgap have a great influence on the storage capacity of K^+. The high delocalization of LUMO orbit is conducive to the high charge delocalization along with the polymer networks, and reduces the charge density of the redox-active site, thus achieving high redox activity and inhibiting side reactions between the polymer and the electrolyte. The electronic structure of CMPs can be adjusted by synthesis control. For example, the LUMO energy level and bandgap of Bz-containing CMPs can drop from PhBT to PyBT. Low LUMO levels and narrow band gaps confer high electron affinity and conductivity on CMPs. Therefore, the polymer PyBT composed of pyrene and benzothiadiazole units exhibits excellent KIB electrochemical properties, such as excellent rate performance at different current densities from 30 to 500 mA g^{-1} (Fig. 43B), a high reversible capacity of 428 mAh g^{-1} at 30 mA g^{-1} and excellent capacity retention of 272 mAh g^{-1} at 50 mA g^{-1} over 500 cycles (Fig. 43C). The K storage mechanism of PyBT (Fig. 43D) was investigated by FTIR spectral analysis under different discharge-charge states (Fig. 43E and F). The introduction of the BT unit is beneficial to the increase of the redox activity of CMP electrodes.

6.4. CMPs for supercapacitors

Supercapacitors, because of their long cycle stability, high energy density, superfast charging and discharging rate, low maintenance costs, and safety of such outstanding features and attention [405-407]. Normally, supercapacitors store energy in two different ways: (i) non-Faradaic processes about electrochemical double-layer (EDL), and (ii) Faradaic processes generated by a reversible redox process (pseudocapacitance) at the electrode interface. In EDL-based supercapacitors, the principle of electrical energy stor-

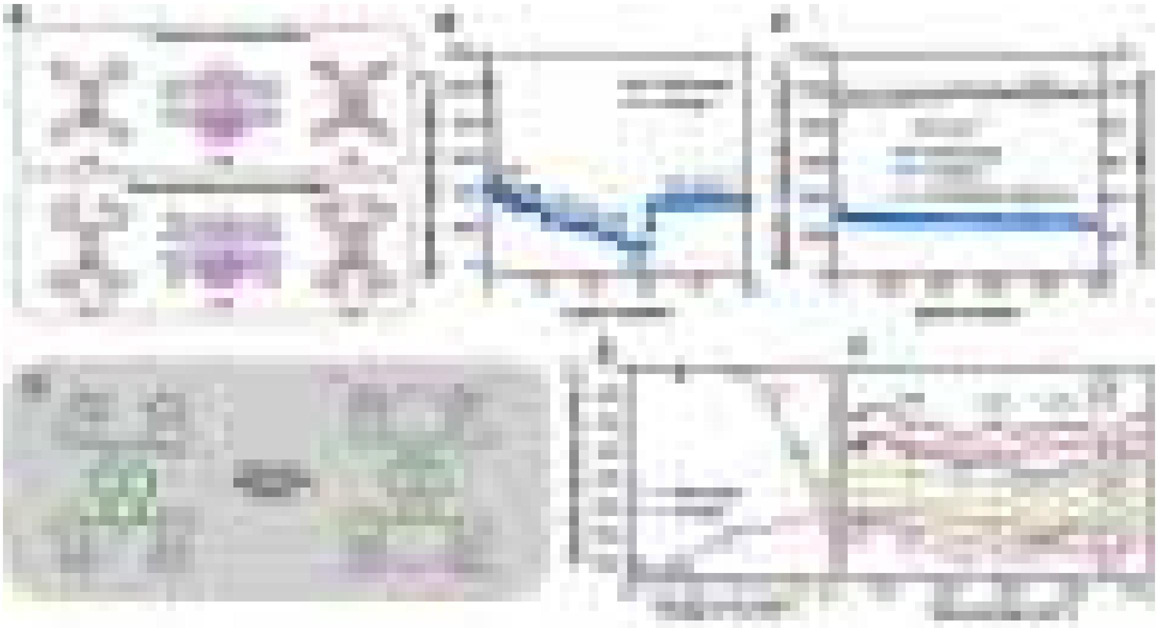

Fig. 43. (A) Notional polymer structures of the Bz-containing CMPs (top) and the BT-containing CMPs (below). (B) Rate performance of PyBT at a current density from 30 to 500 mA g^{-1}. (C) Cycling stability and Coulombic efficiency of PyBT at 50 mA g^{-1}. (D) Proposed K storage mechanism. (E) Charge/discharge curves of the first cycle at 30 mA g^{-1} for PyBT. (F) Ex situ FT-IR spectra of a PyBT-based battery recorded at different states. [345], Copyright 2019. Reproduced with permission from the American Chemical Society.

age is through adsorbing ions to the surface of an electrode in response to the applied potential, and improve the porous electrode can promote maximum capacitance. While in pseudocapacitors, a rapid and reversible redox reaction in the electrode surface produces Faradic pseudocapacitance and can generate the capacitance associated with the electrode charging potential within the entire electrode. Therefore, pseudocapacitors capacitance than involves only the capacitance of EDL.

Carbon and carbon allotropes, such as carbon nanotubes and graphene, are one of the main research materials for electrode materials for commercial supercapacitors owing to their high conductivity, large surface area, good chemical stability, pore structure engineering, heteroatoms doping, and the potential of new carbon materials [408-410]. Additionally, CMPs as an emerging material platform for supercapacitors have got attention from scientific researchers and engineers [343,411-414]. They can be used as the electrode materials or precursors of carbon electrode material for supercapacitors owing to their high surface area, inherent micropore volume, and conductive network skeleton (Table 5) [189,343,412-419].

6.4.1. CMP as electrode materials for supercapacitors

In 2011, Jiang et al. first reported the effect of the synthetic aza-fused CMPs (Aza-CMPs) on supercapacitors' energy storage and power supply [138]. Aza-CMPs have a conductivity aza-fused skeleton, closely aza-fused element, and the inherent micropore and high surface area, prompting the concentration of proton, ion of fast-moving, and the formation of the electrostatic charge separation layer, thus are used as electrode materials for the preparation of supercapacitors with larger capacity, higher energy density, and good cycle life. In 2016, A novel b-ketoenamine-linked CMP (KECMP-1) synthesized by Schiff-base microwave-assisted condensation of 1,3,5-triformylphloroglucinol with m-phenylenediamine [420]. KECMP-1 displays a high specific capacitance of 252 F g^{-1} at 1 A g^{-1}, excellent cycling stability and long cycle life (retaining 130% of the initial capacitance of 160 F g^{-1} at 20 A g^{-1} over 10,000 cycles) for supercapacitors, which is much better than that of similar COF electrodes' electrochemical performance [421]. The remarkable electrochemical properties of KECMP-1 are due to its unique N–H groups and abundant pores that facilitate rapid ion and electron transport through the interface between the electrodes.

The introduction of redox-active structural units into the electrode material [416,422] can significantly enhance the capacitance of the supercapacitor [406]. 1,4-bis(3-phenylpropynoyl)benzene (BPPB) with reversible redox behaviors were crosslinked to form CMP materials, and then form the hollow shell structure H-CMP-BPPB by template synthesis [418]. The hollow structure of H-CMP-BPPB may be beneficial to the diffusion of electrolyte into the CMP material, to make full use of the redox substances in the material [179,423,424]. As shown in Fig. 44A, CMP-BPPB, and a CMP without BPPB are prepared using monodisperse silica spheres as hard templates and 1,3,5-triethynylbenzene and 1,4-diiodobenzene as the reactant, and then obtained H-CMP-BPPB and hollow CMP without BPPB (H-CMP) through etching of silica templates. The hollow structure of the polymer materials is shown in Fig. 44B. H-CMP-BPPB coin type pseudocapacitor has high cycling stability, after 10 000 cycles, maintained capacitances of 90%, and 85% of the first cycle capacitance at 1 and 6A g^{-1}, respectively (Fig. 44C). As well as the Nyquist plots of H-CMP-BPPB and TEM analysis before and after the reaction also indirectly proves the stability of H-CMP-BPPB (Fig. 44D). Furthermore, the introduction of carbonyl groups has very little effect on the chemical composition of CMP, which may be beneficial to the material's weight to the capacitance ratio.

Strong electron donor 2,6-diaminoanthraquinone (DAQ) combined with receptor aryl bromides to form a series of novel CMPs, namely, polyaminoanthraquinone (PAQ) networks such as PAQTA, PAQTB, PAQCB, PAQTM, and PAQSF (Fig. 45A) [412]. The surface area of PAQs can be up to 600m^2 g^{-1}, which has good dispersibility in polar solvents and can be processed into flexible electrodes for supercapacitors. Compared to other electronic donors including triphenylbenzene (TB), carbazole (CB), tetraphenylmethane (TM), and spirobifluorene (SF), the triphenylamine (TA) in PAQTA network is the strongest electron donor, so to the effective combi-

Table 5
Conductive CMPs for supercapacitors in recent years

CMPs	Molecular structure	S_{BET} (m^2 g^{-1})	V_{total} (cm^3 g^{-1})	CD	SC	CR/CN	Electrolyte	Ref.
TAT-CMP-1	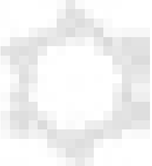	88	–	1	141	83%/10000	1.0 M Na_2SO_4	[416]
TAT-CMP-2	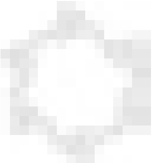	106	–	1	183	95%/10000	1.0 M Na_2SO_4	[416]
Zn-mTCPP	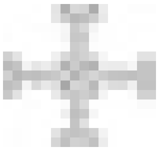	–	–	5	142	–	0.1 M Bu_4NPF_6	[189]
PYBDA		136	–	0.5	456	100%/2000	2 M H_2SO_4	[417]
H-CMP-BPPB		622	0.18	1	189	90%/10000	1 M H_2SO_4	[418]
Fc-CMPs/rGO	–	800.1	–	0.5	470	95%/8000	1 M H_2SO_4	[413]
PAQTA		331	–	1	576	85%/6000	0.5 M H_2SO_4	[412]
CAP-1	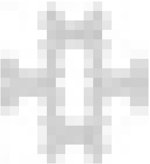	704	0.34	1	81	–	2 M KCl	[414]
CAP-2		594	0.38	1	240	~80%/10000	2 M KCl	[414]
PYT-TABQ/rGO	–	–	–	1	312.5	94.5%/10000	1 M Na_2SO_4	[343]
PTPA-25	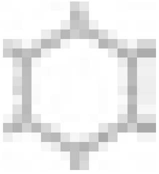	33	–	0.5	335	65%/5000	1.0 M H_2SO_4	[419]
GH-CMP	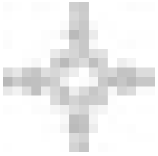	219.2	–	0.2	208	92.6%/10000	1 M H_2SO_4	[415]

CD: current density (A g^{-1}); SC: specific capacitance (F g^{-1}); CR: capacity retention/CN: cycle number.

nation of anthraquinone (AQ) all the charge. Considering the relatively high redox properties of PAQTA and its minimum surface area compared with other PAQs, the larger capacity of PAQTA may depend on the redox activity mechanism rather than the double layer mechanism. The redox mechanism of PAQTA is based on the amalgamation of a strong electron donor unit TA and a receptor unit AQ (Fig. 45B, C, and D), of which AQ's redox mechanism involves the reduction of two electrons (Fig. 45B). TA, which can be oxidized to free radical cations, obtain two-electron delocalized bipolarons (Fig. 45C), providing extra redox-active sites. The total discharge process is shown in Fig. 45D, of which AQ and bipolaron are reduced, AQ ion and TA are oxidized. These two processes involve the concurrent exchange of protons and anions with the electrolyte.

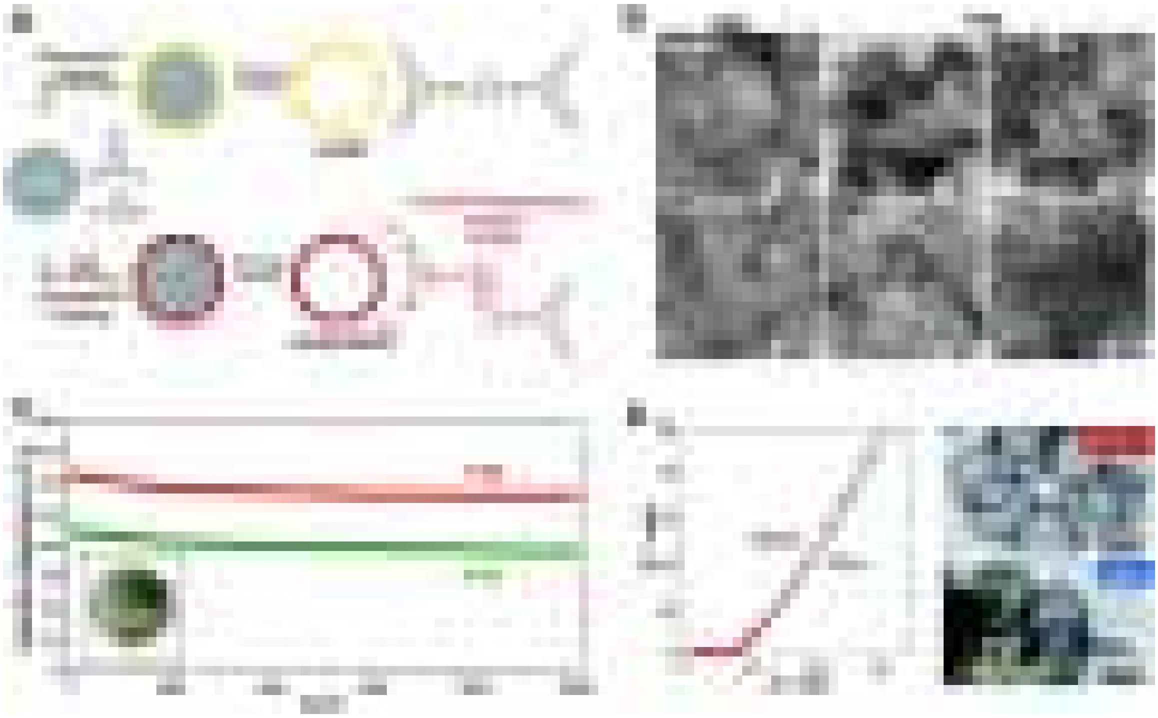

Fig. 44. (A) Synthetic schemes for H-CMP and H-CMP-BPPB. (B) SEM images and TEM images of H-CMP and H-CMP-BPPB. (C) Cycling performance of symmetric coin cell type pseudocapacitors (inset) of H-CMP-BPPB (current densities: 1 and 6 A g^{-1}). (D) Nyquist plots (left) and TEM images (right) of H-CMP-BPPB before and after 10,000 cycles. [418], Copyright 2018. Reproduced with permission from The Royal Society of Chemistry.

Besides, the inimitable nitrogen-rich properties and porous structure of these polymers also contribute to their high electrochemical properties. Two redox-active CMPs (TAT-CMP-1 and TAT-CMP-2) prepared by nitrogen-rich and highly conductive triazatruxene building blocks were used as outstanding electrode materials for supercapacitors application [416]. Fig. 46A display the prepare routes of TAT-CMP-1 and TAT-CMP-2, which show the unique porous and nitrogen-rich structure. Galvanostatic charge-discharge tests (Fig. 46B, C) reveal rapid ion transport and electron propagation in these CMP electrodes. The discharge slopes suggest the relationship between the electrochemical properties of these polymers and their nitrogen content. Due to their inherent porous structure with high N content to provides more redox active sites, they exhibit a high specific capacitance (>160 μF cm $^{-2}$) at a low surface area. Importantly, cyclic experiments (Fig. 46D) of TAT-CMP-1 and TAT-CMP-2 indicate that they have outstanding cyclic stability, with cycle efficiency of 95% and 83%, respectively, at 10 A g^{-1} over 10,000 cycles. The nitrogen groups are conducive to trigger pseudocapacitance and affect the capacitance of the polymer materials, which provides a pathway for the rational design of electrode materials with excellent properties for supercapacitors.

As described in the previous section, 2D CMP materials with high electrical conductivity, good redox activity, and a large porosity rate are prepared. These porous membranes with large surface area, low energy band, and high ion transport rate can be used as electrode materials with high capacity and wide potential window for supercapacitors [413,425]. In 2018, 2D CMP composites (Fc-CMPs/rGO) were prepared using 2D rGO and Fc-CMPs with built-in redox-active ferrocene elements [413]. The covalent binding of Fc-CMPs with rGO through the surface initiates polymerization, and the porous polymer shell completely wraps the outer surface of the graphene nanosheet to form a sandwich structure. The storage mechanism of Fc-CMPs/rGO not only depends on the ion adsorption on the electrode surface but also can store the pseudocapacitance through the redox reaction on the surface, so the total capacitance is increased. Then, the high porosity of Fc-CMPs is beneficial to electrolyte transfer and improves the utilization efficiency of ferrocene units. As well as, the synergy between Fc-CMPs and highly conductive rGO leads to rapid electrochemical reaction kinetics, providing excellent electrical conductivity during the charging and discharging process. This reasonable combination of redox-active CMPs and conductive rGO in a 2D porous skeleton opens a way for the design and manufacture of a new generation of supercapacitors.

6.4.2. CMPs as templates and/or precursors of electrode materials for supercapacitors

CMP materials are conjugated in nature and many of them can be used directly for electrochemical applications. Additionally, some CMP materials are not conductive. High-temperature carbonization can improve the porosity and conductivity of carbon-based materials [426-428]. CMPs can be used as precursors and/or templates to prepare porous carbon materials with excellent electrochemical properties through pyrolysis [90,429,430]. These CMP-derived carbon materials are excellent electrode materials for supercapacitors. For example, compared to porous carbon without a template, the hierarchically porous carbon nanosheets obtained by pyrolysis conversion of carbon-rich graphene-templated CMP hybrids (G-CMPs) that showed better electrochemical performance as electrode material [431]. The use of these porous carbon electrode materials for supercapacitors resulted in a 48% increase in capacitance. Their CV curves show typical symmetrical and rectangular shapes, indicating ideal capacitance behavior. As well as, the layered pore structure of the sandwich with a large aspect ratio is conducive to the rapid ion transport.

Cooper's group directly carbonized poorly conducting CMP electrodes to produce porous engineered carbon, which generally helps ions flow through the electrode [432]. The effect of carbonization activation on the capacitive behavior of CMPs was investigated by using voltammetry and static current charging and discharging

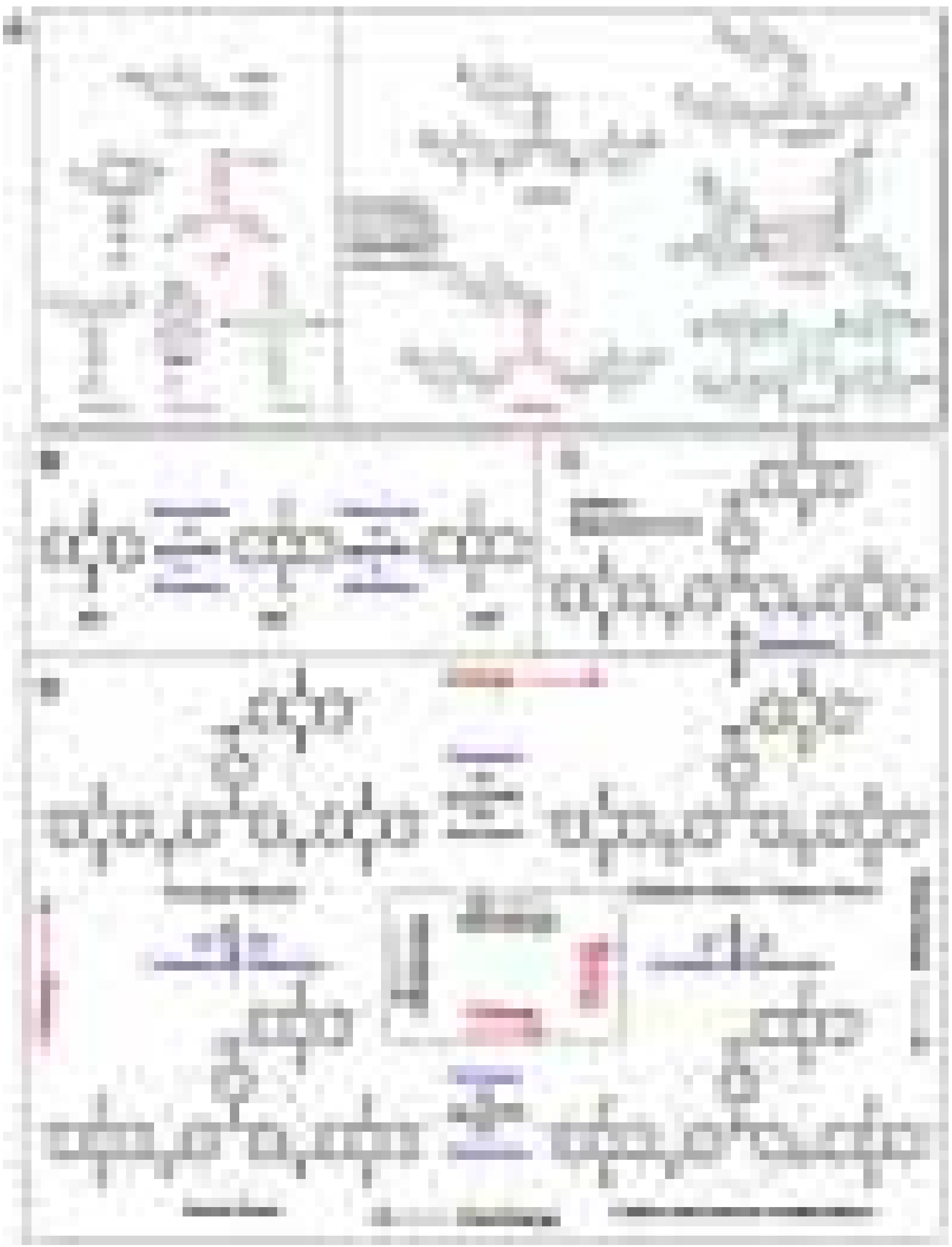

Fig. 45. (A) Synthetic route of the PAQs. (B-D) Proposed redox reactions, i.e., charge/discharge mechanism for PAQTA. [412], Copyright 2018. Reproduced with permission from the John Wiley & Sons Inc.

techniques. These conductive carbonized CMPs exhibit ideal ultracapacitive behavior with a high capacitance of 175 F g^{-1} in an acidic electrolyte and no significant capacitance attenuation after 10,000 cycles. Moreover, the investigation also reveals that the specific capacitance they can reach in alkaline solution is as high as 260 F g^{-1}, and their performance does not decline significantly after 10,000 charge-discharge cycles. Carbonization is an activation method that converts the original CMP materials with poor electrical conductivity into porous carbon materials with better electrical conductivity than the original CMPs and common carbon materials. These preliminary investigations pave the way for further improvements in the performance of supercapacitors.

To directly pyrolysis CMPs into 2D porous carbon nanosheets, Yuan et al., the first to use 4-iodophenylsubstituted graphene (RGO-I) template as a guide to building rich nitrogen graphene CMP sandwich structures (GMPs), then, GMP sandwiches are directly pyrolysis to prepare the structurally clear plastic-doped porous carbon/graphene nanosheets (Fig. 47A) [433]. The microporous polymer shells spontaneously grow on both sides of the graphene 2D template, ensuring the complete separation of sheets of graphene-based complexes even during the subsequent high-temperature treatment. SEM, high-resolution transmission electron microscopy (HRTEM), and atomic force microscopy (AFM) showed that all GMPs have uniform sheet shapes (Fig. 47B). The obtained 2D GMP hybrids have a large aspect ratio and BET specific surface area up to 852 m^2 g^{-1}. Porous carbon and graphene have good electrical conductivity and two-dimensional electron transport capacity, which can realize rapid charge transfer in the process of charging and discharging. As well as the close contact between the porous carbon and the graphene layer, the optimal interface interaction provides a large electrochemically active surface area for charge transfer and a minimum ionic diffusion length during

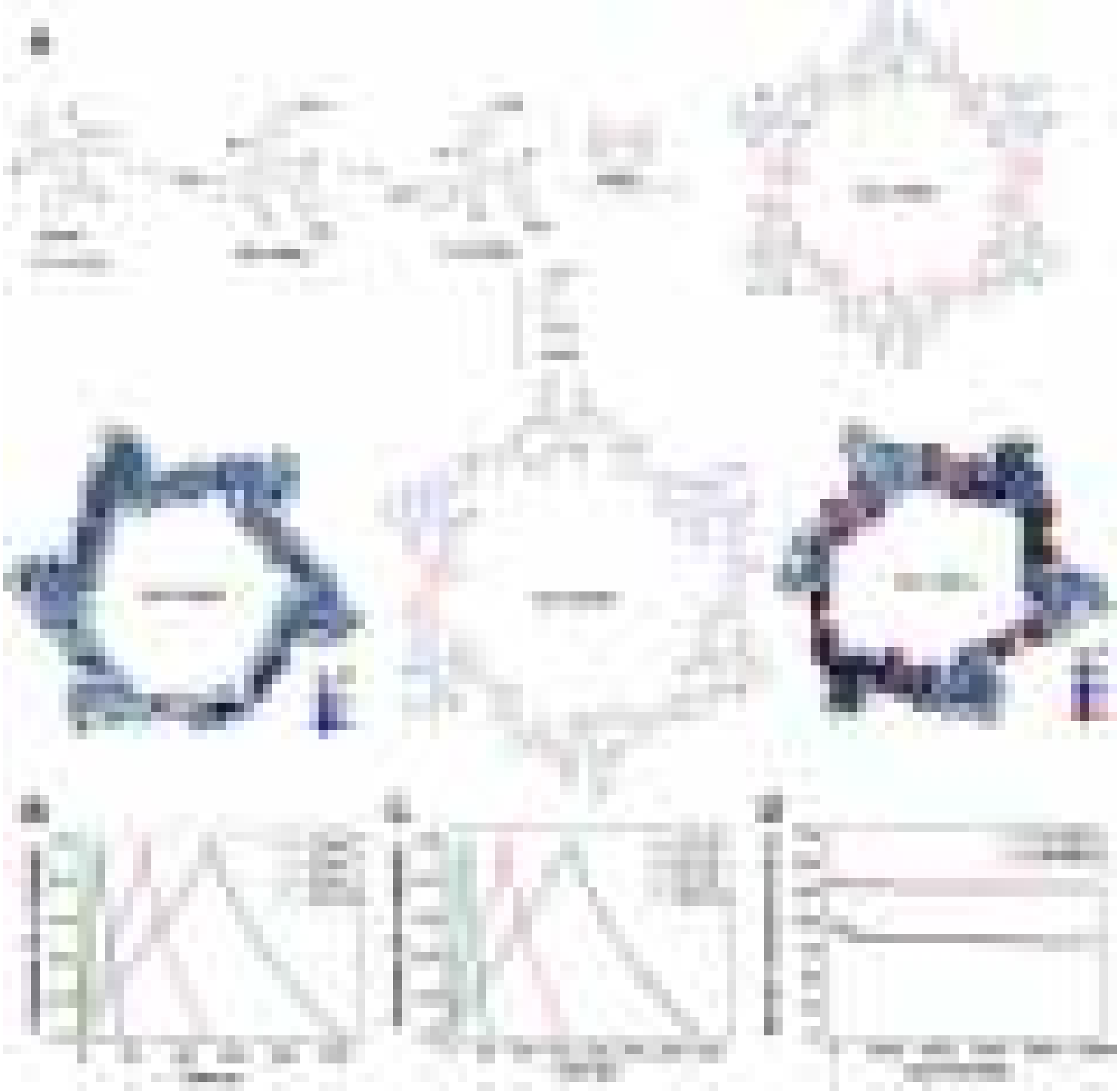

Fig. 46. (A) Synthesis route and the three-dimensional view of TAT-CMP-1 and TAT-CMP-2 in an amorphous periodic cell (gray: carbon, white: hydrogen, blue: nitrogen, red: oxygen and n-hexyl groups (R) are omitted for clarity). Galvanostatic charge-discharge curves of (B) TAT-CMP-1 and (C) TAT-CMP-2 at different current densities, and (D) cycling number for TAT-CMP-1 and TAT-CMP-2. [416], Copyright 2017. Reproduced with permission from The Royal Society of Chemistry.

charging and discharging, thus effectively improving the capacitance performance of the supercapacitor. Interestingly, a series of three separate GMP-based supercapacitors shows enhanced capacitance (Fig. 47C and D). Compared with single-cell supercapacitors, the galvanostatic charge-discharge (GCD) working voltage of three GMP-based supercapacitors connected in series is increased by 3 times at the same current density and almost the same charge and discharge time (Fig. 47D).

Doping and good porosity are two important factors in the application of porous carbon materials. Carbonized doped CMP skeletons is a very advantageous strategy for the preparation of porous carbon electrode materials. Ren's group carbonized reasonably designed n-doped CMP precursor to prepare N-doped porous carbon material (NPCM-1) [434]. Because nitrogen doping improves electrical properties and optimizes pore structure, NPCM-1 shows good performance in ultra-capacitor energy storage. Also, Lim et al. synthesized iron-porphyrin CMP by Suzuki reaction and first time through pyrolysis to obtain Fe-Nx/C electrode material (Fe-P800) [435]. The formation of the M-N-C bond between the metal and the carbon material establishes a direct interaction, which in turn significantly improves the conductivity of the material. Compared with pure nitrogen-doped porous carbon (P800), the specific capacitance of Fe-P800 is increased by twice, showing robust stability. The metal (iron) center has an electronic access point, which provides a fusiform effect for charge transfer to the conductive graphite matrix through its highly reversible redox reaction, thus improving the performance.

6.5. CMPs for fuel cells

Fuel cells first appeared in the 19th century, H. Davy used carbon as fuel, oxygen as oxidant and nitric acid as the electrolyte to prepare carbon and oxygen batteries. In 1839, W. Grove used platinum as the electrode, sulfuric acid as the electrolyte, and oxygen as the fuel and oxidant to obtain electricity from gas and oxygen. The name of "fuel cells" was first proposed by L. Mond and C. Langer in 1889. However, due to the limitation of technological levels, such as the cost of the noble metal platinum electrode, the production of oxygen and many other obstacles cannot be overcome, so people gradually forget about the fuel cells. Today in

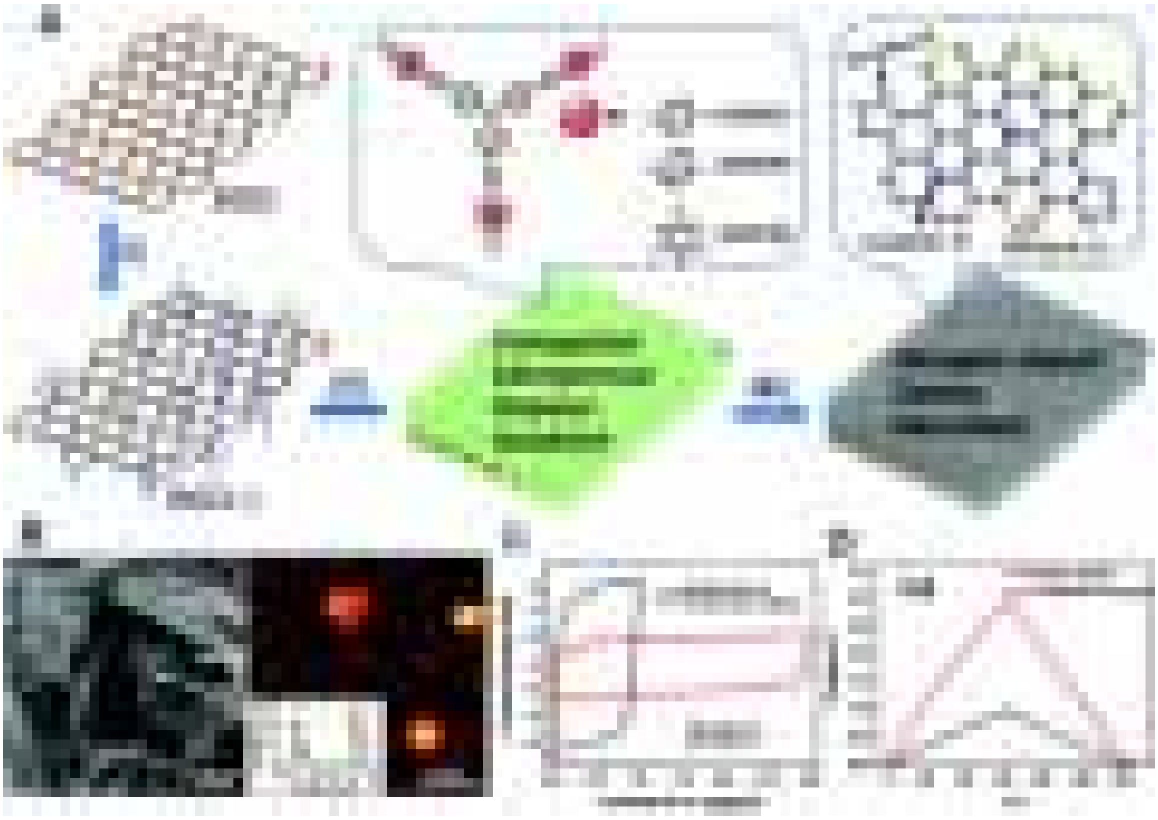

Fig. 47. (A) Preparation of graphene-based conjugated microporous polymer sandwiches and related nitrogen-doped microporous carbon nanosheets. (i) Sodium dodecylbenzenesulfonate, 4-iodophenyl diazonium salt, 0 °C (2 h) to room temperature (RT) (4 h); (ii) building blocks: tris(4-ethynylphenyl)amine and 2,5-dibromopyridine, or 2,5-dibromopyrazine, or 2,4,6-trichloro-1,3,5-triazine, argon, $Pd(PPh_3)_4$,CuI, Et_3N, DMF, 120 °C, 3 days; (iii) argon, RT to 800 °C, 10 °C min $^{-1}$, 2 h. (B) SEM (left), and AFM (right, inset: thickness analyses along the marked line) of GMP2N. (C) CV and (D) GCD curves of three GMP2NC-based supercapacitor devices connected in series. [433], Copyright 2017. Reproduced with permission from The Royal Society of Chemistry and the Chinese Chemical Society.

the 21st century, energy crisis and environmental pollution have become two major problems in human development. Meanwhile, more than 200 years have passed since the concept of fuel cells was proposed, they seem to have become one of the most potential options to solve the energy crisis and environmental pollution. Currently, the use of CMPs as an oxygen reduction electrodes for fuel cells [436-440], in particular, the redox activity and conductive CMPs, is aimed at addressing three essential points that limit the development of oxygen reduction reaction (ORR): (i) construction of low-cost electrode materials, (ii) construction of conductive structures, and (iii) production of sufficient O_2 binding sites in porous networks. Here, recent advances in the use of CMPs as a platform for fuel cells are described (Table 6) [436-438,440-445], including CMPs as an electrode catalyst for fuel cells, and CMPs as catalysts carriers or catalysts precursors for fuel cells.

6.5.1. CMPs as electrode catalysts for fuel cells

Currently, pure metal-free original CMPs as oxygen reduction catalysts used in fuel cells are still rarely reported. Maji et al. prepared electrochemical active CMPs, TPA-BP-1 and TPATPE-2, by Sonogashira–Hagihara coupling of tris(4bromophenyl)amine with 1,1,2,2,–4,4′-diethynylbiphenyl and with tetrakis(4-ethynylphenyl)ethane, respectively (Fig. 48A) [442]. The prepared CMPs system has a dense nitrogen site that is easy to bind to oxygen molecules. The prepared CMPs system has a dense nitrogen site that is easy to bind to oxygen molecules, and tris(4-bromophneyl) amine as hole-transporting bodies, and 1,1,2,2,tetrakis(4-ethynylphenyl)ethane and 4,4′-diethynylbiphenyl as suitable acceptors, the whole system is easier to transfer electrons and easier to carry out electrocatalytic reduction and has appropriate ORR onset potential and good current stability. Cyclic voltammetric curves, linear sweep voltammetric curves, and the chronoamperometric study indicate the potential application of these metal-free CMPs in ORR (Fig. 48B). These metal-free porous organic catalysts open the way for low-cost and effective fuel cells due to the appropriate donor nodes and acceptor units in their structure.

Phthalocyanines (Pcs) and porphyrins (Pors), nitrogen-rich conjugated macrocycles, both have excellent electrocatalytic activity, and CMPs based on Pcs-Pors are still infrequent. Liu et al. proposed a strategy to alternately connect phthalocyanine monomers and porphyrin monomers into 2D conjugated porous networks through aromatic linkage, including FePcZnPor-CMP, ZnPcFePor-CMP, FePcFePor-CMP, and ZnPcZnPor-CMP [441]. The main advantage of this strategy is that the 2D porous network structure composed of conjugated macrocycles and aromatic links and the complete π-conjugated structure is conducive to the complete exposure of the catalytic active sites and the promotion of electron transfer. The results of CV showed that two kinds of FePc-CMPs showed excellent ORR catalytic activity in an alkaline environment, with $E_{1/2}$ up to 0.863–0.866 V. These results are beneficial to the design and synthesis of new catalysts with enhanced ORR catalytic properties.

6.5.2. CMPs as supports of catalysts for fuel cells

CMPs are excellent carriers of catalytic active components because of their highly stable porous skeleton [446]. In the previous discussion, Roy et al. demonstrated the role of TPA as a redox center in electrochemical reduction [442]. Recently, Maji et al. reported a donor-receptor CMPs (TPA-PDI) based on tris-(4-

Table 6
CMPs or CMP derivatives for oxygen reduction reactions of fuel cells.

CMPs		Molecular structure	S_{BET} (m^2 g^{-1})	V_{total} (cm^3 g^{-1})	E_{onset}	$E_{1/2}$	Electrolyte	Ref.
CoPEF		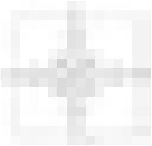	311	–	0.42	–	0.5 M H_2SO_4	[436]
ZnPcFePor-CMP		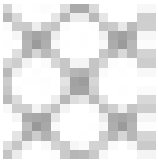	442	0.22	0.902	0.724	0.1 M KOH	[441]
FePcFePor-CMP		–	322	0.17	0.934	0.863	0.1 M KOH	[441]
FePcZnPor-CMP		–	404	0.22	0.936	0.866	0.1 M KOH	[441]
TPA-BP-1		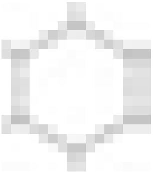	468	–	0.80	–	0.1 M KOH	[442]
TPA-BP-2		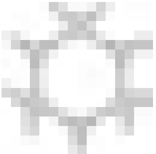	117	–	0.82	–	0.1 M KOH	[442]
CMP derivatives	CMP precursor	Molecular structure[a]	S_{BET}[b] (m^2 g^{-1})	V_{total}[c] (cm^3 g^{-1})	E_{onset}	$E_{1/2}$	Electrolyte	Ref.
Fe/Co-CMP-800	Fe/Co-CMP	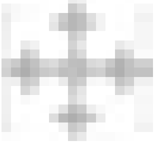	372	–	0.88	0.78	0.5 M H_2SO_4	[437]
N/S-2DPC-60	2DP-S	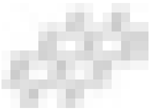	953	0.80	0.86	0.75	0.1 M KOH	[443]
HPC-Fe/N-700	HCMP-Fe	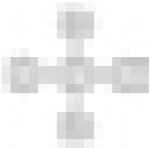	518	–	0.92	0.84	0.1 M KOH	[438]
N-Fc-800	Fc-melamine-POP	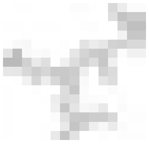	511	–	0.96	0.82	0.1 M KOH	[444]
CoNCs800	CoPc-CMP	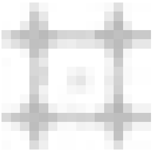	59.8	–	0.905	0.807	0.1 M KOH	[445]
CoO/ZnO@N-PC	ST-CMP	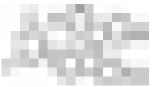	1236	0.68	0.91	0.85	0.1 M KOH	[440]

E_{onset} for onset potential (V vs. RHE); $E_{1/2}$: half-wave potential. [a] molecular structure of precursor. [b, c] BET surface area, and pore volume of CMP derivatives.

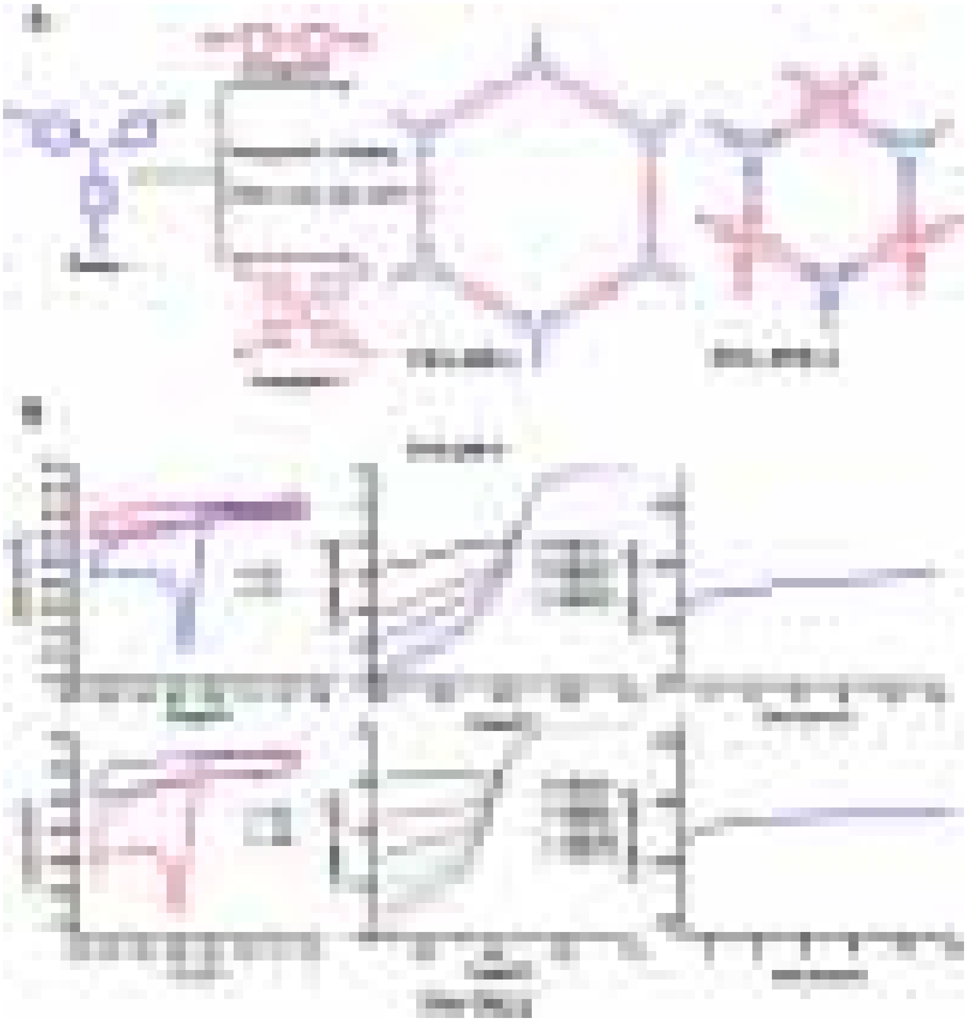

Fig. 48. (A) Synthetic scheme towards the fabrication of two redox-active and semi-conducting CMPs. (B) Cyclic voltammetric curves for TPA-BP-1 under O_2 saturated (blue) and N_2 saturated (red), TPA-TPE-2 under O_2 saturated (red) and N_2 saturated (blue) (left); Linear sweep voltammetric curves observed under different rotation speeds of glassy carbon electrode for TPABP-1 and TPA-TPE-2 (middle); Chronoamperometric study for TPA-BP-1 and TPA-TPE-2 (right). [442], Copyright 2018. Reproduced with permission from The Royal Society of Chemistry.

aminophenyl)amine (TPA) and perylenediimide (PDI) with stable charge separation and semiconductor behavior [212]. PDA and its derivatives are excellent electron acceptor parts that bind to TPA to produce efficient electron transfer within the networks. TPA is the redox catalytic activity center, which can reduce metal salts into their nanoparticles. TPA-PDI, with their conductivity and natural oxygen binding site, is an excellent metal-free catalyst for catalytic ORR, and can also be used as an excellent carrier of metallic (Au and Co) NPs (Fig. 49A). The Au and Co NPs are uniformly and stably loaded on the TPA-PDI matrix (Fig. 49B-E), and the two new nanocomposites (Au@TPA-PDI and Co@TPA-PDI) have significantly improved overall electrocatalytic activity and stability.

6.5.3. CMPs as precursors of catalysts for fuel cells

As mentioned above, the graphene excitation strategy is an emerging strategy for the synthesis of CMP films with large aspect ratio and high specific surface area, which can be used for the pyrolysis of heteroatom-doped 2D porous carbon. Feng's group based on monomers of thiophene-, thiazole- and pyridine- polymerized with 1,3,5-triethynylbenzene on the surface of graphene via Sonogashira-Hagihara reaction to obtain a large aspect ratio and high surface area porous polymer nanosheet (GMPs), thiophene-containing GMP-S, thiazole-containing GMP-NS, and pyridine-containing GMP-N, then template-less thermal carbonization of the polymer nanosheets produced 2D heteroatom-doped porous carbon (GMC), GMC-S, GMC-NS, and GMC-N (Fig. 50A) [430]. The TEM images (Fig. 50B) display many independent flakes in a form like graphene. CV (Fig. 50C) shows that the ORR onset potential of GMC-S is 0.15 V and the peak potential is 0.28 V, lower than that of GMC-NS and GMC-N. The galvanostatic charge/discharge curves experiment (Fig. 50D) shows GMCs' excellent ORR performance and excellent supercapacitive behavior (244–304 F g^{-1} at 0.1 A g^{-1}).

Furthermore, Feng's group prepared templated 1D CMP by the layer-by-layer templating method and used it as a precursor for direct pyrolysis to product 1D three-layers heteroatom-doped porous carbon nanotube (CNT). The CNT has a high specific surface area of up to 750 m^2 g^{-1}, graded porous structure, and outstanding electrochemical catalytic performance for ORR [177]. The Diffusion-limited current density of 4.4 mA cm^{-2} and electron transfer number of 3.8 of three-layer CNT are superior to the correlated arbitrary 1D porous carbon, which shows that reasonable design and control of the shape types of CMP and derived heteroatomized porous carbon is an excellent strategy for the preparation of fuel cells with excellent performance.

Similarly, Scherf et al. prepared a MoS_2 template Co-containing CMP (MoS_2-Co-CMP) sandwich using a structurally oriented, base plane functionalized MoS_2 template [447]. MoS_2-Co-CMP pyrolysis and acid leaching resulted in a MoS_2-cored layered porous car-

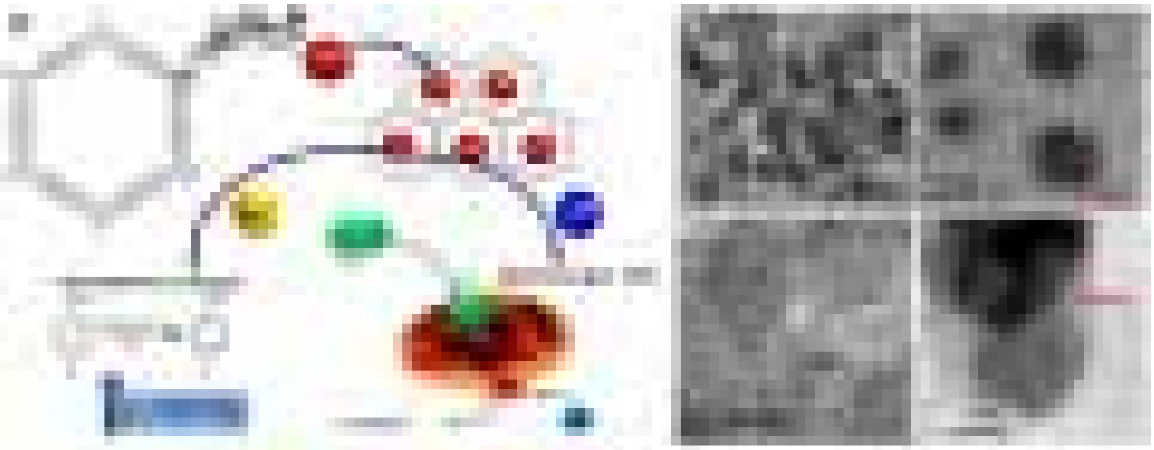

Fig. 49. (A) Schematic Representation Showing in Situ Stabilization of Au and Co NPs in the CMP Matrix. (B) TEM image of Au NPs stabilized in the matrix of TPA–PDI. (C) HRTEM image of Au@TPA–PDI showing lattice fringes. (D) TEM image of Au NPs stabilized in the matrix of TPA–PDI. (E) HRTEM image of Co@TPA–PDI showing lattice fringes. [212], Copyright 2019. Reproduced with permission from the American Chemical Society.

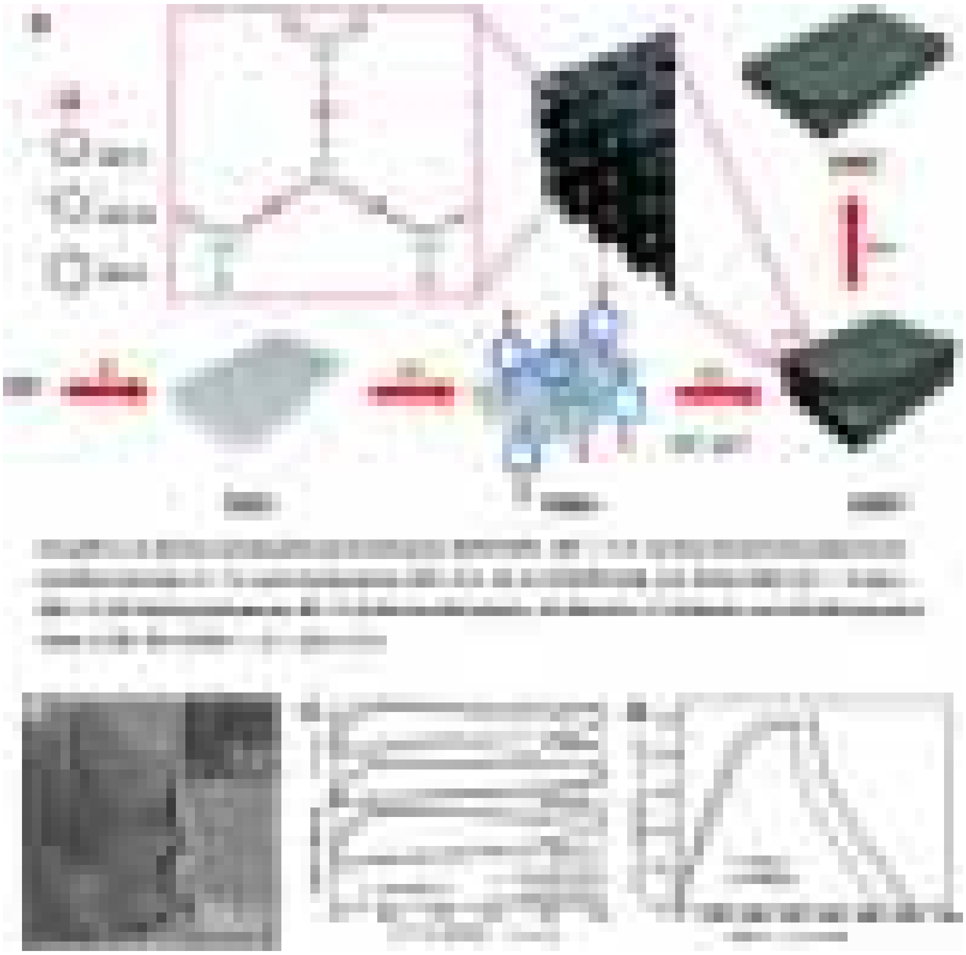

Fig. 50. (A) Preparation of GMPs and related graphene-based microporous carbons (GMCs). Graphene-based 2D porous carbons (GMCs) and their ORR performances: (B) TEM image of GMC-S; (C) CV curves of GMCs in N_2-saturated (dashed line) and O_2-saturated (solid line) 0.1 m KOH at a scan rate of 50 mV s^{-1}; (D) galvanostatic charge/discharge curves of MC-S and GMC-S at a current density of 0.1 Ag $^{-1}$. [430], Copyright 2013. Reproduced with permission from the John Wiley & Sons Inc.

bon hybrid (MoS_2-Co-C) with a high specific surface area. Layered porous carbon shells with uniformly distributed N-doped atoms, and catalysis of CoN and/or CoNC motifs are involved, as well as, there may be a synergistic effect between the MoS_2 template and the heteroatom-doped porous carbon shell. Therefore, the MoS_2-Co-C sample has a high electrochemical energy storage capacity for ORR, its high capacitance value is up to 288 F g^{-1}, and it has significant cycling stability (capacitance retention of 99% at 5 A g^{-1} over 4000 cycles).

Klaus et al. synthesized Fe/Co N-doped carbon without templates using porphyrin-based CMPs as precursors [437]. It has inherent porosity and large surface area, excellent thermal stabil-

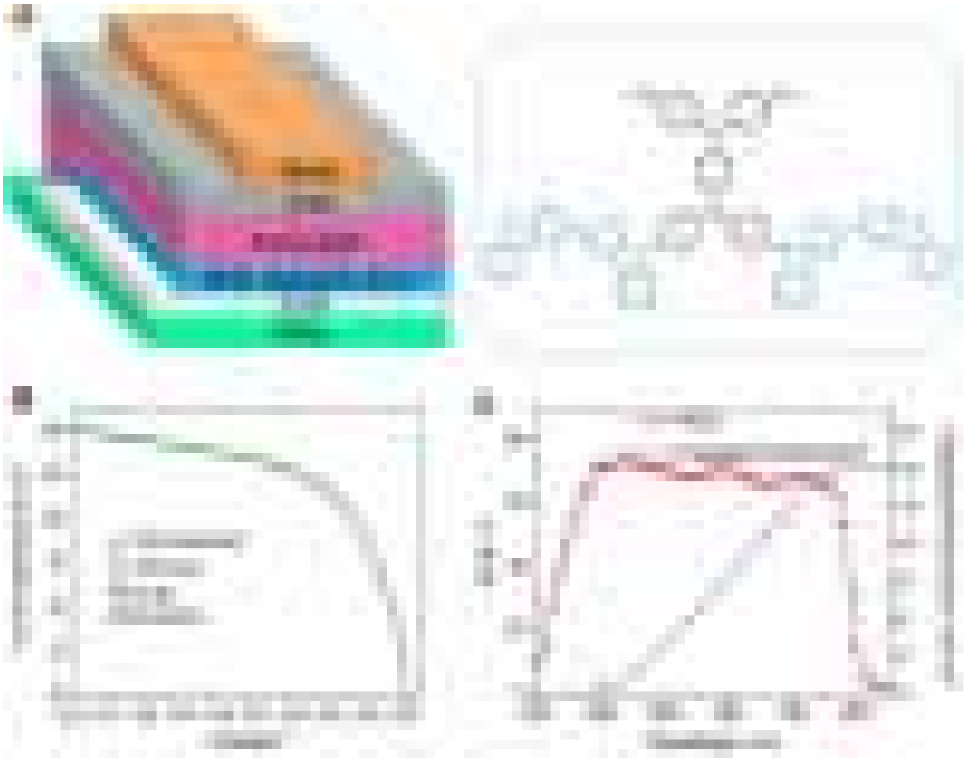

Fig. 51. (A) Schematic representation of the device structure and Structural formula of PAF-86. (B) $J-V$ curve of the PAF film based PSC, and (C) IPCE spectra and integral photocurrent of the PAF film based PSC. [467], Copyright 2017. Reproduced with permission from American Chemical Society.

ity, and high density of MN_4 (CoN_4 and FeN_4) units with precise connections. The reasonable localization of the active site of MN_4 is conducive to enhancing the performance of non-noble metal-based catalysts for ORR. Among them, the presence of CoN_4 contributes to the increase of the ratio of catalytic active substances, and the spatial distance between CoN_4- and FeN_4- sites can compensate for the catalytic selectivity of CoN_4, as well as the FeN_4 site has a higher electron density. Meanwhile, Chen's group prepared N-rich porous organic polymers by Schiff-base method of ferrocene (Fc) with melamine/melem, as a precursor, the polymers were carbonized to obtain N-doped porous carbon nanocomposites [444]. Among them, The N-Fc-800 as a cathode catalyst to assemble a rechargeable zinc-air battery, showed excellent catalytic activity, with a high onset potential of 0.96 V and a half-wave potential of 0.82 V, as well as excellent stability and charging and discharging cycles (200 cycles). These non-noble metal catalysts are conducive to improving the electrochemical performance of the ORR catalytic material, which contributes to the development of new, cost-effective, and environmentally friendly materials for fuel cells.

Wang et al. loaded metal nanoparticles in situ into N-doped carbon matrixes (MNCs) based on heat-treated metallophthalocyanine-CMPs [445]. Various metal nanoparticles, including Co, Fe, and Cu, can be uniformly immobilized in the porous N-doped carbon frameworks and interact with the N active site, which acts as a catalyst for ORR and show enhanced diffusion kinetics. Due to the effective synthesis strategy and specific structure, the obtained MNCs showed high catalytic performance on ORR in both alkaline and acidic media, with a larger half-wave potential and a favorable limiting current, and almost carried out oxygen reduction reaction for the four-electron transfer pathway. MNCs, as a cathode catalyst for Zn-air batteries with stability and methanol acceptance, provides a new strategy for the design and preparation of highly active ORR composite catalysts for fuel cells.

6.6. CMPs for solar cells

Organic photovoltaic (OPV) devices, under irradiation, the active layer is stimulated by light to generate a charge that is transmitted to the electrode to provide a photovoltaic effect, which has always been the star attraction in the field of clean energy [80,448,449]. Among them, perovskite solar cells (PSCs) has the advantages of a high light absorption factor, wide spectral absorption range, rapid carrier migration speed, and long diffusion length, and the solid PSCs can overcome the technical difficulties of encapsulation in practical application, their power conversion efficiency (PCE) has increased from 3.8% to more than 20% in the past few years [450-452]. PSCs generally consist of metal electrode, hole-transporting layer (HTL), perovskite layer, mesoscopic support, and electronic selective layer (ESL). Currently, indium tin oxide (ITO) is usually used as an anode to collect holes, and low-power function metals (such as Al and Ag) are usually used as cathodes to collect electrons. The insertion of the HTL between the ITO electrode and the active layer can facilitate hole extraction and thus enhance PCE [453,454]. Poly(3,4-ethylenedioxythiophene):polystyrenesulfonate (PEDOT:PSS) is used as the main material in the HTL owing to its high conductivity, low opacity, and outstanding film formation [455]. However, the moisture absorption and acidity of PEDOT:PSS tends to erode ITO, resulting in poor chemical stability of PEDOT-based devices and a rapid decline inefficiency, which greatly reduces the actual service life of solar cells. To find the candidate materials of PEDOT:PSS and improve the stability of PSCs, many attempts have been made in the search for new HTL materials, such as transition metal oxides [456-460] and other conducting polymers [461-464]. Although these materials have made progress in some aspects, the search for effective HTL materials remains one of the major challenges for organic photovoltaic cells. CMPs have monomers with non-planar configuration, adjustable morphology and structure, and skeletons

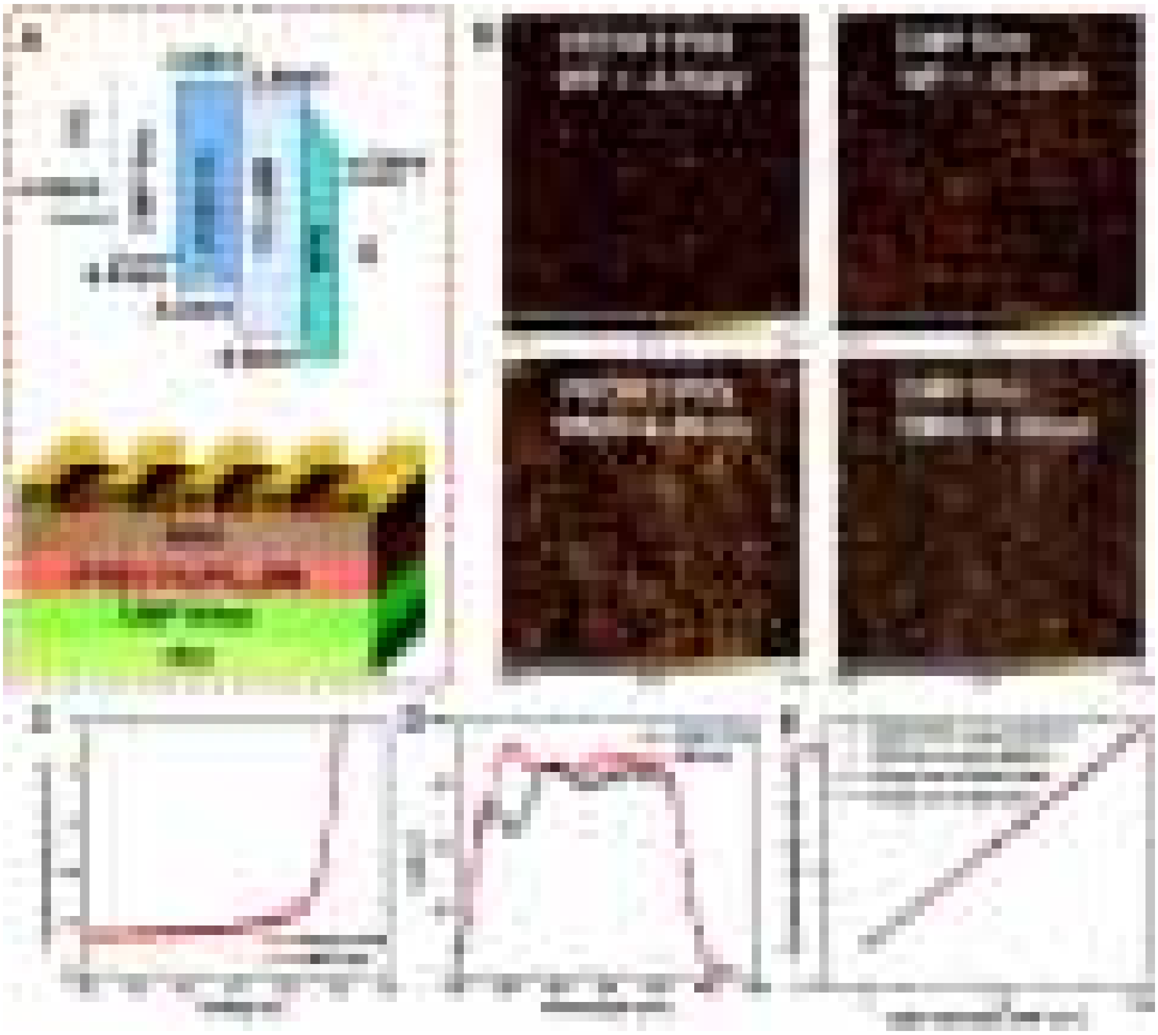

Fig. 52. (A) Energy alignment of the CMP film and other materials (top), and Device configuration of organic solar cells with the CMP film as a hole transporting layer (below). (B) KPFM images of PEDOT:PSS and various CMP films captured by atomic force microscopy in the Kelvin probe mode: WFs of PEDOT:PSS and CMP films, and roughnesses of PEDOT:PSS and CMP films. (C-E) $J-V$ characteristics of devices under 1 sun irradiation (100 mW cm $^{-2}$) based on CMP films prepared under different CV deposition conditions: (C) $J-V$ curves and (D) EQE data of PEDOT:PSS- and CMP-devices, and (E) Irradiation intensity-dependent Jsc of PEDOT:PSS and CMP containing devices. [468], Copyright 2018. Reproduced with permission from The Royal Society of Chemistry.

conducive to charge transmission [86,465,466], which are popular materials for HTL in recent years.

The porous aromatic matrix (PAF-86) thin film prepared by Zhu et al., using the electropolymerization (EP) method, was used as a stable HTL material for the first time in inverted PSCs (Fig. 51A) [467]. The monomer M1 of PAF-86 film not only has the function of electronic and electrochemical (EC) to provide effective active sites. The prepared PAF-86 film has the advantages of dense and smooth surface, reasonable pore structure, strong electronic blocking ability, and good stability. Meanwhile, the EP process is simple, controllable, and operates under environmental conditions, so it is appropriate for industrial large-scale production. The $J-V$ curve of PSC shows that the PAF-86 film has PCE of 9.84%, J_{sc} of 18.23 mA cm $^{-2}$, V_{oc} of 0.91 V, fill factor of 0.59 (Fig. 51B), and the corresponding incident-photon-to-current conversion efficiency (IPCE) spectra (Fig. 51C) showed that the comprehensive current density consistent with the result of $J-V$ was 18.23 mA cm $^{-2}$, the IPCE value can reach about 70% in the range of wavelength 390 ~ 760 nm. At room temperature of 20 ~ 30 °C and relative humidity of 30 ~ 35%, the PAF-86 thin-film PSC has excellent stability and retains about 80% PCE in the air without encapsulation. Under the same condition, the PCE performance of the PSC device based on PEDOT:PSS drops sharply to 4% of the original PSC. Compared with other existing HTL materials, PAF- 86 thin-film has the following advantages, small dosage of monomer, synthesis of mild conditions, energy consumption is reduced, and the cost high polymer chemical and mechanical stability, which is advantageous to the assembly of flexible, lightweight, portable organic photovoltaic devices and provides more choices for PSCs HTL materials.

Based on the carbazole group, Zhou et al. were successfully prepared a pH neutral CMP films by in-situ electrochemical deposition, which were used as HTL materials in OPVs (Fig. 52A) [468]. This strategy has the following advantages: (i) The non-planar configuration of the monomer of the CMP films can promote charge transfer. (ii) The film thickness can be precisely controlled by the scanning cycle and the cost can be saved. (iii) A pH neutral CMP films helps prevent erosion of OPVs. The morphologies and energetics of the synthesized CMP films and PEDOT:PSS are shown in Fig. 52B. Compared with PEDOT:PSS (−4.94 eV), CMP thin films has higher work function (WF, −5.03 eV), which can promote hole extraction of OPVs, and the surface roughness of CMP is slightly lower, which is conducive to solution deposition of OPVs active layer. The $J-V$ curve (Fig. 52C) of the device indicates that the efficiency of CMP device is slightly higher than that of PEDOT:PSS device, V_{oc} increases from 0.78 to 0.80 V, and J_{sc} increases from 15.94 to 16.14 mA cm $^{-2}$, which may be due to the built-in potential, modulated charge composition, and deeper HOMO level of CMP films. It can be seen from the external quantum efficiency spectrum (Fig. 52D) that CMP films have higher external quantum efficiency (EQE) in two spectral ranges (360 nm to 470 nm and 520 nm to 700 nm), which confirms the increase of J-V. Meanwhile, the illumination intensity-dependent J_{sc} in these two devices (Fig. 52E) indicated that the main bimolecular charge was approximately retained in the solar cells of CMP-based HTL. In terms of practical applications, electrochemical polymerization of CMP films shows great potential in OPVs.

7. Conclusions and perspectives

The clean energy systems will be the most important system in the energy field of the future. Compared with other inorganic and organic materials, the unique multi-function CMPs can provide adjustable and improved functions, which has been regarded as a transformational breakthrough in this field. CMPs have organic structures, conductive skeletons, and adjustable energy levels, and scientists are working on using CMP materials for energy-related applications. As previously mentioned, as a classic π-conjugated polymer, they offer a new platform with opportunities in the application of this type of polymers in gas storage, photocatalysis, and energy storage. However, to make these polymer network structures more efficient and able to compete with other excellent materials that have been developed, some significant exploration and improvements are needed. Here, we give a summary and a discussion of the challenges and future directions in the field, including design and synthesis, functionality, and applications.

7.1. Adjustment of pore and bandgap structure

Most CMPs synthesis routes involve metal-catalyzed carbon-carbon cross-coupling reactions. However, simple polymerization techniques without metal catalysts need to be further developed, allowing the use of industrial-scale metal-free polymerization routes while preserving the properties of the polymers. They are amorphous and have no long-period molecular ordering, but the flexibility of molecular design, structural tunability, and variety of synthesis methods give CMP with different structures and function the characteristic of "predictable". Based on carefully selecting the monomer or functional group and the multifunctional connector, CMPs can adjust various properties, including pore properties and electronic structure.

Efforts in design, synthesis, and function over the past few years have led to advances in the field of property regulation of CMPs. As a powerful platform for the design of porous materials, CMPs have made progress in the field of property regulation in design, synthesis, and function over the past few years. They provide an effective strategy for regulating porosity, pore environment, and function. However, the current realization of CMP materials with a high surface area of more than 5000 $m^2\ g^{-1}$ remains a formidable challenge. High surface area, definite pore size, and controlled pore size distribution are important for selective adsorption and storage of fuel molecules or chemicals of CMP. The careful selection of functional groups on the surface of CMP pores is expected to lead to a breakthrough based on synthetic reactions in an adjustment of pore structure and characteristics of CMPs.

Furthermore, as a platform for designing π-conjugated materials, CMPs can be used to develop 3D polymer networks for exciton migration and carrier transport. The enhancement of charge carrier mobility and conductivity of these polymer materials is important for photoelectric applications. In this respect, the synthesis of low bandgap CMPs is particularly important but remains challenging. To systematically study the electronic structure-property correlation of CMPs are needed, which is not clear in many CMP photo- and electro-catalysts but is helpful for their further design. Similarly, the dynamic distribution of charge in these CMP networks is an important aspect to be explored in areas such as energy storage, conversion, and catalysis. Of these challenges, the most immediate concern is controlling the energy levels of such conjugated semiconductor materials. For example, in the process of light energy conversion, one must fully understand the location of the HOMOs and the LUMOs. In fact, in some field, such as photocatalytic devices, a mismatch in the energy levels of equipment components made of polymer materials can lead to inefficiencies in the devices. The development of a reliable method or technique to predict and/or specify their HOMOs and LUMOs levels would be a breakthrough for these materials.

7.2. Development of CMP composites and derived materials

At present, CMP materials serve as promising energy storage materials [75,469] although they have many advantages unmatched by other porous materials, there are still many places to be explored. Doping behavior [360,470] can enhance the catalytic activity and stability of traditional CMP catalysts. As a platform for designing collaborative catalytic systems, the resulting CMP composites can be used in energy conversion systems if different functions, such as photo-capture components, redox-active components, and catalytic centers, can be doped into the networks. However, the intrinsic relationship between doping behavior and the specific properties of these CMPs has not yet been established, by doping accurately obtain excellent features of CMP catalyst still need further exploration.

Besides, CMPs encapsulate nanoparticles [154,471-473] to produce composites that can be used for energy applications in more demanding environments. For our best knowledge, some metal-free CMPs cannot alone provide the energy and environment required for the conversion of light energy. With the further development of CMPs, the research on the reaction mechanism of their light energy conversion extends to how to maximize the utilization of the “naked” CMP materials that have been developed. The features of existing excellent CMPs have not yet been systematically developed and need to be fully explained before CMP application research can be extended. CMPs has design flexibility and diversity of building monomer, in the case that CMPs cannot meet the requirements of light energy conversion. Individuals can through the metal loading or post-synthesis modification to introduced various impurity atoms and metal species into the porous networks effectively to realize the control metal-mixed compound synthesis and heterostructure and to simplify the metal recovery process. As the study continued to expand, CMPs, as a whole platform, show urgency not only in light energy conversion but also in other areas of clean energy, such as electrical energy storage.

Finally, porous carbon is widely used in the field of clean energy [474-478]. CMPs as their precursors’ pyrolysis to prepare CMPs derived porous carbon materials [177,443] is a promising strategy. For example, the pyrolysis of MPc-CMPs is an effective strategy for the construction of N-doped carbon compounds without the need for additional templates [445]. However, the loss of coordination of metal nitrogen during direct pyrolysis requires attention in the synthesis of other CMP-derived materials using this strategy.

7.3. Extend the optoelectronic applications of CMPs

In recent years, it has been found that CMPs can replace the traditional homogeneous catalyst effectively in a variety of optoelectronic applications [72]. In terms of morphology, these polymer materials have broken through simple amorphous powders, such as nanoparticles and nanotubes, thin films, and macroscopic bulks. The further development of CMPs in optoelectronic applications, especially under the condition of a continuous flow of photoreactor, needs to solve the problems of photon flux and continuous reaction. For example, these materials need to be compatible with a variety of solvents in a flow reactor and react very efficiently at low energy wavelengths [117]. Compared with traditional photocatalysts, the construction of CMPs which can absorb low-energy wavelengths of light is conducive to efficient utilization of energy, greater optical stability, and less photodegradation. Most of the reported work has focused on the electron donor (p-type) component, such as carbazole and tetraphenylvinyl, and the corresponding CMPs [49,176,479], as well as the introduction of electron acceptor (n-type) species to build a promising transfer of charge/energy [480,481]. Furthermore, as mentioned in our previous review [72], water wettability and biocompatibility of CMP materials also need to be addressed when attempting to compete with more conventional and mature photocatalysts such as enzymes, especially for larger-scale optoelectronic applications.

7.4. Application prospects of CMPs in clean energy

CMPs as a new class of porous materials still have challenges in practical application [326,482-485]. For example, in the field of hydrogen energy: (i) How to improve the hydrogen adsorption performance of CMPs at a convenient temperature. (ii) How to synthesize more heat-stable CMPs and use them in the pyrolysis of chemical hydrides to produce hydrogen. (iii) How to improve the catalytic activity of CMPs and clarify the specific catalytic mechanism. (iv) How to develop other hydrogen production methods. Meanwhile, LIBs are very common in clean energy devices, and CMPs have shown great potential as an electrode material for LIBs. The integration of the advantages of CMPs into traditional LIB materials would facilitate the development of a new generation of batteries. However, currently, most reported electrochemical properties of CMPs are not comparable to those of commercial electrode materials. The challenges with LIBs are: (i) To prepare stable CMP electrode materials to prevent excessive volume changes during the entire ion insertion/extraction process. (ii) To discover more effective electroactive structures and deeper understand the charge/ion transport mechanism to improve electrode stability. (iii) To solve the compatibility problem between electrode material and electrolyte. (iv) To increase the discharge-recharging cycle, capacity, and cycle life of the electrode material.

For fuel cells, the low cost and adjustable properties of CMPs can act as electrolytes, electrode catalysts, and catalyst precursors for fuel cells. The major challenges that remain are improving efficiency, energy density, and improving reliability and reducing application costs. Meanwhile, as a kind of renewable energy storage device, the supercapacitor has been widely used in various electroluminescent devices. In supercapacitor applications, the development of high specific surface areas, suitable holes, low internal resistance, good cycling performance, and low-cost CMP electrode materials remains a challenge. Therefore, for fuel cells, LIBs, and supercapacitor applications, the industrialization of CMPs as the main catalysts and the precursors or carriers of catalysts still has a long way to go. Additionally, the investigation of the application of CMPs in solar cells has just started, and the corresponding reports are still very few, but the application of CMPs in solar cells is one of the future research priorities.

7.5. Summary

In summary, the past efforts in design, synthesis, and functional exploration have shown that CMPs are a powerful platform for structural and functional design, and many CMP-based materials with high chemical and thermal stability and excellent performance have been reported. We look forward to a bright and promising future for CMPs as a robust platform for addressing challenging environmental and energy issues. Currently, there are two main goals for the development of CMPs in clean energy: One is to maximize the application of existing CMP-based materials in the clean energy field; the other is to synthesize new CMPs by optimizing synthetic monomers, links, and synthesis methods and conditions to develop more outstanding CMP candidate materials for clean energy. Finally, CMP materials and clean energy are a rapidly growing field that will yield many excellent results even as we write this review. Therefore, it is difficult to consider all the work in the limited space and time, and we apologize to our readers for this.

Declaration of Competing Interest

The authors declare that they have no known competing financial interests or personal relationships that could have appeared to influence the work reported in this paper.

CRediT authorship contribution statement

Songhao Luo: Conceptualization, Writing – original draft, Visualization. **Zhuotong Zeng:** Funding acquisition, Writing – review & editing. **Han Wang:** Writing – review & editing, Visualization. **Weiping Xiong:** Funding acquisition, Writing – review & editing. **Biao Song:** Writing – review & editing. **Chengyun Zhou:** Writing – review & editing. **Abing Duan:** Writing – review & editing. **Xiaofei Tan:** Writing – review & editing. **Qingyun He:** Resources. **Guangming Zeng:** Funding acquisition, Project administration, Supervision. **Zhifeng Liu:** Funding acquisition, Supervision, Writing – review & editing. **Rong Xiao:** Funding acquisition, Supervision.

Acknowledgments

The study was financially supported by the Program for Changjiang Scholars and Innovative Research Team in University (IRT-13R17), the National Natural Science Foundation of China (U20A20323, 82003363, 82073449, 52000064, 51521006, 51378190, 51039001, 51979103, 51679085, 51308200), the Fundamental Research Funds for the Central Universities of China (531107050930, 531107051205), the Funds of Hunan Science and Technology Innovation Project (2018RS3115), the Key Research and Development Project of Hunan Province of China (2017SK2241) and the Three Gorges Follow-up Research Project (2017HXXY-05).

References

[1] Davis SJ, Caldeira K, Matthews HD. Future CO2 emissions and climate change from existing energy infrastructure. Science 2010;329:1330–3.
[2] Wang W, Tade MO, Shao Z. Research progress of perovskite materials in photocatalysis- and photovoltaics-related energy conversion and environmental treatment. Chem Soc Rev 2015;44:5371–408.
[3] Le Quere C, Korsbakken JI, Wilson C, Tosun J, Andrew R, Andres RJ, Canadell JG, Jordan A, Peters GP, van Vuuren DP. Drivers of declining CO2 emissions in 18 developed economies. Nat Clim Change 2019;9:213–17.
[4] Li S-L, Xu Q. Metal-organic frameworks as platforms for clean energy. Energy Environ Sci 2013;6:1656–83.
[5] Kittner N, Lill F, Kammen DM. Energy storage deployment and innovation for the clean energy transition. Nature Energy 2017;2:17125 /1-6.
[6] Gao M, Zhu L, Peh CK, Ho GW. Solar absorber material and system designs for photothermal water vaporization towards clean water and energy production. Energy Environ Sci 2019;12:841–64.
[7] Wang Q, Domen K. Particulate photocatalysts for light-driven water splitting: mechanisms, challenges, and design strategies. Chem Rev 2020;120:919–85.
[8] Wang Z, Li C, Domen K. Recent developments in heterogeneous photocatalysts for solar-driven overall water splitting. Chem Soc Rev 2019;48:2109–25.
[9] He T, Pachfule P, Wu H, Xu Q, Chen P. Hydrogen carriers. Nat Rev Mater 2016;1:16067 /1-17.

[10] Li Y, Fu Z-Y, Su B-L. Hierarchically structured porous materials for energy conversion and storage. Adv Funct Mater 2012;22:4634–67.
[11] Ji L, Meduri P, Agubra V, Xiao X, Alcoutlabi M. Graphene-based nanocomposites for energy storage. Adv Energy Mater 2016;6:1502159 /1-73.
[12] Lee S, Kwon G, Ku K, Yoon K, Jung S-K, Lim H-D, Kang K. Recent progress in organic electrodes for li and na rechargeable batteries. Adv Mater 2018;30:1704682 /1-45.
[13] Hwang J-Y, Myung S-T, Sun Y-K. Recent progress in rechargeable potassium batteries. Adv Funct Mater 2018;28:1802938 /1-45.
[14] Hu Z, Zhu Z, Cheng F, Zhang K, Wang J, Chen C, Chen J. Pyrite FeS2 for high-rate and long-life rechargeable sodium batteries. Energy Environ Sci 2015;8:1309–16.
[15] Xia BY, Yan Y, Li N, Wu HB, Lou XW, Wang X. A metal-organic framework-derived bifunctional oxygen electrocatalyst. Nature Energy 2016;1:15006 /1-8.
[16] Nie Y, Li L, Wei Z. Recent advancements in Pt and Pt-free catalysts for oxygen reduction reaction. Chem Soc Rev 2015;44:2168–201.
[17] Borghei M, Lehtonen J, Liu L, Rojas OJ. Advanced biomass-derived electrocatalysts for the oxygen reduction reaction. Adv Mater 2018;30:1703691 /1-27.
[18] Xiao Z, Yuan Y, Shao Y, Wang Q, Dong Q, Bi C, Sharma P, Gruverman A, Huang J. Giant switchable photovoltaic effect in organometal trihalide perovskite devices. Nat Mater 2015;14:193–8.
[19] Cao W, Xue J. Recent progress in organic photovoltaics: device architecture and optical design. Energy Environ Sci 2014;7:2123–44.
[20] Song T-B, Chen Q, Zhou H, Jiang C, Wang H-H, Yang Y, Liu Y, You J, Yang Y. Perovskite solar cells: film formation and properties. J Mater Chem A 2015;3:9032–50.
[21] Wang F, Wu X, Yuan X, Liu Z, Zhang Y, Fu L, Zhu Y, Zhou Q, Wu Y, Huang W. Latest advances in supercapacitors: from new electrode materials to novel device designs. Chem Soc Rev 2017;46:6816–54.
[22] Shao Y, El-Kady MF, Wang LJ, Zhang Q, Li Y, Wang H, Mousavi MF, Kaner RB. Graphene-based materials for flexible supercapacitors. Chem Soc Rev 2015;44:3639–65.
[23] Yang P, Mai W. Flexible solid-state electrochemical supercapacitors. Nano Energy 2014;8:274–90.
[24] Liang Y, Tao Z, Chen J. Organic electrode materials for rechargeable lithium batteries. Adv Energy Mater 2012;2:742–69.
[25] Liang YL, Zhang P, Chen J. Function-oriented design of conjugated carbonyl compound electrodes for high energy lithium batteries. Chem Sci 2013;4:1330–7.
[26] Yokoji T, Kameyama Y, Maruyama N, Matsubara H. High-capacity organic cathode active materials of 2,2′-bis-p-benzoquinone derivatives for rechargeable batteries. J Mater Chem A 2016;4:5457–66.
[27] Ellis BL, Lee KT, Nazar LF. Positive electrode materials for Li-ion and Li-batteries. Chem Mater 2010;22:691–714.
[28] Zhang M, Qu BH, Lei DN, Chen YJ, Yu XZ, Chen LB, Li QH, Wang YG, Wang TH. A green and fast strategy for the scalable synthesis of Fe2O3/graphene with significantly enhanced Li-ion storage properties. J Mater Chem 2012;22:3868–74.
[29] Malavasi L, Fisher CA, Islam MS. Oxide-ion and proton conducting electrolyte materials for clean energy applications: structural and mechanistic features. Chem Soc Rev 2010;39:4370–87.
[30] Wang C, Astruc D. Nanogold plasmonic photocatalysis for organic synthesis and clean energy conversion. Chem Soc Rev 2014;43:7188–7216.
[31] Hossain S, Abdalla AM, Jamain SNB, Zaini JH, Azad AK. A review on proton conducting electrolytes for clean energy and intermediate temperature-solid oxide fuel cells. Renew Sust Energ Rev 2017;79:750–64.
[32] Dawson R, Laybourn A, Clowes R, Khimyak YZ, Adams DJ, Cooper AI. Functionalized conjugated microporous polymers. Macromolecules 2009;42:8809–16.
[33] Wu D, Xu F, Sun B, Fu R, He H, Matyjaszewski K. Design and preparation of porous polymers. Chem Rev 2012;112:3959–4015.
[34] Dawson R, Cooper AI, Adams DJ. Nanoporous organic polymer networks. Prog Polym Sci 2012;37:530–63.
[35] Colson JW, Dichtel WR. Rationally synthesized two-dimensional polymers. Nat Chem 2013;5:453–65.
[36] Taylor D, Dalgarno SJ, Xu Z, Vilela F. Conjugated porous polymers: incredibly versatile materials with far-reaching applications. Chem Soc Rev 2020;49:3981–4042.
[37] Côté AP, Benin AI, Ockwig NW, Keeffe M, Matzger AJ, Yaghi OM. Porous, crystalline, covalent organic frameworks. Science 2005;310:1166–70.
[38] Han SS, Furukawa H, Yaghi OM, Goddard WA. Covalent organic frameworks as exceptional hydrogen storage materials. J Am Chem Soc 2008;130:11580–1.
[39] Ding SY, Wang W. Covalent organic frameworks (COFs): from design to applications. Chem Soc Rev 2013;42:548–68.
[40] Beaudoin D, Maris T, Wuest JD. Constructing monocrystalline covalent organic networks by polymerization. Nat Chem 2013;5:830–4.
[41] Wang H, Zeng Z, Xu P, Li L, Zeng G, Xiao R, Tang Z, Huang D, Tang L, Lai C, Jiang D, Liu Y, Yi H, Qin L, Ye S, Ren X, Tang W. Recent progress in covalent organic framework thin films: fabrications, applications and perspectives. Chem Soc Rev 2019;48:488–516.
[42] Ben T, Ren H, Ma S, Cao D, Lan J, Jing X, Wang W, Xu J, Deng F, Simmons JM, Qiu S, Zhu G. Targeted synthesis of a porous aromatic framework with high stability and exceptionally high surface area. Angew Chem Int Ed 2009;48:9457–60.
[43] McKeown NB, Gahnem B, Msayib KJ, Budd PM, Tattershall CE, Mahmood K, Tan S, Book D, Langmi HW, Walton A. Towards polymer-based hydrogen storage materials: engineering ultramicroporous cavities within polymers of intrinsic microporosity. Angew Chem Int Ed 2006;45:1804–7.
[44] Carta M, Malpass-Evans R, Croad M, Rogan Y, Jansen JC, Bernardo P, Bazzarelli F, McKeown NB. An efficient polymer molecular sieve for membrane gas separations. Science 2013;339:303–7.
[45] Fischer S, Schmidt J, Strauch P, Thomas A. An anionic microporous polymer network prepared by the polymerization of weakly coordinating anions. Angew Chem Int Ed 2013;52:12174–8.
[46] Zhao Q, Dunlop JW, Qiu X, Huang F, Zhang Z, Heyda J, Dzubiella J, Antonietti M, Yuan J. An instant multi-responsive porous polymer actuator driven by solvent molecule sorption. Nat Commun 2014;5:4293 /1-8.
[47] Jiang J-X, Su F, Trewin A, Wood CD, Campbell NL, Niu H, Dickinson C, Ganin AY, Rosseinsky MJ, Khimyak YZ, Cooper AI. Conjugated microporous poly(aryleneethynylene) networks. Angew Chem Int Ed 2007;46:8574–8.
[48] Cooper AI. Conjugated microporous polymers. Adv Mater 2009;21:1291–5.
[49] Xu Y, Chen L, Guo Z, Nagai A, Jiang D. Light-emitting conjugated polymers with microporous network architecture: interweaving scaffold promotes electronic conjugation, facilitates exciton migration, and improves luminescence. J Am Chem Soc 2011;133:17622–5.
[50] Ren S, Bojdys MJ, Dawson R, Laybourn A, Khimyak YZ, Adams DJ, Cooper AI. Porous, fluorescent, covalent triazine-based frameworks via room-temperature and microwave-assisted synthesis. Adv Mater 2012;24:2357–61.
[51] Bunz UH, Seehafer K, Geyer FL, Bender M, Braun I, Smarsly E, Freudenberg J. Porous polymers based on aryleneethynylene building blocks. Macromol Rapid Commun 2014;35:1466–96.
[52] Xu S, Luo Y, Tan B. Recent development of hypercrosslinked microporous organic polymers. Macromol Rapid Commun 2013;34:471–84.
[53] Budd PM, Ghanem BS, Makhseed S, McKeown NB, Msayib KJ, Tattershall CE. Polymers of intrinsic microporosity (PIMs): robust, solution-processable, organic nanoporous materials. Chem Commun 2004:230–1.
[54] El-Kaderi HM, Hunt JR, Mendoza-Cortes JL, Cote AP, Taylor RE, O'Keeffe M, Yaghi OM. Designed synthesis of 3D covalent organic frameworks. Science 2007;316:268–72.
[55] Kuhn P, Antonietti M, Thomas A. Porous, covalent triazine-based frameworks prepared by ionothermal synthesis. Angew Chem Int Ed 2008;47:3450–3.
[56] Uribe-Romo FJ, Hunt JR, Furukawa H, Klock C, O'Keeffe M, Yaghi OM. A crystalline imine-linked 3-D porous covalent organic framework. J Am Chem Soc 2009;131:4570–1.
[57] Jiang J-X, Wang C, Laybourn A, Hasell T, Clowes R, Khimyak YZ, Xiao J, Higgins SJ, Adams DJ, Cooper AI. Metal-organic conjugated microporous polymers. Angew Chem Int Ed 2011;50:1072–5.
[58] Linares N, Silvestre-Albero AM, Serrano E, Silvestre-Albero J, Garcia–Martinez J. Mesoporous materials for clean energy technologies. Chem Soc Rev 2014;43:7681–717.
[59] Lin CY, Zhang D, Zhao Z, Xia Z. Covalent organic framework electrocatalysts for clean energy conversion. Adv Mater 2018;30:1703646 /1-16.
[60] Lee J-SM, Cooper AI. Advances in conjugated microporous polymers. Chem Rev 2020;120:2171–214.
[61] Chen Q, Luo M, Hammershoj P, Zhou D, Han Y, Laursen BW, Yan CG, Han BH. Microporous polycarbazole with high specific surface area for gas storage and separation. J Am Chem Soc 2012;134:6084–7.
[62] Zhang C, Yang X, Zhao Y, Wang XY, Yu M, Jiang JX. Bifunctionalized conjugated microporous polymers for carbon dioxide capture. Polymer (Guildf) 2015;61:36–41.
[63] Xie Y, Wang T-T, Liu X-H, Zou K, Deng W-Q. Capture and conversion of CO2 at ambient conditions by a conjugated microporous polymer. Nat Commun 2013;4:1960 /1-7.
[64] Yang C, Ma BC, Zhang L, Lin S, Ghasimi S, Landfester K, Zhang KA, Wang X. Molecular engineering of conjugated polybenzothiadiazoles for enhanced hydrogen production by photosynthesis. Angew Chem Int Ed 2016;55:9202–6.
[65] Xu Y, Mao N, Zhang C, Wang X, Zeng J, Chen Y, Wang F, Jiang J-X. Rational design of donor-pi-acceptor conjugated microporous polymers for photocatalytic hydrogen production. Appl Catal B 2018;228:1–9.
[66] Wang Z, Yang X, Yang T, Zhao Y, Wang F, Chen Y, Zeng JH, Yan C, Huang F, Jiang J-X. Dibenzothiophene dioxide based conjugated microporous polymers for visible-light-driven hydrogen production. ACS Catal 2018;8:8590–6.
[67] Chen L, Honsho Y, Seki S, Jiang DL. Light-harvesting conjugated microporous polymers: rapid and highly efficient flow of light energy with a porous polyphenylene framework as antenna. J Am Chem Soc 2010;132:6742–8.
[68] Rao KV, Haldar R, Maji TK, George SJ. Dynamic, conjugated microporous polymers: visible light harvesting via guest-responsive reversible swelling. PCCP 2016;18:156–63.
[69] Jiang J-X, Trewin A, Adams DJ, Cooper AI. Band gap engineering in fluorescent conjugated microporous polymers. Chem Sci 2011;2:1777–81.
[70] Gu C, Huang N, Chen Y, Zhang H, Zhang S, Li F, Ma Y, Jiang D. Porous organic polymer films with tunable work functions and selective hole and electron flows for energy conversions. Angew Chem Int Ed 2016;55:3049–53.
[71] Gu C, Huang N, Chen Y, Qin L, Xu H, Zhang S, Li F, Ma Y, Jiang D. π-Conjugated microporous polymer films: designed synthesis, conducting properties, and photoenergy conversions. Angew Chem Int Ed 2015;54:13594–8.
[72] Luo S, Zeng Z, Zeng G, Liu Z, Xiao R, Xu P, Wang H, Huang D, Liu Y, Shao B, Liang Q, Wang D, He Q, Qin L, Fu Y. Recent advances in conjugated micro-

porous polymers for photocatalysis: designs, applications, and prospects. J Mater Chem A 2020;8:6434–70.

[73] Zhang C, Yang X, Ren WF, Wang YH, Su FB, Jiang JX. Microporous organic polymer-based lithium ion batteries with improved rate performance and energy density. J Power Sources 2016;317:49–56.

[74] Su C, He H, Xu L, Zhao K, Zheng C, Zhang C. A mesoporous conjugated polymer based on a high free radical density polytriphenylamine derivative: its preparation and electrochemical performance as a cathode material for Li-ion batteries. J Mater Chem A 2017;5:2701–9.

[75] Zhang C, He Y, Mu P, Wang X, He Q, Chen Y, Zeng J, Wang F, Xu Y, Jiang J-X. Toward high performance thiophene-containing conjugated microporous polymer anodes for lithium-ion batteries through structure design. Adv Funct Mater 2018;28:1705432 /1-9.

[76] Xu F, Chen X, Tang Z, Wu D, Fu R, Jiang D. Redox-active conjugated microporous polymers: a new organic platform for highly efficient energy storage. Chem Commun 2014;50:4788–90.

[77] Xu Y, Jin S, Xu H, Nagai A, Jiang D. Conjugated microporous polymers: design, synthesis and application. Chem Soc Rev 2013;42:8012–8031.

[78] Vilela F, Zhang K, Antonietti M. Conjugated porous polymers for energy applications. Energy Environ Sci 2012;5:7819–32.

[79] Jiang J-X, Su F, Niu H, Wood CD, Campbell NL, Khimyak YZ, Cooper AI. Conjugated microporous poly(phenylene butadiynylene)s. Chem Commun 2008:486–8.

[80] Weber J, Thomas A. Toward stable interfaces in conjugated polymers: microporous poly(p-phenylene) and poly(phenyleneethynylene) based on a spirobifluorene building block. J Am Chem Soc 2008;130:6334–6335.

[81] Schmidt J, Weber J, Epping JD, Antonietti M, Thomas A. Microporous conjugated poly(thienylene arylene) networks. Adv Mater 2009;21:702–5.

[82] Chen L, Yang Y, Jiang D. CMPs as scaffolds for constructing porous catalytic frameworks: a built-in heterogeneous catalyst with high activity and selectivity based on nanoporous metalloporphyrin polymers. J Am Chem Soc 2010;132:9138–43.

[83] Li A, Sun H-X, Tan Dd-Z, Fan W-J, Wen S-H, Qing X-J, Li G-X, Li S-Y, Deng W-Q. Superhydrophobic conjugated microporous polymers for separation and adsorption. Energy Environ Sci 2011;4:2062–5.

[84] Cheng G, Hasell T, Trewin A, Adams DJ, Cooper AI. Soluble conjugated microporous polymers. Angew Chem Int Ed 2012;51:12727–31.

[85] Liu X, Xu Y, Jiang D. Conjugated microporous polymers as molecular sensing devices: microporous architecture enables rapid response and enhances sensitivity in fluorescence-on and fluorescence-off sensing. J Am Chem Soc 2012;134:8738–41.

[86] Gu C, Chen Y, Zhang Z, Xue S, Sun S, Zhang K, Zhong C, Zhang H, Pan Y, Lv Y, Yang Y, Li F, Zhang S, Huang F, Ma Y. Electrochemical route to fabricate film–like conjugated microporous polymers and application for organic electronics. Adv Mater 2013;25:3443–8.

[87] Xu Y, Nagai A, Jiang D. Core–shell conjugated microporous polymers: a new strategy for exploring color-tunable and -controllable light emissions. Chem Commun 2013;49:1591–3.

[88] A S, Zhang Y, Li Z, Xia H, Xue M, Liu X, Mu Y. Highly efficient and reversible iodine capture using a metalloporphyrin-based conjugated microporous polymer. Chem Commun 2014;50:8495–8.

[89] Ding X, Han B-H. Metallophthalocyanine-based conjugated microporous polymers as highly efficient photosensitizers for singlet oxygen generation. Angew Chem Int Ed 2015;54:6536–9.

[90] Zhuang X, Gehrig D, Forler N, Liang H, Wagner M, Hansen MR, Laquai F, Zhang F, Feng X. Conjugated microporous polymers with dimensionality-controlled heterostructures for green energy devices. Adv Mater 2015;27:3789–96.

[91] Liao Y, Weber J, Mills BM, Ren Z, Faul CFJ. Highly efficient and reversible iodine capture in hexaphenylbenzene-based conjugated microporous polymers. Macromolecules 2016;49:6322–33.

[92] Wang L, Wan Y, Ding Y, Wu S, Zhang Y, Zhang X, Zhang G, Xiong Y, Wu X, Yang J, Xu H. Conjugated microporous polymer nanosheets for overall water splitting using visible light. Adv Mater 2017;29:1702428 /1-8.

[93] Li Y, Duan Q, Wang H, Gao B, Qiu N, Li Y. Construction of two-dimensional porphyrin-based fully conjugated microporous polymers as highly efficient photocatalysts. Journal of Photochemistry and Photobiology A-Chemistry 2018;356:370–8.

[94] Mu P, Zhang Z, Bai W, He J, Sun H, Zhu Z, Liang W, Li A. Superwetting monolithic hollow-carbon-nanotubes aerogels with hierarchically nanoporous structure for efficient solar steam generation. Adv Energy Mater 2019;9:1802158 /1-9.

[95] Jiang J-X, Su F, Trewin A, Wood CD, Niu H, Jones JTA, Khimyak YZ, Cooper AI. Synthetic control of the pore dimension and surface area in conjugated microporous polymer and copolymer networks. J Am Chem Soc 2008;130:7710–20.

[96] Thomas A, Kuhn P, Weber J, Titirici M-M, Antonietti M. Porous polymers: enabling solutions for energy applications. Macromol Rapid Commun 2009;30:221–36.

[97] Wang X, Maeda K, Thomas A, Takanabe K, Xin G, Carlsson JM, Domen K, Antonietti M. A metal-free polymeric photocatalyst for hydrogen production from water under visible light. Nat Mater 2009;8:76–80.

[98] Wong YL, Tobin JM, Xu Z, Vilela F. Conjugated porous polymers for photocatalytic applications. J Mater Chem A 2016;4:18677–86.

[99] Wang X, Zhao Y, Wei L, Zhang C, Jiang J-X. Nitrogen-rich conjugated microporous polymers: impact of building blocks on porosity and gas adsorption. J Mater Chem A 2015;3:21185–93.

[100] Sun L, Liang Z, Yu J, Xu R. Luminescent microporous organic polymers containing the 1,3,5-tri(4-ethenylphenyl)benzene unit constructed by Heck coupling reaction. Polym Chem 2013;4:1932–8.

[101] Gu C, Bao Y, Huang W, Liu D, Yang R. Four simple structure carbazole-based conjugated microporous polymers with different soft connected chains. Macromol Chem Phys 2016;217:748–56.

[102] Chai S, Liu H, Zhang X, Han Y, Hu N, Wei L, Cong F, Wei H, Wang L. Synthesis of a novel beta-ketoenamine-linked conjugated microporous polymer with N-H functionalized pore surface for carbon dioxide capture. Appl Surf Sci 2016;384:539–43.

[103] Biswal BP, Becker D, Chandrasekhar N, Seenath JS, Paasch S, Machill S, Hennersdorf F, Brunner E, Weigand JJ, Berger R, Feng X. Exploration of thiazolo[5,4-*d*]thiazole linkages in conjugated porous organic polymers for chemoselective molecular sieving. Chemistry-A European Journal 2018;24:10868–75.

[104] Marco AB, Cortizo-Lacalle D, Perez-Miqueo I, Valenti G, Boni A, Plas J, Strutyński K, De Feyter S, Paolucci F, Montes M, Khlobystov AN, Melle-Franco M, Mateo-Alonso A. Twisted aromatic frameworks: readily exfoliable and solution-processable two-dimensional conjugated microporous polymers. Angew Chem Int Ed 2017;56:6946–51.

[105] Deng S, Zhao P, Dai Y, Huang B, Hu A. Synthesis of soluble conjugated polymeric nanoparticles through heterogeneous Suzuki coupling reaction. Polymer (Guildf) 2015;64:216–20.

[106] Chen Y, Sun H, Yang R, Wang T, Pei C, Xiang Z, Zhu Z, Liang W, Li A, Deng W. Synthesis of conjugated microporous polymer nanotubes with large surface areas as absorbents for iodine and CO2 uptake. J Mater Chem A 2015;3:87–91.

[107] Holst JR, Stöckel E, Adams DJ, Cooper AI. High surface area networks from tetrahedral monomers: metal-catalyzed coupling, thermal polymerization, and “click” chemistry. Macromolecules 2010;43:8531–8.

[108] Ren S, Dawson R, Laybourn A, Jiang J-x, Khimyak Y, Adams DJ, Cooper AI. Functional conjugated microporous polymers: from 1,3,5-benzene to 1,3,5-triazine. Polym Chem 2012;3:928–34.

[109] Jiang J-X, Trewin A, Su F, Wood CD, Niu H, Jones JTA, Khimyak YZ, Cooper AI. Microporous poly(tri(4-ethynylphenyl)amine) networks: synthesis, properties, and atomistic simulation. Macromolecules 2009;42:2658–66.

[110] Qian X, Zhu Z-Q, Sun H-X, Ren F, Mu P, Liang W, Chen L, Li A. Capture and reversible storage of volatile iodine by novel conjugated microporous polymers containing thiophene units. ACS Appl Mater Inter 2016;8:21063–9.

[111] Zang JK, Zhu ZQ, Sun HX, Liang WD, Li A. Synthesis of functional conjugated microporous polymers containing pyridine units with high BET surface area for reversible CO2 storage. React Funct Polym 2016;99:95–9.

[112] Tan D, Fan W, Xiong W, Sun H, Li A, Deng W, Meng C. Study on adsorption performance of conjugated microporous polymers for hydrogen and organic solvents: the role of pore volume. Eur Polym J 2012;48:705–11.

[113] Bao L, Sun H, Zhu Z, Liang W, Mu P, Zang J, Li A. Synthesis and properties of tubular-shape conjugated microporous polymers with high purity. Mater Lett 2016;178:5–9.

[114] Wang X, Chen B, Dong W, Zhang X, Li Z, Xiang Y, Chen H. Hydrophilicity-controlled conjugated microporous polymers for enhanced visible-light-driven photocatalytic H2 evolution. Macromol Rapid Commun 2019;40:1800494 /1-8.

[115] Miyaura N, Suzuki A. Stereoselective synthesis of arylated (E)-alkenes by the reaction of alk-1-enylboranes with aryl halides in the presence of palladium catalyst. J Chem Soc, Chem Commun 1979:866–7.

[116] Miyaura N, Yamada K, Suzuki A. A new stereospecific cross-coupling by the palladium-catalyzed reaction of 1-alkenylboranes with 1-alkenyl or 1-alkynyl halides. Tetrahedron Lett 1979;20:3437–40.

[117] Tobin JM, Liu J, Hayes H, Demleitner M, Ellis D, Arrighi V, Xu Z, Vilela F. BODIPY-based conjugated microporous polymers as reusable heterogeneous photosensitisers in a photochemical flow reactor. Polym Chem 2016;7:6662–70.

[118] Xu M, Han X, Wang T, Li S, Hua D. Conjugated microporous polymers bearing phosphonate ligands as an efficient sorbent for potential uranium extraction from high- level liquid wastes. J Mater Chem A 2018;6:13894–900.

[119] Sun L, Zou Y, Liang Z, Yu J, Xu R. A one-pot synthetic strategy via tandem Suzuki–Heck reactions for the construction of luminescent microporous organic polymers. Polym Chem 2014;5:471–8.

[120] Ampelli C, Genovese C, Errahali M, Gatti G, Marchese L, Perathoner S, Centi G. CO2 capture and reduction to liquid fuels in a novel electrochemical setup by using metal-doped conjugated microporous polymers. J Appl Electrochem 2015;45:701–13.

[121] Zhang Q, Yu S, Wang Q, Xiao Q, Yue Y, Ren S. Fluorene-based conjugated microporous polymers: preparation and chemical sensing application. Macromol Rapid Commun 2017;38:1700445 /1-6.

[122] Yuan Y, Huang H, Chen L, Chen YN, ’-bicarbazole N. A versatile building block toward the construction of conjugated porous polymers for CO2 capture and dyes adsorption. Macromolecules 2017;50:4993–5003.

[123] Liu Q, Li G, Tang Z, Chen L, Liao B, Ou B, Zhou Z, Zhou H. Design and synthesis of conjugated polymers of tunable pore size distribution. Mater Chem Phys 2017;186:11–18.

[124] Mane S, Li Y-X, Liu X-Q, Yue MB, Sun Ll-B. Development of adsorbents for selective carbon capture: role of homo- and cross-coupling in conjugated mi-

croporous polymers and their carbonized derivatives. ACS Sustain Chem Eng 2018;6:17419–26.

[125] Schmidt J, Werner M, Thomas A. Conjugated microporous polymer networks via yamamoto polymerization. Macromolecules 2009;42:4426–9.

[126] Liao Y, Cheng Z, Trunk M, Thomas A. Targeted control over the porosities and functionalities of conjugated microporous polycarbazole networks for CO2-selective capture and H-2 storage. Polym Chem 2017;8:7240–7.

[127] Germain J, Svec F, Fréchet JMJ. Preparation of size-selective nanoporous polymer networks of aromatic rings: potential adsorbents for hydrogen storage. Chem Mater 2008;20:7069–76.

[128] Liao Y, Weber J, Faul CFJ. Conjugated microporous polytriphenylamine networks. Chem Commun 2014;50:8002–5.

[129] Ueda M, Abe T, Awano H. Synthesis of poly (2, 5-dialkoxyphenylene). Macromolecules 1992;25:5125–30.

[130] Chen Q, Liu Dd-P, Luo M, Feng Ll-J, Zhao Y-C, Han B-H. Nitrogen-containing microporous conjugated polymers via carbazole-based oxidative coupling polymerization: preparation, porosity, and gas uptake. Small 2014;10:308–315.

[131] Zhang Y, A S, Zou Y, Luo X, Li Z, Xia H, Liu X, Mu Y. Gas uptake, molecular sensing and organocatalytic performances of a multifunctional carbazole-based conjugated microporous polymer. J Mater Chem A 2014;2:13422–30.

[132] Zhi Y, Ma S, Xia H, Zhang Y, Shi Z, Mu Y, Liu X. Construction of donor-acceptor type conjugated microporous polymers: a fascinating strategy for the development of efficient heterogeneous photocatalysts in organic synthesis. Appl Catal B 2019;244:36–44.

[133] Xu Y, Cui D, Zhang S, Xu G, Su Z. Facile synthesis of conjugated microporous polymer-based porphyrin units for adsorption of CO2 and organic vapors. Polym Chem 2019;10:819–22.

[134] Singh A, Roy S, Das C, Samanta D, Maji TK. Metallophthalocyanine-based redox active metal-organic conjugated microporous polymers for OER catalysis. Chem Commun 2018;54:4465–8.

[135] Wang Y, Tao J, Xiong S, Lu P, Tang J, He J, Javaid MU, Pan C, Yu G. Ferrocene-based porous organic polymers for high-affinity iodine capture. Chem Eng J 2020;380:122420 /1-5.

[136] Rabbani MG, El-Kaderi HM. Template-free synthesis of a highly porous benzimidazole-linked polymer for CO2 capture and H2 storage. Chem Mater 2011;23:1650–3.

[137] Zhu X, Tian C, Jin T, Wang J, Mahurin SM, Mei W, Xiong Y, Hu J, Feng X, Liu H, Dai S. Thiazolothiazole-linked porous organic polymers. Chem Commun 2014;50:15055–8.

[138] Kou Y, Xu Y, Guo Z, Jiang D. Supercapacitive energy storage and electric power supply using an aza-fused π-conjugated microporous framework. Angew Chem Int Ed 2011;50:8753–7.

[139] Wang H, Jiang D, Huang D, Zeng G, Xu P, Lai C, Chen M, Cheng M, Zhang C, Wang Z. Covalent triazine frameworks for carbon dioxide capture. J Mater Chem A 2019;7:22848–70.

[140] Kuhn P, Forget A, Su D, Thomas A, Antonietti M. From microporous regular frameworks to mesoporous materials with ultrahigh surface area: dynamic reorganization of porous polymer networks. J Am Chem Soc 2008;130:13333–7.

[141] Kuhn P, Forget A, Hartmann J, Thomas A, Antonietti M. Template-free tuning of nanopores in carbonaceous polymers through ionothermal synthesis. Adv Mater 2009;21:897–901.

[142] Kuhn P, Thomas A, Antonietti M. Toward tailorable porous organic polymer networks: a high-temperature dynamic polymerization scheme based on aromatic nitriles. Macromolecules 2009;42:319–26.

[143] Yuan S, Dorney B, White D, Kirklin S, Zapol P, Yu L, Liu Dd-J. Microporous polyphenylenes with tunable pore size for hydrogen storage. Chem Commun 2010;46:4547–9.

[144] Qiao S, Du Z, Yang R. Design and synthesis of novel carbazole-spacer-carbazole type conjugated microporous networks for gas storage and separation. J Mater Chem A 2014;2:1877–85.

[145] Qiao S, Du Z, Huang W, Yang R. Influence of aggregated morphology on carbon dioxide uptake of polythiophene conjugated organic networks. J Solid State Chem 2014;212:69–72.

[146] Qiao S, Wang T, Huang W, Jiang J-X, Du Z, Shieh F-K, Yang R. Dendrimer-like conjugated microporous polymers. Polym Chem 2016;7:1281–9.

[147] Sun C-J, Wang P-F, Wang H, Han B-H. All-thiophene-based conjugated porous organic polymers. Polym Chem 2016;7:5031–8.

[148] Geng T, Zhu Z, Wang X, Xia H, Wang Y, Li D. Poly{tris 4-(2-Thienyl)phenyl amine} fluorescent conjugated microporous polymer for selectively sensing picric acid. Sens Actuators, B 2017;244:334–43.

[149] Pandey P, Katsoulidis AP, Eryazici I, Wu Y, Kanatzidis MG, Nguyen ST. Imine-linked microporous polymer organic frameworks. Chem Mater 2010;22:4974–9.

[150] Rabbani MG, Sekizkardes AK, El-Kadri OM, Kaafarani BR, El-Kaderi HM. Pyrene-directed growth of nanoporous benzimidazole-linked nanofibers and their application to selective CO2 capture and separation. J Mater Chem 2012;22:25409–17.

[151] Xu C, Hedin N. Synthesis of microporous organic polymers with high CO2-over-N2 selectivity and CO2 adsorption. J Mater Chem A 2013;1:3406–14.

[152] Haikal RR, Soliman AB, Amin M, Karakalos SG, Hassan YS, Elmansi AM, Hafez IH, Berber MR, Hassanien A, Alkordi MH. Synergism of carbon nanotubes and porous-organic polymers (POPs) in CO2 fixation: one-pot approach for bottom-up assembly of tunable heterogeneous catalyst. Appl Catal B 2017;207:347–57.

[153] Shanmugaraju S, Umadevi D, Savyasachi AJ, Byrne K, Ruether M, Schmitt W, Watson GW, Gunnlaugsson T. Reversible adsorption and storage of secondary explosives from water using a Troger's base-functionalised polymer. J Mater Chem A 2017;5:25014–24.

[154] Zhou H, Wu C, Wu Q, Guo B, Liu W, Li G, Su Q, Mu Y. Palladium nanoparticles supported on a carbazole functionalized mesoporous organic polymer: synthesis and their application as efficient catalysts for the Suzuki-Miyaura cross coupling reaction. Polym Chem 2017;8:1488–94.

[155] Zhi Y, Li K, Xia H, Xue M, Mu Y, Liu X. Robust porous organic polymers as efficient heterogeneous organo-photocatalysts for aerobic oxidation reactions. J Mater Chem A 2017;5:8697–704.

[156] Cai L, Li Y, Li Y, Wang H, Yu Y, Liu Y, Duan Q. Synthesis of zincphthalocyanine-based conjugated microporous polymers with rigid-linker as novel and green heterogeneous photocatalysts. J Hazard Mater 2018;348:47–55.

[157] Ju P, Wu S, Su Q, Li X, Liu Z, Li G, Wu Q. Salen-porphyrin-based conjugated microporous polymer supported Pd nanoparticles: highly efficient heterogeneous catalysts for aqueous C-C coupling reactions. J Mater Chem A 2019;7:2660–6.

[158] Iha RK, Wooley KL, Nyström AM, Burke DJ, Kade MJ, Hawker CJ. Applications of orthogonal “click” chemistries in the synthesis of functional soft materials. Chem Rev 2009;109:5620–86.

[159] Lowe AB, Hoyle CE, Bowman CN. Thiol-yne click chemistry: a powerful and versatile methodology for materials synthesis. J Mater Chem 2010;20:4745–50.

[160] Liang L, Astruc D. The copper(I)-catalyzed alkyne-azide cycloaddition (CuAAC) “click” reaction and its applications. An overview. Coord Chem Rev 2011;255:2933–45.

[161] An Q, Hassan Y, Yan X, Krolla-Sidenstein P, Mohammed T, Lang M, Braese S, Tsotsalas M. Fast and efficient synthesis of microporous polymer nanomembranes via light-induced click reaction. Beilstein J Org Chem 2017;13:558–63.

[162] Yao B, Mei J, Li J, Wang J, Wu H, Sun JZ, Qin A, Tang BZ. Catalyst-free thiol–yne click polymerization: a powerful and facile tool for preparation of functional poly(vinylene sulfide)s. Macromolecules 2014;47:1325–33.

[163] Schwab MG, Crespy D, Feng X, Landfester K, Mullen K. Preparation of microporous melamine-based polymer networks in an anhydrous high-temperature miniemulsion. Macromol Rapid Commun 2011;32:1798–803.

[164] Liu Y, Cui Y, Zhang C, Du J, Wang S, Bai Y, Liang Z, Song X. Post-cationic modification of a pyrimidine-based conjugated microporous polymer for enhancing the removal performance of anionic dyes in water. Chemistry-A European Journal 2018;24:7480–8.

[165] Kiskan B, Weber J. Versatile postmodification of conjugated microporous polymers using thiol-yne chemistry. ACS Macro Lett 2012;1:37–40.

[166] Ratvijitvech T, Dawson R, Laybourn A, Khimyak YZ, Adams DJ, Cooper AI. Post-synthetic modification of conjugated microporous polymers. Polymer (Guildf) 2014;55:321–5.

[167] Cui D, Yao C, Xu Y. Conjugated microporous polymers with azide groups: a new strategy for postsynthetic fluoride functionalization and effectively enhanced CO2 adsorption properties. Chem Commun 2017;53:11422–5.

[168] Yang S-J, Ding X, Han B-H. Conjugated microporous polymers with extended pi-structures for organic vapor adsorption. Macromolecules 2018;51:947–53.

[169] Liu L, Deng Q-F, Hou X-X, Yuan Z-Y. User-friendly synthesis of nitrogen-containing polymer and microporous carbon spheres for efficient CO2 capture. J Mater Chem 2012;22:15540–8.

[170] Gao PF, Zheng LL, Liang LJ, Yang XX, Li YF, Huang CZ. A new type of pH-responsive coordination polymer sphere as a vehicle for targeted anticancer drug delivery and sustained release. J Mater Chem B 2013;1:3202–8.

[171] Tabata K, Braam D, Kushida S, Tong L, Kuwabara J, Kanbara T, Beckel A, Lorke A, Yamamoto Y. Self-assembled conjugated polymer spheres as fluorescent microresonators. Sci Rep 2014;4:5902 /1-5.

[172] Chen JS, Archer LA, Wen Lou X. SnO2 hollow structures and TiO2 nanosheets for lithium-ion batteries. J Mater Chem 2011;21:9912–24.

[173] Mahmoud MA, Narayanan R, El-Sayed MA. Enhancing colloidal metallic nanocatalysis: sharp edges and corners for solid nanoparticles and cage effect for hollow ones. Acc Chem Res 2013;46:1795–805.

[174] Li G, Li Y, Liu H, Guo Y, Li Y, Zhu D. Architecture of graphdiyne nanoscale films. Chem Commun 2010;46:3256–8.

[175] Wu K, Guo J, Wang C. Dispersible and discrete metalloporphyrin-based CMP nanoparticles enabling colorimetric detection and quantitation of gaseous SO2. Chem Commun 2014;50:695–7.

[176] Gu C, Huang N, Gao J, Xu F, Xu Y, Jiang D. Controlled synthesis of conjugated microporous polymer films: versatile platforms for highly sensitive and label-free chemo- and biosensing. Angew Chem Int Ed 2014;53:4850–5.

[177] He Y, Gehrig D, Zhang F, Lu C, Zhang C, Cai M, Wang Y, Laquai F, Zhuang X, Feng X. Highly efficient electrocatalysts for oxygen reduction reaction based on 1D ternary doped porous carbons derived from carbon nanotube directed conjugated microporous polymers. Adv Funct Mater 2016;26:8255–65.

[178] Senkovskyy V, Senkovska I, Kiriy A. Surface-initiated synthesis of conjugated microporous polymers: chain-growth kumada catalyst-transfer polycondensation at work. ACS Macro Lett 2012;1:494–8.

[179] Kang N, Park JH, Jin M, Park N, Lee SM, Kim HJ, Kim JM, Son SU. Microporous organic network hollow spheres: useful templates for nanoparticulate Co3O4 hollow oxidation catalysts. J Am Chem Soc 2013;135:19115–18.

[180] Li B, Yang X, Xia L, Majeed MI, Tan B. Hollow microporous organic capsules. Sci Rep 2013;3:2128 /1-6.

[181] Stöber W, Fink A, Bohn E. Controlled growth of monodisperse silica spheres in the micron size range. J Colloid Interface Sci 1968;26:62–9.
[182] Ji G, Yang Z, Zhao Y, Zhang H, Yu B, Xu J, Xu H, Liu Z. Synthesis of metalloporphyrin-based conjugated microporous polymer spheres directed by bipyridine-type ligands. Chem Commun 2015;51:7352–5.
[183] Schwab MG, Fassbender B, Spiess HW, Thomas A, Feng X, Mullen K. Catalyst-free preparation of melamine-based microporous polymer networks through Schiff base chemistry. J Am Chem Soc 2009;131:7216–17.
[184] Silverstein MS. PolyHIPEs: recent advances in emulsion-templated porous polymers. Prog Polym Sci 2014;39:199–234.
[185] Kim M, Byeon M, Bae J-S, Moon S-Y, Yu G, Shin K, Basarir F, Yoon T-H, Park J-W. Preparation of ultrathin films of molecular networks through layer-by-layer cross-linking polymerization of tetrafunctional monomers. Macromolecules 2011;44:7092–5.
[186] Palma-Cando A, Scherf U. Electrochemically generated thin films of microporous polymer networks: synthesis, properties, and applications. Macromol Chem Phys 2016;217:827–41.
[187] Zhang Q, Dong H, Hu W. Electrochemical polymerization for two-dimensional conjugated polymers. Journal of Materials Chemistry C 2018;6:10672–86.
[188] Lindemann P, Tsotsalas M, Shishatskiy S, Abetz V, Krolla-Sidenstein P, Azucena C, Monnereau L, Beyer A, Gölzhäuser A, Mugnaini V, Gliemann H, Bräse S, Wöll C. Preparation of freestanding conjugated microporous polymer nanomembranes for gas separation. Chem Mater 2014;26:7189–93.
[189] Zhang H, Zhang Y, Gu C, Ma Y. Electropolymerized conjugated microporous poly(zinc-porphyrin) films as potential electrode materials in supercapacitors. Adv Energy Mater 2015;5:1402175 /1-6.
[190] Chen Z, Chen M, Yu Y, Wu L. Robust synthesis of free-standing and thickness controllable conjugated microporous polymer nanofilms. Chem Commun 2017;53:1989–92.
[191] Liang B, Wang H, Shi X, Shen B, He X, Ghazi ZA, Khan NA, Sin H, Khattak AM, Li L, Tang Z. Microporous membranes comprising conjugated polymers with rigid backbones enable ultrafast organic-solvent nanofiltration. Nat Chem 2018;10:961–7.
[192] Raaijmakers MJT, Benes NE. Current trends in interfacial polymerization chemistry. Prog Polym Sci 2016;63:86–142.
[193] Gu C, Zhang Z, Sun S, Pan Y, Zhong C, Lv Y, Li M, Ariga K, Huang F, Ma Y. In situ electrochemical deposition and doping of C60 films applied to high-performance inverted organic photovoltaics. Adv Mater 2012;24:5727–31.
[194] Zhao R, Zhan X, Yao L, Chen Q, Xie Z, Ma Y. Electrochemical deposition of azobenzene-containing network films with high-contrast and stable photoresponse. Macromol Rapid Commun 2016;37:610–15.
[195] Gu C, Fei T, Yao L, Lv Y, Lu D, Ma Y. Multilayer polymer stacking by in situ electrochemical polymerization for color-stable white electroluminescence. Adv Mater 2011;23:527–30.
[196] Lv Y, Yao L, Gu C, Xu Y, Liu D, Lu D, Ma Y. Electroactive self-assembled monolayers for enhanced efficiency and stability of electropolymerized luminescent films and devices. Adv Funct Mater 2011;21:2896–900.
[197] Gu C, Dong W, Yao L, Lv Y, Zhang Z, Lu D, Ma Y. Cross-linked multifunctional conjugated polymers prepared by in situ electrochemical deposition for a highly-efficient blue-emitting and electron-transport layer. Adv Mater 2012;24:2413–17.
[198] Li M, Ishihara S, Ohkubo K, Liao M, Ji Q, Gu C, Pan Y, Jiang X, Akada M, Hill JP, Nakanishi T, Ma Y, Yamauchi Y, Fukuzumi S, Ariga K. Electrochemical synthesis of transparent, amorphous, C60-rich, photoactive, and low-doped film with an interconnected structure. Small 2013;9:2064–8.
[199] Mergel O, Kühn PT, Schneider S, Simon U, Plamper FA. Influence of polymer architecture on the electrochemical deposition of polyelectrolytes. Electrochim Acta 2017;232:98–105.
[200] Gu C, Huang N, Wu Y, Xu H, Jiang D. Design of highly photofunctional porous polymer films with controlled thickness and prominent microporosity. Angew Chem Int Ed 2015;54:11540–4.
[201] Zhao R, Han J, Huang M, Liu F, Wang L, Ma Y. Photoresponsive conjugated microporous polymer films fabricated by electrochemical deposition for controlled release. Macromol Rapid Commun 2017;38:1700274 /1-6.
[202] Lindemann P, Schade A, Monnereau L, Feng W, Batra K, Gliemann H, Levkin P, Braese S, Woell C, Tsotsalas M. Surface functionalization of conjugated microporous polymer thin films and nanomembranes using orthogonal chemistries. J Mater Chem A 2016;4:6815–18.
[203] Zhu J, Yang C, Lu C, Zhang F, Yuan Z, Zhuang X. Two-dimensional porous polymers: from sandwich-like structure to layered skeleton. Acc Chem Res 2018;51:3191–202.
[204] Wang S, Wang Q, Shao P, Han Y, Gao X, Ma L, Yuan S, Ma X, Zhou J, Feng X, Wang B. Exfoliation of covalent organic frameworks into few-layer redox-active nanosheets as cathode materials for lithium-ion batteries. J Am Chem Soc 2017;139:4258–61.
[205] Bunck DN, Dichtel WR. Bulk synthesis of exfoliated two-dimensional polymers using hydrazone-linked covalent organic frameworks. J Am Chem Soc 2013;135:14952–5.
[206] Chandra S, Kandambeth S, Biswal BP, Lukose B, Kunjir SM, Chaudhary M, Babarao R, Heine T, Banerjee R. Chemically stable multilayered covalent organic nanosheets from covalent organic frameworks via mechanical delamination. J Am Chem Soc 2013;135:17853–61.
[207] Mitra S, Kandambeth S, Biswal BP, Khayum MA, Choudhury CK, Mehta M, Kaur G, Banerjee S, Prabhune A, Verma S, Roy S, Kharul UK, Banerjee R. Self--exfoliated guanidinium-based ionic covalent organic nanosheets (iCONs). J Am Chem Soc 2016;138:2823–8.
[208] Liu W, Wang C, Zhang L, Pan H, Liu W, Chen J, Yang D, Xiang Y, Wang K, Jiang J, Yao X. Exfoliation of amorphous phthalocyanine conjugated polymers into ultrathin nanosheets for highly efficient oxygen reduction. J Mater Chem A 2019;7:3112–19.
[209] Tabor DP, Roch LM, Saikin SK, Kreisbeck C, Sheberla D, Montoya JH, Dwaraknath S, Aykol M, Ortiz C, Tribukait H, Amador-Bedolla C, Brabec CJ, Maruyama B, Persson KA. Aspuru-Guzik A. Accelerating the discovery of materials for clean energy in the era of smart automation. Nat Rev Mater 2018;3:5–20.
[210] Wu T, Wang T, Sun L, Deng K, Deng W, Lu R. A DFT exploration of efficient catalysts based on metal-salen monomers for the cycloaddition reaction of CO2 to propylene oxide. Chemistryselect 2017;2:4533–7.
[211] Yang Z-D, Wu W, Zeng XC. Electronic and transport properties of porous graphenes: two-dimensional benzo- and aza-fused pi-conjugated-microporous-polymer sheets and boron-nitrogen co-doped derivatives. Journal of Materials Chemistry C 2014;2:2902–7.
[212] Bhattacharyya S, Samanta D, Roy S, Radhakantha VPH, Maji TK. In situ stabilization of Au and Co nanoparticles in a redox-active conjugated microporous polymer matrix: facile heterogeneous catalysis and electrocatalytic oxygen reduction reaction activity. ACS Appl Mater Inter 2019;11:5455–5461.
[213] Li S, Yang Z-D, Zhang G, Zeng XC. Electronic and transport properties of porous graphene sheets and nanoribbons: benzo-CMPs and BN codoped derivatives. Journal of Materials Chemistry C 2015;3:9637–49.
[214] Fan W-J, Yang G-J, Chi J-W, Yu Y, Tan Dd-Z. Theoretical study of the physisorption of organic molecules on conjugated microporous polymers: the critical role of skeleton structures on binding strength. RSC Adv 2016;6:54841–7.
[215] Srinivasu K, Ghosh SK. Hydrogen adsorption in lithium decorated conjugated microporous polymers: a DFT investigation. RSC Adv 2014;4:4170–6.
[216] Fan W-J, Zhao Y-L, Hu Y-C, Shi H, Tan Dd-Z, Zhang R-Q. Design of conjugated microporous polymer nanotubes for efficient benzene molecular adsorptions. Int J Quantum Chem 2018;118:25492 /1-10.
[217] Chen C, Tang C, Xu W, Li Y, Xu L. Design of iron atom modified thiophene-linked metalloporphyrin 2D conjugated microporous polymer as CO2 reduction photocatalyst. PCCP 2018;20:9536–42.
[218] Xu L. Design of open-shell pi-conjugated microporous polymer film with super-high conductivity. Macromol Chem Phys 2018;219:1700600 /1-6.
[219] Marcus RA. Chemical and electrochemical electron-transfer theory. Annu Rev Phys Chem 1964;15:155–96.
[220] Marcus RA. Electron transfer reactions in chemistry. Theory and experiment. Rev Mod Phys 1993;65:599–610.
[221] Zwijnenburg MA, Cheng G, McDonald TO, Jelfs KE, Jiang J-X, Ren S, Hasell T, Blanc F, Cooper AI, Adams DJ. Shedding light on structure-property relationships for conjugated microporous polymers: the importance of rings and strain. Macromolecules 2013;46:7696–704.
[222] Wang L, Wan Y, Ding Y, Niu Y, Xiong Y, Wu X, Xu H. Photocatalytic oxygen evolution from low-bandgap conjugated microporous polymer nanosheets: a combined first-principles calculation and experimental study. Nanoscale 2017;9:4090–6.
[223] Das S, Heasman P, Ben T, Qiu S. Porous organic materials: strategic design and structure–function correlation. Chem Rev 2017;117:1515–63.
[224] Jiang S, Jelfs KE, Holden D, Hasell T, Chong SY, Haranczyk M, Trewin A, Cooper AI. Molecular dynamics simulations of gas selectivity in amorphous porous molecular solids. J Am Chem Soc 2013;135:17818–30.
[225] Thomas JMH, Trewin A. Amorphous PAF-1: guiding the rational design of ultraporous materials. J Physl Chem C 2014;118:19712–22.
[226] Fayon P, Trewin A. Formation mechanism of ultra porous framework materials. PCCP 2016;18:16840–7.
[227] Abbott LJ, Colina CM. Atomistic structure generation and gas adsorption simulations of microporous polymer networks. Macromolecules 2011;44:4511–19.
[228] Suresh VM, Bonakala S, Roy S, Balasubramanian S, Maji TK. Synthesis, characterization, and modeling of a functional conjugated microporous polymer: CO2 storage and light harvesting. J Physl Chem C 2014;118:24369–76.
[229] Abbott LJ, Colina CM. Porosity and ring formation in conjugated microporous polymers. J Chem Eng Data 2014;59:3177–82.
[230] Plimpton S. Fast parallel algorithms for short-range molecular dynamics. J Comput Phys 1995;117:1–19.
[231] Abbott LJ, Colina CM. Formation of microporosity in hyper-cross-linked polymers. Macromolecules 2014;47:5409–15.
[232] Asahi R, Morikawa T, Irie H, Ohwaki T. Nitrogen-doped titanium dioxide as visible-light-sensitive photocatalyst: designs, developments, and prospects. Chem Rev 2014;114:9824–52.
[233] Zhang J, Chen Y, Wang X. Two-dimensional covalent carbon nitride nanosheets: synthesis, functionalization, and applications. Energy Environ Sci 2015;8:3092–108.
[234] Foit SR, Vinke IC, de Haart LGJ, Eichel R-A. Power-to-syngas: an enabling technology for the transition of the energy system? Angew Chem Int Ed 2017;56:5402–11.
[235] NoneHydrogen Council launched in Davos as 13 major companies join to promote hydrogen. Fuel Cells Bulletin 2017;1. doi:10.1016/S464-2859(17)30001-9.
[236] Chen Q, Luo M, Wang T, Wang J-X, Zhou D, Han Y, Zhang C-S, Yan C-G, Han B-H. Porous organic polymers based on propeller-like hexaphenylbenzene building units. Macromolecules 2011;44:5573–7.

[237] Chen Q, Wang J-X, Yang F, Zhou D, Bian N, Zhang X-J, Yan C-G, Han B-H. Tetraphenylethylene-based fluorescent porous organic polymers: preparation, gas sorption properties and photoluminescence properties. J Mater Chem 2011;21:13554–60.

[238] Li A, Lu R-F, Wang Y, Wang X, Han K-L, Deng W-Q. Lithium-doped conjugated microporous polymers for reversible hydrogen storage. Angew Chem Int Ed 2010;49:3330–3.

[239] Reich TE, Jackson KT, Li S, Jena P, El-Kaderi HM. Synthesis and characterization of highly porous borazine-linked polymers and their performance in hydrogen storage application. J Mater Chem 2011;21:10629–32.

[240] Reich TE, Behera S, Jackson KT, Jena P, El-Kaderi HM. Highly selective CO2/CH4 gas uptake by a halogen-decorated borazine-linked polymer. J Mater Chem 2012;22:13524–8.

[241] Bhunia A, Vasylyeva V, Janiak C. From a supramolecular tetranitrile to a porous covalent triazine-based framework with high gas uptake capacities. Chem Commun 2013;49:3961–3.

[242] Yang L, Ma Y, Xu Y, Chang G. Cation-π induced lithium-doped conjugated microporous polymer with remarkable hydrogen storage performance. Chem Commun 2019;55:11227–30.

[243] Zeng W, Zhang Y, Zhao X, Qin M, Li X, Jin W, Zhang D. One-pot synthesis of conjugated microporous polymers based on extended molecular graphenes for hydrogen storage. Polymer (Guildf) 2019;174:96–100.

[244] Rao KV, Mohapatra S, Kulkarni C, Maji TK, George SJ. Extended phenylene based microporous organic polymers with selective carbon dioxide adsorption. J Mater Chem 2011;21:12958–63.

[245] Zhang W, Li C, Yuan Y-P, Qiu Ll-G, Xie A-J, Shen Y-H, Zhu J-F. Highly energy- and time-efficient synthesis of porous triazine-based framework: microwave-enhanced ionothermal polymerization and hydrogen uptake. J Mater Chem 2010;20:6413–15.

[246] Xu D, Sun L, Li G, Shang J, Yang R-X, Deng W-Q. Methyllithium-doped naphthyl-containing conjugated microporous polymer with enhanced hydrogen storage performance. Chemistry-A European Journal 2016;22:7944–9.

[247] Mulfort KL, Hupp JT. Chemical reduction of metal−organic framework materials as a method to enhance gas uptake and binding. J Am Chem Soc 2007;129:9604–5.

[248] Rangnekar N, Mittal N, Elyassi B, Caro J, Tsapatsis M. Zeolite membranes – a review and comparison with MOFs. Chem Soc Rev 2015;44:7128–54.

[249] Jeon MY, Kim D, Kumar P, Lee PS, Rangnekar N, Bai P, Shete M, Elyassi B, Lee HS, Narasimharao K, Basahel SN, Al-Thabaiti S, Xu W, Cho HJ, Fetisov EO, Thyagarajan R, DeJaco RF, Fan W, Mkhoyan KA, Siepmann JI, Tsapatsis M. Ultra-selective high-flux membranes from directly synthesized zeolite nanosheets. Nature 2017;543:690–4.

[250] Peng Y, Li Y, Ban Y, Jin H, Jiao W, Liu X, Yang W. Metal-organic framework nanosheets as building blocks for molecular sieving membranes. Science 2014;346:1356–9.

[251] Wang X, Chi C, Zhang K, Qian Y, Gupta KM, Kang Z, Jiang J, Zhao D. Reversed thermo-switchable molecular sieving membranes composed of two-dimensional metal-organic nanosheets for gas separation. Nat Commun 2017;8:14460 /1-10.

[252] Song Q, Jiang S, Hasell T, Liu M, Sun S, Cheetham AK, Sivaniah E, Cooper AI. Porous organic cage thin films and molecular-sieving membranes. Adv Mater 2016;28:2629–37.

[253] Hasell T, Cooper AI. Porous organic cages: soluble, modular and molecular pores. Nat Rev Mater 2016;1:16053 /1-14.

[254] Holst JR, Trewin A, Cooper AI. Porous organic molecules. Nat Chem 2010;2:915–20.

[255] Song Q, Cao S, Zavala-Rivera P, Ping Lu L, Li W, Ji Y, Al-Muhtaseb SA, Cheetham AK, Sivaniah E. Photo-oxidative enhancement of polymeric molecular sieve membranes. Nat Commun 2013;4:1918 /1-9.

[256] Jimenez-Solomon MF, Song Q, Jelfs KE, Munoz-Ibanez M, Livingston AG. Polymer nanofilms with enhanced microporosity by interfacial polymerization. Nat Mater 2016;15:760–7.

[257] Rose I, Bezzu CG, Carta M, Comesaña-Gándara B, Lasseuguette E, Ferrari MC, Bernardo P, Clarizia G, Fuoco A, Jansen JC, Hart Kyle E, Liyana-Arachchi TP, Colina CM, McKeown NB. Polymer ultrapermeability from the inefficient packing of 2D chains. Nat Mater 2017;16:932–7.

[258] Liu W, Jiang S-D, Yan Y, Wang W, Li J, Leng K, Japip S, Liu J, Xu H, Liu Y, Park I-H, Bao Y, Yu W, Guiver MD, Zhang S, Loh KP. A solution-processable and ultra-permeable conjugated microporous thermoset for selective hydrogen separation. Nat Commun 2020;11:1633 /1-7.

[259] Chong MN, Jin B, Chow CWK, Saint C. Recent developments in photocatalytic water treatment technology: a review. Water Res 2010;44:2997–3027.

[260] Liu Y, Liu Z, Huang D, Cheng M, Zeng G, Lai C, Zhang C, Zhou C, Wang W, Jiang D, Wang H, Shao B. Metal or metal-containing nanoparticle@MOF nanocomposites as a promising type of photocatalyst. Coord Chem Rev 2019;388:63–78.

[261] Jiang L, Yuan X, Pan Y, Liang J, Zeng G, Wu Z, Wang H. Doping of graphitic carbon nitride for photocatalysis: a reveiw. Appl Catal B 2017;217:388–406.

[262] Liu J, Liu Y, Liu N, Han Y, Zhang X, Huang H, Lifshitz Y, Lee S-T, Zhong J, Kang Z. Metal-free efficient photocatalyst for stable visible water splitting via a two-electron pathway. Science 2015;347:970–4.

[263] Zou W, Zhang L, Liu L, Wang X, Sun J, Wu S, Deng Y, Tang C, Gao F, Dong L. Engineering the Cu2O–reduced graphene oxide interface to enhance photocatalytic degradation of organic pollutants under visible light. Appl Catal B 2016;181:495–503.

[264] Yu H, Shi R, Zhao Y, Waterhouse GIN, Wu Ll-Z, Tung C-H, Zhang T. Smart utilization of carbon dots in semiconductor photocatalysis. Adv Mater 2016;28:9454–77.

[265] Zhang G, Lan Z-A, Wang X. Surface engineering of graphitic carbon nitride polymers with cocatalysts for photocatalytic overall water splitting. Chem Sci 2017;8:5261–74.

[266] Mahmood J, Li F, Jung S-M, Okyay MS, Ahmad I, Kim S-J, Park N, Jeong HY, Baek J-B. An efficient and pH-universal ruthenium-based catalyst for the hydrogen evolution reaction. Nat Nanotechnol 2017;12:441–6.

[267] Chen X, Shen S, Guo L, Mao SS. Semiconductor-based photocatalytic hydrogen generation. Chem Rev 2010;110:6503–70.

[268] Li Y, Wang H, Xie L, Liang Y, Hong G, Dai H. MoS2 nanoparticles grown on graphene: an advanced catalyst for the hydrogen evolution reaction. J Am Chem Soc 2011;133:7296–9.

[269] Sprick RS, Bonillo B, Clowes R, Guiglion P, Brownbill NJ, Slater BJ, Blanc F, Zwijnenburg MA, Adams DJ, Cooper AI. Visible-light-driven hydrogen evolution using planarized conjugated polymer photocatalysts. Angew Chem Int Ed 2016;55:1792–6.

[270] Yu H, Shi R, Zhao Y, Bian T, Zhao Y, Zhou C, Waterhouse GIN, Wu Ll-Z, Tung C-H, Zhang T. Alkali-assisted synthesis of nitrogen deficient graphitic carbon nitride with tunable band structures for efficient visible-light-driven hydrogen evolution. Adv Mater 2017;29:1605148 /1-7.

[271] Cheng W, Su H, Tang F, Che W, Huang Y, Zheng X, Yao T, Liu J, Hu F, Jiang Y, Liu Q, Wei S. Synergetic enhancement of plasmonic hot-electron injection in Au cluster-nanoparticle/C3N4 for photocatalytic hydrogen evolution. J Mater Chem A 2017;5:19649–55.

[272] Wang Y, Silveri F, Bayazit MK, Ruan Q, Li Y, Xie J, Catlow CRA, Tang J. Bandgap engineering of organic semiconductors for highly efficient photocatalytic water splitting. Adv Energy Mater 2018;8:1801084 /1-10.

[273] Yu Y, Yan W, Wang X, Li P, Gao W, Zou H, Wu S, Ding K. Surface engineering for extremely enhanced charge separation and photocatalytic hydrogen evolution on g-C3N4. Adv Mater 2018;30:1705060 /1-8.

[274] Kong D, Zheng Y, Kobielusz M, Wang Y, Bai Z, Macyk W, Wang X, Tang J. Recent advances in visible light-driven water oxidation and reduction in suspension systems. Mater Today 2018;21:897–924.

[275] Vyas VS, Lau VW-h, Lotsch BV. Soft photocatalysis: organic polymers for solar fuel production. Chem Mater 2016;28:5191–204.

[276] Li L, Cai Z, Wu Q, Lo W-Y, Zhang N, Chen LX, Yu L. Rational design of porous conjugated polymers and roles of residual palladium for photocatalytic hydrogen production. J Am Chem Soc 2016;138:7681–6.

[277] Han XL, Xu MY, Yang S, Qian J, Hua DB. Acetylcysteine-functionalized microporous conjugated polymers for potential separation of uranium from radioactive effluents. J Mater Chem A 2017;5:5123–8.

[278] Wang F, Ren F, Mu P, Zhu ZQ, Sun HX, Ma CH, Xiao CH, Liang WD, Chen LH, Li A. Hierarchical porous spherical-shaped conjugated microporous polymers for the efficient removal of antibiotics from water. J Mater Chem A 2017;5:11348–56.

[279] Liras M, Iglesias M, Sanchez F. Conjugated microporous polymers incorporating bodipy moieties as light-emitting materials and recyclable visible-light photocatalysts. Macromolecules 2016;49:1666–73.

[280] Sprick RS, Bonillo B, Sachs M, Clowes R, Durrant JR, Adams DJ, Cooper AI. Extended conjugated microporous polymers for photocatalytic hydrogen evolution from water. Chem Commun 2016;52:10008–11.

[281] Xu Y, Mao N, Feng S, Zhang C, Wang F, Chen Y, Zeng J, Jiang J-X. Perylene–containing conjugated microporous polymers for photocatalytic hydrogen evolution. Macromol Chem Phys 2017;218:1700049 /1-9.

[282] Xu YF, Zhang C, Mu P, Mao N, Wang X, He Q, Wang F, Jiang JX. Tetra-armed conjugated microporous polymers for gas adsorption and photocatalytic hydrogen evolution. Sci China Chem 2017;60:1075–83.

[283] Zhao Y, Ma W, Xu Y, Zhang C, Wang Q, Yang T, Gao X, Wang F, Yan C, Jiang J-X. Effect of linking pattern of dibenzothiophene-s,s-dioxide-containing conjugated microporous polymers on the photocatalytic performance. Macromolecules 2018;51:9502–8.

[284] Mothika VS, Sutar P, Verma P, Das S, Pati SK, Maji TK. Regulating charge–transfer in conjugated microporous polymers for photocatalytic hydrogen evolution. Chemistry-A European Journal 2019;25:3867–74.

[285] Wang X, Chen L, Chong SY, Little MA, Wu Y, Zhu W-H, Clowes R, Yan Y, Zwijnenburg MA, Sprick RS, Cooper AI. Sulfone-containing covalent organic frameworks for photocatalytic hydrogen evolution from water. Nat Chem 2018;10:1180–9.

[286] Wang H, Wang H, Wang Z, Tang L, Zeng G, Xu P, Chen M, Xiong T, Zhou C, Li X, Huang D, Zhu Y, Wang Z, Tang J. Covalent organic framework photocatalysts: structures and applications. Chem Soc Rev 2020;49:4135–65.

[287] Slater AG, Cooper AI. Function-led design of new porous materials. Science 2015;348 aaa8075/1-10.

[288] Wan S, Gándara F, Asano A, Furukawa H, Saeki A, Dey SK, Liao L, Ambrogio MW, Botros YY, Duan X, Seki S, Stoddart JF, Yaghi OM. Covalent organic frameworks with high charge carrier mobility. Chem Mater 2011;23:4094–4097.

[289] Biswal BP, Kandambeth S, Chandra S, Shinde DB, Bera S, Karak S, Garai B, Kharul UK, Banerjee R. Pore surface engineering in porous, chemically stable covalent organic frameworks for water adsorption. J Mater Chem A 2015;3:23664–9.

[290] Guan X, Li H, Ma Y, Xue M, Fang Q, Yan Y, Valtchev V, Qiu S. Chemically stable polyarylether-based covalent organic frameworks. Nat Chem 2019;11:587–94.

[291] Soliman AB, Hassan MH, Tran Ngoc H, Abugable AA, Elmehalmey WA, Karakalos SG, Tsotsalas M, Heinle M, Elbahri M, Fontecave M, Alkordi MH. Pt Immobilization within a tailored porous-organic polymer graphene composite: opportunities in the hydrogen evolving reaction. ACS Catal 2017;7:7847–7854.

[292] Lu C, Tranca D, Zhang J, Rodrıǵuez Hernández Fn, Su Y, Zhuang X, Zhang F, Seifert G, Feng X. Molybdenum carbide-embedded nitrogen-doped porous carbon nanosheets as electrocatalysts for water splitting in alkaline media. ACS Nano 2017;11:3933–42.

[293] Liao Y, Cheng Z, Zuo W, Thomas A, Faul CFJ. Nitrogen-rich conjugated microporous polymers: facile synthesis, efficient gas storage, and heterogeneous catalysis. ACS Appl Mater Inter 2017;9:38390–400.

[294] Xu F, Wu D, Fu R, Wei B. Design and preparation of porous carbons from conjugated polymer precursors. Mater Today 2017;20:629–56.

[295] Wang H, Cheng Z, Liao Y, Li J, Weber J, Thomas A, Faul CFJ. Conjugated microporous polycarbazole networks as precursors for nitrogen-enriched microporous carbons for CO2 storage and electrochemical capacitors. Chem Mater 2017;29:4885–93.

[296] Cui S, Qian M, Liu X, Sun Z, Du P. A copper porphyrin-based conjugated mesoporous polymer-derived bifunctional electrocatalyst for hydrogen and oxygen evolution. ChemSusChem 2016;9:2365–73.

[297] Su J, Yang Y, Xia G, Chen J, Jiang P, Chen Q. Ruthenium-cobalt nanoalloys encapsulated in nitrogen-doped graphene as active electrocatalysts for producing hydrogen in alkaline media. Nat Commun 2017;8:14969 /1-10.

[298] Zhang L, Xiao J, Wang H, Shao M. Carbon-based electrocatalysts for hydrogen and oxygen evolution reactions. ACS Catal 2017;7:7855–65.

[299] Qu K, Zheng Y, Jiao Y, Zhang X, Dai S, Qiao S-Z. Polydopamine-inspired, dual heteroatom-doped carbon nanotubes for highly efficient overall water splitting. Adv Energy Mater 2017;7:1602068 /1-8.

[300] Wang H, Hou B, Yang Y, Chen Q, Zhu M, Thomas A, Liao Y. Cobalt nanocrystals encapsulated in heteroatom-rich porous carbons derived from conjugated microporous polymers for efficient electrocatalytic hydrogen evolution. Small 2018;14:1803232 /1-6.

[301] Arakawa H, Aresta M, Armor JN, Barteau MA, Beckman EJ, Bell AT, Bercaw JE, Creutz C, Dinjus E, Dixon DA, Domen K, DuBois DL, Eckert J, Fujita E, Gibson DH, Goddard WA, Goodman DW, Keller J, Kubas GJ, Kung HH, Lyons JE, Manzer LE, Marks TJ, Morokuma K, Nicholas KM, Periana R, Que L, Rostrup-Nielson J, Sachtler WMH, Schmidt LD, Sen A, Somorjai GA, Stair PC, Stults BR, Tumas W. Catalysis research of relevance to carbon management: Progress, challenges, and opportunities. Chem Rev 2001;101:953–96.

[302] Pervaiz M, Sain MM. Carbon storage potential in natural fiber composites. Resour Conserv Recy 2003;39:325–40.

[303] Gray HB. Powering the planet with solar fuel. Nat Chem 2009;1(7). doi:10.1038/nchem.141.

[304] Farha OK, Özgür Yazaydın A, Eryazici I, Malliakas CD, Hauser BG, Kanatzidis MG, Nguyen ST, Snurr RQ, Hupp JT. De novo synthesis of a metal–organic framework material featuring ultrahigh surface area and gas storage capacities. Nat Chem 2010;2:944–8.

[305] Yang Dd-A, Cho H-Y, Kim J, Yang S-T, Ahn W-S. CO2 capture and conversion using Mg-MOF-74 prepared by a sonochemical method. Energy Environ Sci 2012;5:6465–73.

[306] Ampelli C, Centi G, Passalacqua R, Perathoner S. Synthesis of solar fuels by a novel photoelectrocatalytic approach. Energy Environ Sci 2010;3:292–301.

[307] Herron JA, Kim J, Upadhye AA, Huber GW, Maravelias CT. A general framework for the assessment of solar fuel technologies. Energy Environ Sci 2015;8:126–57.

[308] Yu M, Wang X, Yang X, Zhao Y, Jiang J-X. Conjugated microporous copolymer networks with enhanced gas adsorption. Polym Chem 2015;6:3217–23.

[309] Wang W, Zhouab M, Yuan D. Carbon dioxide capture in amorphous porous organic polymers. J Mater Chem A 2017;5:1334–47.

[310] Rabbani MG, Islamoglu T, El-Kaderi HM. Benzothiazole- and benzoxazole-linked porous polymers for carbon dioxide storage and separation. J Mater Chem A 2017;5:258–65.

[311] Zhou H, Zhang QY, Lu XB. Synthesis and catalytic application of N-heterocyclic carbene copper complex functionalized conjugated microporous polymer. RSC Adv 2016;6:44995–5000.

[312] Yuan R, Ren H, Yan Z, Wang A, Zhu G. Robust tri(4-ethynylphenyl)amine-based porous aromatic frameworks for carbon dioxide capture. Polym Chem 2014;5:2266–72.

[313] Dawson R, Adams DJ, Cooper AI. Chemical tuning of CO2 sorption in robust nanoporous organic polymers. Chem Sci 2011;2:1173–7.

[314] Ma H, Ren H, Zou X, Meng S, Sun F, Zhu G. Post-metalation of porous aromatic frameworks for highly efficient carbon capture from CO2 + N-2 and CH4 + N-2 mixtures. Polym Chem 2014;5:144–52.

[315] Zhang X, Lu J, Zhang J. Porosity enhancement of carbazolic porous organic frameworks using dendritic building blocks for gas storage and separation. Chem Mater 2014;26:4023–9.

[316] Jeon HJ, Choi JH, Lee Y, Choi KM, Park JH, Kang JK. Highly selective CO2-capturing polymeric organic network structures. Adv Energy Mater 2012;2:225–8.

[317] Jiang F, Sun J, Yang R, Qiao S, An Z, Huang J, Mao H, Chen G, Ren Y. A facile approach to prepare a microporous polycarbazole P-tetra(4-(N-carbazolyl)phenyl)silane network with high CO2 storage and separation properties. New J Chem 2016;40:4969–73.

[318] Qiao S, Wei H, Wang T, Huang W, Gu C, Yang R, Li X. A ribbon-like ultramicroporous conjugated polycarbazole network for gas storage and separation. New J Chem 2016;40:3172–6.

[319] Qiao S, Huang W, Wei H, Wang T, Yang R. Fine tailoring the steric configuration of initial building blocks to construct ultramicroporous polycarbazole networks with high CO2 uptake and selectivity of CO2 over N-2. Polymer (Guildf) 2015;70:52–8.

[320] Qiao S, Huang W, Du Z, Chen X, Shieh F-K, Yang R. Phosphine oxide-based conjugated microporous polymers with excellent CO2 capture properties. New J Chem 2015;39:136–41.

[321] Wang S, Liu Y, Yu Y, Du J, Cui Y, Song X, Liang Z. Conjugated microporous polymers based on biphenylene for CO2 adsorption and luminescence detection of nitroaromatic compounds. New J Chem 2018;42:9482–7.

[322] Banerjee R, Furukawa H, Britt D, Knobler C, O'Keeffe M, Yaghi OM. Control of pore size and functionality in isoreticular zeolitic imidazolate frameworks and their carbon dioxide selective capture properties. J Am Chem Soc 2009;131:3875–7.

[323] Vaidhyanathan R, Iremonger SS, Shimizu GKH, Boyd PG, Alavi S, Woo TK. Direct observation and quantification of CO2 binding within an amine-functionalized nanoporous solid. Science 2010;330:650–3.

[324] Lu W, Yuan D, Sculley J, Zhao D, Krishna R, Zhou H-C. Sulfonate-grafted porous polymer networks for preferential CO2 adsorption at low pressure. J Am Chem Soc 2011;133:18126–9.

[325] Xie Ll-H, Suh MP. High CO2-capture ability of a porous organic polymer bifunctionalized with carboxy and triazole groups. Chemistry-A European Journal 2013;19:11590–7.

[326] Qin L, Xu G-J, Yao C, Xu Y-H. Conjugated microporous polymer networks with adjustable microstructures for high CO2 uptake capacity and selectivity. Chem Commun 2016;52:12602–5.

[327] Yassin A, Trunk M, Czerny F, Fayon P, Trewin A, Schmidt J, Thomas A. Structure-thermodynamic-property relationships in cyanovinyl-based microporous polymer networks for the future design of advanced carbon capture materials. Adv Funct Mater 2017;27:1700233 /1-9.

[328] North M, Pasquale R, Young C. Synthesis of cyclic carbonates from epoxides and CO2. Green Chem 2010;12:1514–39.

[329] Xie K, Umezawa N, Zhang N, Reunchan P, Zhang Y, Ye J. Self-doped SrTiO3$-\delta$ photocatalyst with enhanced activity for artificial photosynthesis under visible light. Energy Environ Sci 2011;4:4211–19.

[330] Cheng H, Huang B, Liu Y, Wang Z, Qin X, Zhang X, Dai Y. An anion exchange approach to Bi2WO6 hollow microspheres with efficient visible light photocatalytic reduction of CO2 to methanol. Chem Commun 2012;48:9729–31.

[331] Broicher C, Foit SR, Rose M, Hausoul PJC, Palkovits R. A bipyridine-based conjugated microporous polymer for the ir-catalyzed dehydrogenation of formic acid. ACS Catal 2017;7:8413–19.

[332] Qiao J, Liu Y, Hong F, Zhang J. A review of catalysts for the electroreduction of carbon dioxide to produce low-carbon fuels. Chem Soc Rev 2014;43:631–75.

[333] Zhang S, Huang W, Hu P, Huang C, Shang C, Zhang C, Yang R, Cui G. Conjugated microporous polymers with excellent electrochemical performance for lithium and sodium storage. J Mater Chem A 2015;3:1896–901.

[334] Lin Z-Q, Xie J, Zhang B-W, Li J-W, Weng J, Song R-B, Huang X, Zhang H, Li H, Liu Y, Xu ZJ, Huang W, Zhang Q. Solution-processed nitrogen-rich graphene–like holey conjugated polymer for efficient lithium ion storage. Nano Energy 2017;41:117–27.

[335] Chen Z, Li W, Dai Y, Xu N, Su C, Liu J, Zhang C. Conjugated microporous polymer based on star-shaped triphenylamine-benzene structure with improved electrochemical performances as the organic cathode material of Li-ion battery. Electrochim Acta 2018;286:187–94.

[336] Wang J, Chen CS, Zhang Y. Hexaazatrinaphthylene-based porous organic polymers as organic cathode materials for lithium-ion batteries. ACS Sustain Chem Eng 2018;6:1772–9.

[337] Wei W, Chang G, Xu Y, Yang L. An indole-based conjugated microporous polymer: a new and stable lithium storage anode with high capacity and long life induced by cation-pi interactions and a N-rich aromatic structure. J Mater Chem A 2018;6:18794–8.

[338] Wang X, Zhang C, Xu Y, He Q, Mu P, Chen Y, Zeng J, Wang F, Jiang J-X. Conjugated microporous polytetra(2-thienyl)ethylene as high performance anode material for lithium- and sodium-ion batteries. Macromol Chem Phys 2018;219:1700524 /1-8.

[339] Chen Z, Xu N, Li W, Zhao R, Dong Y, Liu J, Su C, Wang J, Zhang C. Effect of trace hydrofluoric acid in a LiPF6 electrolyte on the performance of a Li-organic battery with an N-heterocycle based conjugated microporous polymer as the cathode. J Mater Chem A 2019;7:16347–55.

[340] Meng L, Ren S, Ma C, Yu Y, Lou Y, Zhang D, Shi Z. Synthesis of a 2D nitrogen-rich pi-conjugated microporous polymer for high performance lithium-ion batteries. Chem Commun 2019;55:9491–4.

[341] Molina A, Patil N, Ventosa E, Liras M, Palma J, Marcilla R. New anthraquinone-based conjugated microporous polymer cathode with ultrahigh specific surface area for high-performance lithium-ion batteries. Adv Funct Mater 2020;30:1908074 /1-11.

[342] Ren S-B, Ma W, Zhang C, Chen L, Wang K, Li R-R, Shen M, Han Dd-M, Chen Y, Jiang J-X. Exploiting polythiophenyl-triazine-based conjugated microporous polymer with superior lithium-storage performance. ChemSusChem 2020;13:1–9.

[343] Chen Y, Li H, Tang M, Zhuo S, Wu Y, Wang E, Wang S, Wang C, Hu W. Capacitive conjugated ladder polymers for fast-charge and -discharge sodium-ion batteries and hybrid supercapacitors. J Mater Chem A 2019;7:20891–8.

[344] Weeraratne KS, Alzharani AA, El-Kaderi HM. Redox-active porous organic polymers as novel electrode materials for green rechargeable sodium-ion batteries. ACS Appl Mater Inter 2019;11:23520–6.

[345] Zhang C, Qao Y, Xiong P, Ma W, Bai P, Wang X, Li Q, Zhao J, Xu Y, Chen Y, Zeng JH, Wang F, Xu Y, Jiang J-X. Conjugated microporous polymers with tunable electronic structure for high-performance potassium-ion batteries. ACS Nano 2019;13:745–54.

[346] Tian B, Zheng J, Zhao C, Liu C, Su C, Tang W, Li X, Ning G-H. Carbonyl-based polyimide and polyquinoneimide for potassium-ion batteries. J Mater Chem A 2019;7:9997–10003.

[347] Balogun M-S, Qiu W, Wang W, Fang P, Lu X, Tong Y. Recent advances in metal nitrides as high-performance electrode materials for energy storage devices. J Mater Chem A 2015;3:1364–87.

[348] Zhu G-N, Wang Y-G, Xia Y-Y. Ti-based compounds as anode materials for Li-ion batteries. Energy Environ Sci 2012;5:6652–67.

[349] Trogadas P, Ramani V, Strasser P, Fuller TF, Coppens M-O. Hierarchically structured nanomaterials for electrochemical energy conversion. Angew Chem Int Ed 2016;55:122–48.

[350] Chan CK, Peng H, Liu G, McIlwrath K, Zhang XF, Huggins RA, Cui Y. High-performance lithium battery anodes using silicon nanowires. Nat Nanotechnol 2008;3:31–5.

[351] Scrosati B, Garche J. Lithium batteries: status, prospects and future. J Power Sources 2010;195:2419–30.

[352] Mao Y, Duan H, Xu B, Zhang L, Hu Y, Zhao C, Wang Z, Chen L, Yang Y. Lithium storage in nitrogen-rich mesoporous carbon materials. Energy Environ Sci 2012;5:7950–5.

[353] Kang N, Park JH, Choi J, Jin J, Chun J, Jung IG, Jeong J, Park J-G, Lee SM, Kim HJ, Son SU. Nanoparticulate iron oxide tubes from microporous organic nanotubes as stable anode materials for lithium ion batteries. Angew Chem Int Ed 2012;51:6626–30.

[354] Jiang J, Zhu J, Ai W, Fan Z, Shen X, Zou C, Liu J, Zhang H, Yu T. Evolution of disposable bamboo chopsticks into uniform carbon fibers: a smart strategy to fabricate sustainable anodes for Li-ion batteries. Energy Environ Sci 2014;7:2670–9.

[355] Janoschka T, Hager MD, Schubert US. Powering up the future: radical polymers for battery applications. Adv Mater 2012;24:6397–409.

[356] Su C, Ye Y, Xu L, Zhang C. Synthesis and charge–discharge properties of a ferrocene-containing polytriphenylamine derivative as the cathode of a lithium ion battery. J Mater Chem 2012;22:22658–62.

[357] Renault S, Oltean VA, Araujo CM, Grigoriev A, Edström K, Brandell D. Superlithiation of organic electrode materials: the case of dilithium benzenedipropiolate. Chem Mater 2016;28:1920–6.

[358] Lee KY, Hwang H, Shin D, Choi W. Enhanced thermopower wave via nanowire bonding and grain boundary fusion in combustion of fuel/CuO–Cu2O–Cu hybrid composites. J Mater Chem A 2015;3:5457–66.

[359] Kim S-M, Kim MH, Choi SY, Lee JG, Jang J, Lee JB, Ryu JH, Hwang SS, Park J-H, Shin K, Kim YG, Oh SM. Poly(phenanthrenequinone) as a conductive binder for nano-sized silicon negative electrodes. Energy Environ Sci 2015;8:1538–43.

[360] Novák P, Müller K, Santhanam KSV, Haas O. Electrochemically active polymers for rechargeable batteries. Chem Rev 1997;97:207–82.

[361] Zhu LM, Lei AW, Cao YL, Ai XP, Yang HX. An all-organic rechargeable battery using bipolar polyparaphenylene as a redox-active cathode and anode. Chem Commun 2013;49:567–9.

[362] Casado N, Hernández G, Veloso A, Devaraj S, Mecerreyes D, Armand M. PEDOT radical polymer with synergetic redox and electrical properties. ACS Macro Lett 2016;5:59–64.

[363] Armand M, Tarascon JM. Building better batteries. Nature 2008;451:652–7.

[364] Song Z, Zhou H. Towards sustainable and versatile energy storage devices: an overview of organic electrode materials. Energy Environ Sci 2013;6:2280–301.

[365] Shi Y, Peng L, Ding Y, Zhao Y, Yu G. Nanostructured conductive polymers for advanced energy storage. Chem Soc Rev 2015;44:6684–96.

[366] Zhu Z, Hong M, Guo D, Shi J, Tao Z, Chen J. All-solid-state lithium organic battery with composite polymer electrolyte and pillar[5]quinone cathode. J Am Chem Soc 2014;136:16461–4.

[367] Patra BC, Khilari S, Satyanarayana L, Pradhan D, Bhaumik A. A new benzimidazole based covalent organic polymer having high energy storage capacity. Chem Commun 2016;52:7592–5.

[368] Dai Y, Li W, Chen Z, Zhu X, Liu J, Zhao R, Wright DS, Noori A, Mousavi MF, Zhang C. An air-stable electrochromic conjugated microporous polymer as an emerging electrode material for hybrid energy storage systems. J Mater Chem A 2019;7:16397–405.

[369] Mahadevi AS, Sastry GN. Cation−π interaction: its role and relevance in chemistry, biology, and material science. Chem Rev 2013;113:2100–38.

[370] Craven TW, Cho M-K, Traaseth NJ, Bonneau R, Kirshenbaum K. A miniature protein stabilized by a cation−π interaction network. J Am Chem Soc 2016;138:1543–50.

[371] Chang G, Yang L, Yang J, Stoykovich MP, Deng X, Cui J, Wang D. High-performance pH-switchable supramolecular thermosets via cation–π interactions. Adv Mater 2018;30:1704234 /1-6.

[372] Alzubi M, Arias S, Louzao I, Quiñoá E, Riguera R, Freire F. Multipodal dynamic coordination involving cation–π interactions to control the structure of helical polymers. Chem Commun 2017;53:8573–6.

[373] Gebbie MA, Wei W, Schrader AM, Cristiani TR, Dobbs HA, Idso M, Chmelka BF, Waite JH, Israelachvili JN. Tuning underwater adhesion with cation–π interactions. Nat Chem 2017;9:473–9.

[374] Han X, Chang C, Yuan L, Sun T, Sun J. Aromatic carbonyl derivative polymers as high-performance li-ion storage materials. Adv Mater 2007;19:1616–21.

[375] Sakaushi K, Nickerl G, Wisser FM, Nishio-Hamane D, Hosono E, Zhou H, Kaskel S, Eckert J. An energy storage principle using bipolar porous polymeric frameworks. Angew Chem Int Ed 2012;51:7850–4.

[376] Wu J, Rui X, Wang C, Pei W-B, Lau R, Yan Q, Zhang Q. Nanostructured conjugated ladder polymers for stable and fast lithium storage anodes with high–capacity. Adv Energy Mater 2015;5:1402189 /1-6.

[377] González-García P. Activated carbon from lignocellulosics precursors: a review of the synthesis methods, characterization techniques and applications. Renew Sust Energ Rev 2018;82:1393–414.

[378] Rashidi NA, Yusup S. A review on recent technological advancement in the activated carbon production from oil palm wastes. Chem Eng J 2017;314:277–90.

[379] Titirici M-M, Antonietti M. Chemistry and materials options of sustainable carbon materials made by hydrothermal carbonization. Chem Soc Rev 2010;39:103–16.

[380] Soleimani M, Kaghazchi T. Agricultural waste conversion to activated carbon by chemical activation with phosphoric acid. Chem Eng Technal 2007;30:649–54.

[381] Furukawa H, Cordova KE, O'Keeffe M, Yaghi OM. The chemistry and applications of metal-organic frameworks. Science 2013;341:123044 /1-12.

[382] Salunkhe RR, Kaneti YV, Kim J, Kim JH, Yamauchi Y. Nanoarchitectures for metal-organic framework-derived nanoporous carbons toward supercapacitor applications. Acc Chem Res 2016;49:2796–806.

[383] Chen Y-Z, Zhang R, Jiao L, Jiang H-L. Metal-organic framework-derived porous materials for catalysis. Coord Chem Rev 2018;362:1–23.

[384] Li X, Zheng S, Jin L, Li Y, Geng P, Xue H, Pang H, Xu Q. Metal-organic framework-derived carbons for battery applications. Adv Energy Mater 2018;8:1800716 /1-25.

[385] Luo S, Zeng Z, Zeng G, Liu Z, Xiao R, Chen M, Tang L, Tang W, Lai C, Cheng M, Shao B, Liang Q, Wang H, Jiang D. Metal organic frameworks as robust host of palladium nanoparticles in heterogeneous catalysis: synthesis, application, and prospect. ACS Appl Mater Inter 2019;11:32579–98.

[386] Zhang Q, Sun H, Wang X, Zhu Z, Liang W, Li A, Wen S, Deng W. Conjugated microporous polymer-derived porous hard carbon as high-rate long-life anode materials for lithium ion batteries. Energy Technology 2013;1:721–5.

[387] Zhang Q, Dai Q, Yan C, Su C, Li A. Nitrogen-doped porous carbon nanoparticle derived from nitrogen containing conjugated microporous polymer as high performance lithium battery anode. J Alloys Compd 2017;714:204–12.

[388] Qin Dd-D, Wang T, Song Y-M, Tao C-L. Reduced monoclinic BiVO4 for improved photoelectrochemical oxidation of water under visible light. Dalton Transactions 2014;43:7691–4.

[389] Li X, Zhu X, Zhu Y, Yuan Z, Si L, Qian Y. Porous nitrogen-doped carbon vegetable-sponges with enhanced lithium storage performance. Carbon N Y 2014;69:515–24.

[390] Han X, Han P, Yao J, Zhang S, Cao X, Xiong J, Zhang J, Cui G. Nitrogen-doped carbonized polyimide microsphere as a novel anode material for high performance lithium ion capacitors. Electrochim Acta 2016;196:603–10.

[391] Zhang QT, Ge SW, Wang XM, Sun HX, Zhu ZQ, Liang WD, Li A. Novel MnO/conjugated microporous polymer derived-porous hard carbon nanocomposite for superior lithium storage. RSC Adv 2014;4:41649–53.

[392] Zhang Q, Dai Q, Li M, Wang X, Li A. Incorporation of MnO nanoparticles inside porous carbon nanotubes originated from conjugated microporous polymers for lithium storage. J Mater Chem A 2016;4:19132–9.

[393] Li X, Niu S, Nan D, Li B, He Y-B, Kang F. Sp-sp(2) hybrid-conjugated microporous polymer-derived Pd-encapsulated porous carbon materials for lithium–sulfur batteries. Chem Commun 2019;55:10084–7.

[394] Zhang Q, Meng Y, Li M, Wang X. Thiophene containing conjugated microporous polymers derived sulfur-enriched porous carbon supported Fe3O4 nanoparticles with superior lithium storage properties. Journal of Materials Science-Materials in Electronics 2019;30:1425–33.

[395] Hu Y-Y, Liu Z, Nam K-W, Borkiewicz OJ, Cheng J, Hua X, Dunstan MT, Yu X, Wiaderek KM, Du Ll-S, Chapman KW, Chupas PJ, Yang X-Q, Grey CP. Origin of additional capacities in metal oxide lithium-ion battery electrodes. Nat Mater 2013;12:1130–6.

[396] Pan L, Zhu X-D, Xie X-M, Liu Y-T. Smart hybridization of TiO2 nanorods and Fe3O4 nanoparticles with pristine graphene nanosheets: hierarchically nanoengineered ternary heterostructures for high-rate lithium storage. Adv Funct Mater 2015;25:3341–50.

[397] Okubo M, Hosono E, Kim J, Enomoto M, Kojima N, Kudo T, Zhou H, Honma I. Nanosize effect on high-rate li-ion intercalation in LiCoO2 electrode. J Am Chem Soc 2007;129:7444–52.

[398] Okubo M, Kim J, Kudo T, Zhou H, Honma I. Anisotropic surface effect on electronic structures and electrochemical properties of LiCoO2. J Physl Chem C 2009;113:15337–42.

[399] Eftekhari A, Jian Z, Ji X. Potassium secondary batteries. ACS Appl Mater Inter 2017;9:4404–19.

[400] Chen Y, Luo W, Carter M, Zhou L, Dai J, Fu K, Lacey S, Li T, Wan J, Han X, Bao Y, Hu L. Organic electrode for non-aqueous potassium-ion batteries. Nano Energy 2015;18:205–11.

[401] Lei K, Li F, Mu C, Wang J, Zhao Q, Chen C, Chen J. High K-storage performance based on the synergy of dipotassium terephthalate and ether-based electrolytes. Energy Environ Sci 2017;10:552–7.

[402] Jian Z, Luo W, Ji X. Carbon electrodes for K-Ion batteries. J Am Chem Soc 2015;137:11566–9.

[403] Zhang W, Mao J, Li S, Chen Z, Guo Z. Phosphorus-based alloy materials for advanced potassium-ion battery anode. J Am Chem Soc 2017;139:3316–3319.

[404] Han C, Han K, Wang X, Wang C, Li Q, Meng J, Xu X, He Q, Luo W, Wu L, Mai L. Three-dimensional carbon network confined antimony nanoparticle anodes for high-capacity K-ion batteries. Nanoscale 2018;10:6820–6.

[405] Béguin F, Presser V, Balducci A, Frackowiak E. Carbons and electrolytes for advanced supercapacitors. Adv Mater 2014;26:2219–51.

[406] Wang Q, Yan J, Fan Z. Carbon materials for high volumetric performance supercapacitors: design, progress, challenges and opportunities. Energy Environ Sci 2016;9:729–62.

[407] Niu H, Zhou D, Yang X, Li X, Wang Q, Qu F. Towards three-dimensional hierarchical ZnO nanofiber@Ni(OH)2 nanoflake core–shell heterostructures for high-performance asymmetric supercapacitors. J Mater Chem A 2015;3:18413–21.

[408] Yu D, Goh K, Wang H, Wei L, Jiang W, Zhang Q, Dai L, Chen Y. Scalable synthesis of hierarchically structured carbon nanotube–graphene fibres for capacitive energy storage. Nat Nanotechnol 2014;9:555–62.

[409] Xu Y, Tao Y, Zheng X, Ma H, Luo J, Kang F, Yang Q-H. A metal-free supercapacitor electrode material with a record high volumetric capacitance over 800 F cm − 3. Adv Mater 2015;27:8082–7.

[410] Xu F, Tang Z, Huang S, Chen L, Liang Y, Mai W, Zhong H, Fu R, Wu D. Erratum: facile synthesis of ultrahigh-surface-area hollow carbon nanospheres for enhanced adsorption and energy storage. Nat Commun 2015;6:7863 /1-2.

[411] Ringk A, Lignie A, Hou Y, Alshareef HN, Beaujuge PM. Electropolymerized star-shaped benzotrithiophenes yield pi-conjugated hierarchical networks with high areal capacitance. ACS Appl Mater Inter 2016;8:12091–100.

[412] Liao Y, Wang H, Zhu M, Thomas A. Efficient supercapacitor energy storage using conjugated microporous polymer networks synthesized from Buchwald-Hartwig coupling. Adv Mater 2018;30:1705710 /1-10.

[413] Khattak AM, Sin H, Ghazi ZA, He X, Liang B, Khan NA, Alanagh HR, Iqbal A, Li L, Tang Z. Controllable fabrication of redox-active conjugated microporous polymers on reduced graphene oxide for high performance faradaic energy storage. J Mater Chem A 2018;6:18827–32.

[414] Liu W, Ulaganathan M, Abdelwahab I, Luo X, Chen Z, Tan SJR, Wang X, Liu Y, Geng D, Bao Y, Chen J, Loh KP. Two-dimensional polymer synthesized via solid-state polymerization for high-performance supercapacitors. ACS Nano 2018;12:852–60.

[415] Zhang M, Zhao T, Dou J, Xu Z, Zhang W, Chen X, Wang X, Zhou B. Bottom-up construction of conjugated microporous polyporphyrin-coated graphene hydrogel composites with hierarchical pores for high-performance capacitors. Chemelectrochem 2019;6:5946. doi:10.1002/celc.201901586.

[416] Li X-C, Zhang Y, Wang C-Y, Wan Y, Lai W-Y, Pang H, Huang W. Redox-active triazatruxene-based conjugated microporous polymers for high-performance supercapacitors. Chem Sci 2017;8:2959–65.

[417] Bandyopadhyay S, Singh C, Jash P, Hussain MW, Paul A, Patra A. Redox-active, pyrene-based pristine porous organic polymers for efficient energy storage with exceptional cyclic stability. Chem Commun 2018;54:6796–9.

[418] Choi J, Ko JH, Kang CW, Lee SM, Kim HJ, Ko Y-J, Yang M, Son SU. Enhanced redox activity of a hollow conjugated microporous polymer through the generation of carbonyl groups by carbonylative Sonogashira coupling. J Mater Chem A 2018;6:6233–7.

[419] Li H, Lyu W, Liao Y. Engineering redox activity in conjugated microporous polytriphenylamine networks using pyridyl building blocks toward efficient supercapacitors. Macromol Rapid Commun 2019;40:1900455 /1-7.

[420] Chai S, Hu N, Han Y, Zhang X, Yang Z, Wei L, Wang L, Wei H. The microwave-assisted solvothermal synthesis of a novel beta-ketoenamine-linked conjugated microporous polymer for supercapacitors. RSC Adv 2016;6:49425–8.

[421] Wei H, Chai S, Hu N, Yang Z, Wei L, Wang L. The microwave-assisted solvothermal synthesis of a crystalline two-dimensional covalent organic framework with high CO2 capacity. Chem Commun 2015;51:12178–81.

[422] Choi J, Kim ES, Ko JH, Lee SM, Kim HJ, Ko Y-J, Son SU. Hollow and microporous triphenylamine networks post-modified with TCNE for enhanced organocathode performance. Chem Commun 2017;53:8778–81.

[423] Wang X, Feng J, Bai Y, Zhang Q, Yin Y. Synthesis, properties, and applications of hollow micro-/nanostructures. Chem Rev 2016;116:10983–1060.

[424] Cho K, Yoo J, Noh H-W, Lee SM, Kim HJ, Ko Y-J, Jang H-Y, Son SU. Hollow structural effect of microporous organocatalytic polymers with pyrrolidines: dramatic enhancement of catalytic performance. J Mater Chem A 2017;5:8922–6.

[425] Sun M, Kuang P, Qin L, Gu C, Xie Z, Ma Y. In situ synthesis of electroactive conjugated microporous fullerene films capable of supercapacitive energy storage. Chem Commun 2017;53:9602–5.

[426] Zhu Y, Murali S, Stoller MD, Ganesh KJ, Cai W, Ferreira PJ, Pirkle A, Wallace RM, Cychosz KA, Thommes M, Su D, Stach EA, Ruoff RS. Carbon-based supercapacitors produced by activation of graphene. Science 2011;332:1537–41.

[427] Li Y, Zhu H, Shen F, Wan J, Han X, Dai J, Dai H, Hu L. Highly conductive microfiber of graphene oxide templated carbonization of nanofibrillated cellulose. Adv Funct Mater 2014;24:7366–72.

[428] Zheng S, Ju H, Lu X. A high-performance supercapacitor based on KOH activated 1D C70 microstructures. Adv Energy Mater 2015;5:1500871 /1-9.

[429] Ashourirad B, Sekizkardes AK, Altarawneh S, El-Kaderi HM. Exceptional gas adsorption properties by nitrogen-doped porous carbons derived from benzimidazole-linked polymers. Chem Mater 2015;27:1349–58.

[430] Zhuang X, Zhang F, Wu D, Forler N, Liang H, Wagner M, Gehrig D, Hansen MR, Laquai F, Feng X. Two-dimensional sandwich-type, graphene-based conjugated microporous polymers. Angew Chem Int Ed 2013;52:9668–72.

[431] Yuan K, Guo-Wang P, Hu T, Shi L, Zeng R, Forster M, Pichler T, Chen Y, Scherf U. Nanofibrous and graphene-templated conjugated microporous polymer materials for flexible chemosensors and supercapacitors. Chem Mater 2015;27:7403–11.

[432] Lee J-SM, Wu T-H, Alston BM, Briggs ME, Hasell T, Hu C-C, Cooper AI. Porosity-engineered carbons for supercapacitive energy storage using conjugated microporous polymer precursors. J Mater Chem A 2016;4:7665–73.

[433] Yuan K, Hu T, Xu Y, Graf R, Shi L, Forster M, Pichler T, Riedl T, Chen Y, Scherf U. Nitrogen-doped porous carbon/graphene nanosheets derived from two-dimensional conjugated microporous polymer sandwiches with promising capacitive performance. Mater Chem Front 2017;1:278–85.

[434] Xu Y, Wu S, Ren S, Ji J, Yue Y, Shen J. Nitrogen-doped porous carbon materials generated via conjugated microporous polymer precursors for CO2 capture and energy storage. RSC Adv 2017;7:32496–501.

[435] Lim AC, Jadhav HS, Seo JG. Electron transport shuttle mechanism via an Fe-N-C bond derived from a conjugated microporous polymer for a supercapacitor. Dalton Transactions 2018;47:852–8.

[436] Lu G, Yang H, Zhu Y, Huggins T, Ren ZJ, Liu Z, Zhang W. Synthesis of a conjugated porous Co(II) porphyrinylene-ethynylene framework through alkyne metathesis and its catalytic activity study. J Mater Chem A 2015;3:4954–4959.

[437] Brüller S, Liang H-W, Kramm UI, Krumpfer JW, Feng X, Müllen K. Bimetallic porous porphyrin polymer-derived non-precious metal electrocatalysts for oxygen reduction reactions. J Mater Chem A 2015;3:23799–808.

[438] Zhang W, Cui T, Yang L, Zhang C, Cai M, Sun S, Yao Y, Zhuang X, Zhang F. Hollow-structured conjugated porous polymer derived Iron/Nitrogen-codoped hierarchical porous carbons as highly efficient electrocatalysts. J Colloid Interface Sci 2017;497:108–16.

[439] Yang S-J, Ding X, Han B-H. Conjugated microporous polymers with dense sulfonic acid groups as efficient proton conductors. Langmuir 2018;34:7640–6.

[440] Hu L, Gu S, Yu W, Zhang W, Xie Q, Pan C, Tang J, Yu G. Facile preparation of CoO nanoparticles embedded N-doped porous carbon from conjugated microporous polymer for oxygen reduction reaction. J Colloid Interface Sci 2019;562:550–7.

[441] Liu W, Wang K, Wang C, Liu W, Pan H, Xiang Y, Qi D, Jiang J. Mixed phthalocyanine-porphyrin-based conjugated microporous polymers towards unveiling the activity origin of Fe-N-4 catalysts for the oxygen reduction reaction. J Mater Chem A 2018;6:22851–7.

[442] Roy S, Bandyopadhyay A, Das M, Ray PP, Pati SK, Maji TK. Redox-active and semi-conducting donor-acceptor conjugated microporous polymers as metal-free ORR catalysts. J Mater Chem A 2018;6:5587–91.

[443] Su Y, Yao Z, Zhang F, Wang H, Mics Z, Canovas E, Bonn M, Zhuang X, Feng X. Sulfur-enriched conjugated polymer nanosheet derived sulfur and nitrogen co-doped porous carbon nanosheets as electrocatalysts for oxygen reduction reaction and zinc-air battery. Adv Funct Mater 2016;26:5893–902.

[444] Zhou B, Liu L, Cai P, Zeng G, Li X, Wen Z, Chen L. Ferrocene-based porous organic polymer derived high-performance electrocatalysts for oxygen reduction. J Mater Chem A 2017;5:22163–9.

[445] Li Q, Shao Q, Wu Q, Duan Q, Li Y, Wang H-g. In situ anchoring of metal nanoparticles in the N-doped carbon framework derived from conjugated microporous polymers towards an efficient oxygen reduction reaction. Catal Sci Technol 2018;8:3572–9.

[446] Kim S-J, Mahmood J, Kim C, Han G-F, Kim S-W, Jung S-M, Zhu G, De Yoreo JJ, Kim G, Baek J-B. Defect-free encapsulation of Fe-0 in 2D fused organic networks as a durable oxygen reduction electrocatalyst. J Am Chem Soc 2018;140:1737–42.

[447] Yuan K, Zhuang X, Hu T, Shi L, Sfaelou S, Polnick U, Forster M, Pichler T, Riedl T, Feng X, Chen Y, Scherf U. 2D heterostructures derived from MoS2-templated, cobalt-containing conjugated microporous polymer sandwiches for the oxygen reduction reaction and electrochemical energy storage. ChemElectroChem 2017;4:709–15.

[448] Bildirir H, Gregoriou VG, Avgeropoulos A, Scherfd U, Chochos CL. Porous organic polymers as emerging new materials for organic photovoltaic applications: current status and future challenges. Mate Horiz 2017;4:546–56.

[449] An Y, Liao X, Chen L, Yin J, Ai Q, Xie Q, Huang B, Liu F, Jen AKY, Chen Y. Nonhalogen solvent-processed asymmetric wide-bandgap polymers for nonfullerene organic solar cells with over 10% efficiency. Adv Funct Mater 2018;28:1706517 /1-9.

[450] Saliba M, Matsui T, Seo J-Y, Domanski K, Correa-Baena J-P, Nazeeruddin MK, Zakeeruddin SM, Tress W, Abate A, Hagfeldt A, Grätzel M. Cesium-containing triple cation perovskite solar cells: improved stability, reproducibility and high efficiency. Energy Environ Sci 2016;9:1989–97.

[451] Chen W, Zhang J, Xu G, Xue R, Li Y, Zhou Y, Hou J, Li Y. A semitransparent inorganic perovskite film for overcoming ultraviolet light instability of organic solar cells and achieving 14.03% efficiency. Adv Mater 2018;30:1800855 /1-10.

[452] Wang Y, Wu T, Barbaud J, Kong W, Cui D, Chen H, Yang X, Han L. Stabilizing heterostructures of soft perovskite semiconductors. Science 2019;365:687–91.

[453] Za Tan, Li S, Wang F, Qian D, Lin J, Hou J, Li Y. High performance polymer solar cells with as-prepared zirconium acetylacetonate film as cathode buffer layer. Sci Rep 2014;4:4691 /1-9.

[454] Egger DA, Edri E, Cahen D, Hodes G. Perovskite solar cells: do we know what we do not know? J Phys Chem Lett 2015;6:279–82.

[455] Jeng J-Y, Chiang Y-F, Lee M-H, Peng S-R, Guo T-F, Chen P, Wen T-C. CH3NH3PbI3 perovskite/fullerene planar-heterojunction hybrid solar cells. Adv Mater 2013;25:3727–32.

[456] Li X, Choy WCH, Xie F, Zhang S, Hou J. Room-temperature solution-processed molybdenum oxide as a hole transport layer with Ag nanoparticles for highly efficient inverted organic solar cells. J Mater Chem A 2013;1:6614–21.

[457] Za Tan, Qian D, Zhang W, Li L, Ding Y, Xu Q, Wang F, Li Y. Efficient and stable polymer solar cells with solution-processed molybdenum oxide interfacial layer. J Mater Chem A 2013;1:657–64.

[458] Park JH, Seo J, Park S, Shin SS, Kim YC, Jeon NJ, Shin H-W, Ahn TK, Noh JH, Yoon SC, Hwang CS, Seok SI. Efficient CH3NH3PbI3 perovskite solar cells employing nanostructured p-type nio electrode formed by a pulsed laser deposition. Adv Mater 2015;27:4013–19.

[459] Zuo C, Ding L. Solution-processed Cu2O and CuO as hole transport materials for efficient perovskite solar cells. Small 2015;11:5528–32.

[460] Chen W-Y, Deng Ll-L, Dai S-M, Wang X, Tian C-B, Zhan X-X, Xie S-Y, Huang R-B, Zheng Ll-S. Low-cost solution-processed copper iodide as an alternative to PEDOT:PSS hole transport layer for efficient and stable inverted planar heterojunction perovskite solar cells. J Mater Chem A 2015;3:19353–9.

[461] Fang Z, Chellappan V, Webster RD, Ke L, Zhang T, Liu B, Lai Y-H. Bridged-triarylamine starburst oligomers as hole transporting materials for electroluminescent devices. J Mater Chem 2012;22:15397–404.

[462] Henson ZB, Zhang Y, Nguyen T-Q, Seo JH, Bazan GC. Synthesis and properties of two cationic narrow band gap conjugated polyelectrolytes. J Am Chem Soc 2013;135:4163–6.

[463] Zhou H, Zhang Y, Mai C-K, Seifter J, Nguyen T-Q, Bazan GC, Heeger AJ. Solution-processed pH-neutral conjugated polyelectrolyte improves interfacial contact in organic solar cells. ACS Nano 2015;9:371–7.

[464] Cui Y, Jia G, Zhu J, Kang Q, Yao H, Lu L, Xu B, Hou J. The critical role of anode work function in non-fullerene organic solar cells unveiled by counterion-size-controlled self-doping conjugated polymers. Chem Mater 2018;30:1078–84.

[465] Ren S, Dawson R, Adams DJ, Cooper A. Low band-gap benzothiadiazole conjugated microporous polymers. Polym Chem 2013;4:5585–90.

[466] Vinodh R, Babu CM, Abidov A, Peng MM, Palanichamy M, Cha WS, Jang HT. Microporous spheres of tiny semiconducting graphene sheets from hyper-cross-linked polymers: absorption and CO2 sorption characteristics. Adv Polym Tech 2018;37:714–23.

[467] Wang Y, Zhang S, Wu J, Liu K, Li D, Meng Q, Zhu G. Electropolymerization porous aromatic framework film as a hole-transport layer for inverted perovskite solar cells with superior stability. ACS Appl Mater Inter 2017;9:43688–95.

[468] Yang S, Yang C, Zhang X, Zheng Z, Bi S, Zhang Y, Zhou H. A conjugated microporous polymer film fabricated by in situ electro-chemical deposition as a hole transporting layer in organic photovoltaics. Journal of Materials Chemistry C 2018;6:9044–8.

[469] Su Y, Liu Y, Liu P, Wu D, Zhuang X, Zhang F, Feng X. Compact coupled graphene and porous polyaryltriazine-derived frameworks as high performance cathodes for lithium-ion batteries. Angew Chem Int Ed 2015;54:1812–16.

[470] Hu Z, Chen Z, Zhang K, Zheng N, Xie R, Liu X, Yang X, Huang F, Cao Y. Self-doped N-type water/alcohol soluble-conjugated polymers with tailored backbones and polar groups for highly efficient polymer solar cells. Solar RRL 2017;1:1700055 /1-12.

[471] Wang ZJ, Ghasimi S, Landfester K, Zhang KAI. Photocatalytic suzuki coupling reaction using conjugated microporous polymer with immobilized palladium nanoparticles under visible light. Chem Mater 2015;27:1921–4.

[472] Wei F, Cai X, Nie J, Wang F, Lu C, Yang G, Chen Z, Ma C, Zhang Y. A 1, 2, 3-triazolyl based conjugated microporous polymer for sensitive detection of p-nitroaniline and Au nanoparticle immobilization. Polym Chem 2018;9:3832–9.

[473] Ayed C, Huang W, Li R, da Silva LC, Wang D, Suraeva O, Najjar W, Zhang KAI. Conjugated microporous polymers with immobilized TiO2 nanoparticles for enhanced visible light photocatalysis. Part Part Syst Char 2018;35:1700234 /1-10.

[474] Yang XW, Zhuang XD, Huang YJ, Jiang JZ, Tian H, Wu DQ, Zhang F, Mai YY, Feng XL. Nitrogen-enriched hierarchically porous carbon materials fabricated by graphene aerogel templated Schiff-base chemistry for high performance electrochemical capacitors. Polym Chem 2015;6:1088–95.

[475] Zhuang X, Zhang F, Wu D, Feng X. Graphene coupled Schiff-base porous polymers: towards nitrogen-enriched porous carbon nanosheets with ultrahigh electrochemical capacity. Adv Mater 2014;26:3081–6.

[476] Katekomol P, Roeser J, Bojdys M, Weber J, Thomas A. Covalent triazine frameworks prepared from 1,3,5-tricyanobenzene. Chem Mater 2013;25:1542–8.

[477] Roberts AD, Li X, Zhang H. Porous carbon spheres and monoliths: morphology control, pore size tuning and their applications as Li-ion battery anode materials. Chem Soc Rev 2014;43:4341–56.

[478] Hao L, Ning J, Luo B, Wang B, Zhang Y, Tang Z, Yang J, Thomas A, Zhi L. Structural evolution of 2D microporous covalent triazine-based framework toward the study of high-performance supercapacitors. J Am Chem Soc 2015;137:219–25.

[479] Liu J, Yee KK, Lo KK, Zhang KY, To WP, Che CM, Xu Z. Selective Ag(I) binding, H2S sensing, and white-light emission from an easy-to-make porous conjugated polymer. J Am Chem Soc 2014;136:2818–24.

[480] Guo J, Xu Y, Jin S, Chen L, Kaji T, Honsho Y, Addicoat MA, Kim J, Saeki A, Ihee H. Conjugated organic framework with three-dimensionally ordered stable structure and delocalized π clouds. Nat Commun 2013;4:2736 /1-8.

[481] Chen L, Furukawa K, Gao J, Nagai A, Nakamura T, Dong Y, Jiang D. Photoelectric covalent organic frameworks: converting open lattices into ordered donor–acceptor heterojunctions. J Am Chem Soc 2014;136:9806–9.

[482] Jin S, Supur M, Addicoat M, Furukawa K, Chen L, Nakamura T, Fukuzumi S, Irle S, Jiang D. Creation of superheterojunction polymers via direct polycondensation: segregated and bicontinuous donor–acceptor π-columnar arrays in covalent organic frameworks for long-lived charge separation. J Am Chem Soc 2015;137:7817–27.

[483] Wang ZJ, Garth K, Ghasimi S, Landfester K, Zhang KA. Conjugated microporous poly(benzochalcogenadiazole)s for photocatalytic oxidative coupling of amines under visible light. ChemSusChem 2015;8:3459–64.

[484] Huang N, Wang P, Jiang DL. Covalent organic frameworks: a materials platform for structural and functional designs. Nat Rev Mater 2016;1:16068 /1-19.

[485] Zeng Y, Zou R, Zhao Y. Covalent organic frameworks for CO2 capture. Adv Mater 2016;28:2855–73.